

TRANSDUCING LANGUAGE MODELS

Vésteinn Snæbjarnarson*^{Q,R} Samuel Kieglend*^{Q,X} Tianyu Liu^Q
 Reda Bouasmoud^Q Ryan Cotterell^Q Tim Vieira^Q
^QETH Zürich ^RUniversity of Copenhagen ^XCHI-FRO
 {vest.snae, tim.f.vieira}@gmail.com reda.bouasmoud@math.ethz.ch
 {samuel.kieglend, tianyu.liu, ryan.cotterell}@inf.ethz.ch

ABSTRACT

Modern language models define distributions over strings, but downstream tasks often require different output formats. For instance, a model that generates byte-pair strings does not directly produce word-level predictions, and a DNA model does not directly produce amino-acid sequences. In such cases, a deterministic string-to-string transformation can convert the model’s output to the desired form. This is a familiar pattern in probability theory: applying a function f to a random variable $X \sim p$ yields a transformed random variable $f(X)$ with an induced distribution. While such transformations are occasionally used in language modeling, prior work does not treat them as yielding new, fully functional language models. We formalize this perspective and introduce a general framework for language models derived from deterministic string-to-string transformations. We focus on transformations representable as finite-state transducers—a commonly used state-machine abstraction for efficient string-to-string mappings. We develop algorithms that compose a language model with an FST to *marginalize* over source strings mapping to a given target, propagating probabilities through the transducer without altering model parameters and enabling *conditioning* on transformed outputs. We present an exact algorithm, an efficient approximation, and a theoretical analysis. We conduct experiments in three domains: converting language models from tokens to bytes, from tokens to words, and from DNA to amino acids. These experiments demonstrate inference-time adaptation of pretrained language models to match application-specific output requirements.

 <https://github.com/rycolab/transducing-language-models>

1 INTRODUCTION

Language models (LMs) define distributions over strings. Yet, the strings they produce often do not match the requirements of downstream applications, so practitioners resort to ad hoc post-processing. We call this the **string mismatch problem**. For example, in natural language processing, modern language models typically generate byte-pair encoded strings (Sennrich et al., 2016), while downstream tasks may require words or characters instead (see Ex. (2), below). Similarly, DNA language models generate nucleobase sequences, whereas many applications require amino acid sequences (Ex. (5)).

Adding a string-to-string transformation to a generation pipeline is a common engineering solution, such as normalizing output or mapping subword tokens to bytes. Formally, this defines a new language model over *transformed* strings. However, while sampling remains straightforward, other operations—such as computing the probability of a transformed string or conditioning on transformed outputs—become intractable. Consider, for instance, the mapping from a string in any casing to its lowercase version, as in the use-case depicted in Fig. 1. While lowercasing a given input is trivial, converting the original distribution to a distribution over lowercased words is not.

This work treats string-to-string transformations as a first-class component of the language modeling pipeline. We show how to equip these transformed models with the familiar autoregressive interface—incremental next-symbol distributions and prefix probabilities—making them interoperable with

*Equal contribution.

pose pretrained language models with transducers that encode such transformations, and refer to the compositions as *transduced language models*. FSTs provide explicit structure for tracing how probabilities from the original model should map to output sequences. This allows us to develop exact and approximate algorithms for efficient sampling, scoring, and conditioning on transformed strings, all without modifying the underlying language model. We give sufficient conditions for when the transformations can be made exactly (§6) and approximations when exact transformations are infeasible (§5).

To validate our approach, we construct FSTs for the three use cases above: (i) converting tokens to bytes, (ii) inserting orthographic boundaries following the Penn Treebank tokenizer, and (iii) converting DNA sequences to sequences over amino acids. We then employ commonly used pretrained language models over the input units of the FSTs, and compose them with the FSTs to obtain language models over the output tokens. Finally, we use these settings to benchmark the theoretical and algorithmic contributions. In particular, we find that using a practical approximation is sufficient to obtain a good estimate at a fraction of the computational cost.

2 BACKGROUND⁴

Strings. Let \mathcal{X} be an **alphabet** (i.e., a finite, non-empty set). Let \mathcal{X}^* denote the set of all finite strings over \mathcal{X} , including the empty string $\varepsilon_{\mathcal{X}}$. When there is no risk of ambiguity with other alphabets, we simply write ε . We use $\mathbf{x}, \mathbf{x}' \in \mathcal{X}^*$ to denote strings and $Z, Z' \subseteq \mathcal{X}^*$ to denote sets of strings. Let \mathbf{xx}' denote **concatenation**. Similarly, we define the concatenation of sets of strings as $ZZ' \stackrel{\text{def}}{=} \{\mathbf{xx}' \mid \mathbf{x} \in Z, \mathbf{x}' \in Z'\}$, and in the singleton case as $\mathbf{x}Z' \stackrel{\text{def}}{=} \{\mathbf{x}\}Z'$, and $Z\mathbf{x}' \stackrel{\text{def}}{=} Z\{\mathbf{x}'\}$. We write $\mathbf{x} \preceq \mathbf{x}'$ when \mathbf{x} is a **prefix** of \mathbf{x}' , and $\mathbf{x} \prec \mathbf{x}'$ when it is a **strict-prefix**. Conversely, if $\mathbf{x} \preceq \mathbf{x}'$, we say \mathbf{x}' is an **extension** of \mathbf{x} (a **strict extension** when $\mathbf{x} \prec \mathbf{x}'$).

Language models. A **language model** $p_{\mathcal{X}}$ is a probability distribution over a set of strings \mathcal{X}^* . Let $\text{EOS} \notin \mathcal{X}$ be a special **end-of-string symbol**. We define the **prefix probability** of $p_{\mathcal{X}}$ as the probability that a string $X \sim p_{\mathcal{X}}$ starts with a given prefix \mathbf{x} , and the **conditional prefix probability**:

$$\vec{p}_{\mathcal{X}}(\mathbf{x}) \stackrel{\text{def}}{=} \sum_{\mathbf{x}' \in \mathcal{X}^*} p_{\mathcal{X}}(\mathbf{xx}') \quad \vec{p}_{\mathcal{X}}(\mathbf{x}' \mid \mathbf{x}) \stackrel{\text{def}}{=} \frac{\vec{p}_{\mathcal{X}}(\mathbf{xx}')}{\vec{p}_{\mathcal{X}}(\mathbf{x})} \quad \vec{p}_{\mathcal{X}}(\text{EOS} \mid \mathbf{x}) \stackrel{\text{def}}{=} \frac{p_{\mathcal{X}}(\mathbf{x})}{\vec{p}_{\mathcal{X}}(\mathbf{x})} \quad (1)$$

when $\vec{p}_{\mathcal{X}}(\mathbf{x}) > 0$; otherwise we set $\vec{p}_{\mathcal{X}}(\mathbf{x}' \mid \mathbf{x}) \stackrel{\text{def}}{=} 0$ and $\vec{p}_{\mathcal{X}}(\text{EOS} \mid \mathbf{x}) \stackrel{\text{def}}{=} 1$. Therefore, $\vec{p}_{\mathcal{X}}(\cdot \mid \mathbf{x})$ is a probability distribution over $\mathcal{X} \sqcup \{\text{EOS}\}$ for all $\mathbf{x} \in \mathcal{X}^*$. Using this structure, any language model $p_{\mathcal{X}}$ may be factorized as $p_{\mathcal{X}}(\mathbf{x}) = \vec{p}_{\mathcal{X}}(\text{EOS} \mid \mathbf{x}) \prod_{t=1}^{|\mathbf{x}|} \vec{p}_{\mathcal{X}}(x_t \mid \mathbf{x}_{<t})$. This factorization defines a left-to-right generative process: starting from $\mathbf{x} = \varepsilon$, we repeatedly sample $x' \sim \vec{p}_{\mathcal{X}}(\cdot \mid \mathbf{x})$; if $x' = \text{EOS}$, we stop, otherwise we update \mathbf{x} to \mathbf{xx}' . Conditional generation simply starts from the conditioning prefix instead of the empty string. We refer to the quantities in Eq. (1) as the **autoregressive interface** to the language model $p_{\mathcal{X}}$.

Cylindrical sets. A cylindrical set is the set of all strings with a given prefix. Let $Z, Z' \subseteq \mathcal{X}^*$; we define the **cylinder** over Z as $\langle Z \rangle \stackrel{\text{def}}{=} ZX^*$. We say that Z is **cylindrical** if $Z = \langle Z \rangle$. The union of cylinder sets is again a cylinder set, since cylinders are upward-closed. We define the **basic cylinder** for \mathbf{x} as $\langle \mathbf{x} \rangle \stackrel{\text{def}}{=} \{\{\mathbf{x}\}\}$. The **prefix-base** operation $\text{pf}(Z)$ is defined by $\text{pf}(Z) \stackrel{\text{def}}{=} \{\mathbf{x} \in Z : \nexists \mathbf{x}' \in Z : \mathbf{x}' \prec \mathbf{x}\}$; this operation uniquely partitions $\langle Z \rangle$ into basic cylinders over $\text{pf}(Z)$. We say that Z is **prefix-free** if $\text{pf}(Z) = Z$. Since $\text{pf}(Z)$ is prefix-free, the basic cylinders $\{\langle \mathbf{x} \rangle \mid \mathbf{x} \in \text{pf}(Z)\}$ are pairwise disjoint, and $\langle Z \rangle = \bigsqcup_{\mathbf{x} \in \text{pf}(Z)} \langle \mathbf{x} \rangle$.

Transducers. A **transducer** is a state-machine that encodes string-to-string relations $f \subseteq \mathcal{X}^* \times \mathcal{Y}^*$. When we express a relationship defined by f as a transducer, we expose the computational structure needed to develop efficient algorithms. Formally, a **finite-state transducer**⁵ (**FST**) \mathfrak{f} is a tuple $(S, \mathcal{X}, \mathcal{Y}, I, F, T)$ where S is a finite set of **states** and \mathcal{X} and \mathcal{Y} are alphabets of **input** and **output** symbols, respectively. The sets $I, F \subseteq S$ are the **initial** and **accepting** states. $T \subseteq S \times (\mathcal{X} \cup \{\varepsilon\}) \times (\mathcal{Y} \cup \{\varepsilon\}) \times S$ is a set of **transitions**. We render transitions $(s, \mathbf{x}, y, s') \in T$ as $s \xrightarrow{\mathbf{x}:y} s'$; we say the transition **scans** \mathbf{x} and **emits** y . We write $T(s)$ for the set of outgoing transitions from state s , and $T(s, \mathbf{x})$ for those that scan \mathbf{x} .⁶ The transducer \mathfrak{f} defines a set of **paths** Π . Each

⁴§A provides a notation glossary.

⁵We refer to Pin (2021, Ch. 2 & 3) for a detailed treatment of transducers.

⁶I.e., $T(s'') \stackrel{\text{def}}{=} \{(s \xrightarrow{\mathbf{x}:y} s') \in T : s = s''\}$, and $T(s'', \mathbf{x}'') \stackrel{\text{def}}{=} \{(s \xrightarrow{\mathbf{x}:y} s') \in T : s = s'', \mathbf{x} = \mathbf{x}''\}$.

path $\pi \in \Pi$ is a sequence of transitions of the form $s_0 \xrightarrow{x_1:y_1} s_1 \xrightarrow{x_2:y_2} s_2 \cdots s_{N-1} \xrightarrow{x_N:y_N} s_N$. We call π an **accepting path** if $s_0 \in I$ and $s_N \in F$. The **relation defined** by f is given by $[[f]] \stackrel{\text{def}}{=} \{(\mathbf{x}, \mathbf{y}) \mid s_0 \xrightarrow{x_1:y_1} s_1 \cdots s_{N-1} \xrightarrow{x_N:y_N} s_N \in \Pi: s_0 \in I, s_N \in F\}$, i.e., each accepting path contributes (not necessarily uniquely) a pair of scanned and emitted strings. When every transition of a transducer scans and emits the same symbol ($x = y$), the machine acts as a **finite-state automaton (acceptor)** that recognizes a **language** $L \subseteq \mathcal{X}^*$ —the set of strings admitted by at least one accepting path. Such a machine is a **nondeterministic finite automaton (NFA)** in general; it is a **deterministic finite automaton (DFA)** if it has a single initial state, no ε -transitions, and at most one transition per state and input symbol. Every NFA can be converted to an equivalent DFA by **determinization** (Rabin & Scott, 1959). For completeness, §B provides additional background.

3 TRANSDUCED LANGUAGE MODELS

A **transduced language model** $p_{\mathcal{Y}}$ arises from applying a string-to-string **transformation** $f: \mathcal{X}^* \rightarrow \mathcal{Y}^*$, encoded by a transducer f , to a string drawn from a **source language model** $p_{\mathcal{X}}$. Formally, if $X \sim p_{\mathcal{X}}$, then $f(X)$ has the following probability mass function:

$$p_{\mathcal{Y}}(\mathbf{y}) \stackrel{\text{def}}{=} \Pr_{X \sim p_{\mathcal{X}}} [\mathbf{y} = f(X)] = \sum_{\mathbf{x} \in f^{-1}(\mathbf{y})} p_{\mathcal{X}}(\mathbf{x}) \quad (2)$$

where $f^{-1}(\mathbf{y})$ is the **preimage** of \mathbf{y} , $f^{-1}(\mathbf{y}) \stackrel{\text{def}}{=} \{\mathbf{x} \in \mathcal{X}^* : \mathbf{y} = f(\mathbf{x})\}$. Put differently, in Eq. (2), we sum over the strings \mathbf{x} such that $f(\mathbf{x}) = \mathbf{y}$. Unfortunately, evaluating $p_{\mathcal{Y}}(\mathbf{y})$ exactly using Eq. (2) is generally infeasible (since the preimage $f^{-1}(\mathbf{y})$ can be very large), even though exact sampling from $p_{\mathcal{Y}}$ is efficient (by sampling $\mathbf{x} \sim p_{\mathcal{X}}$ and applying f). Like all language models, a transduced language model $p_{\mathcal{Y}}$ has prefix and conditional prefix probability functions; its prefix probability is

$$\vec{p}_{\mathcal{Y}}(\mathbf{y}) = \Pr_{X \sim p_{\mathcal{X}}} [\mathbf{y} \preceq f(X)] = \sum_{\mathbf{x} \in \mathcal{P}(\mathbf{y})} p_{\mathcal{X}}(\mathbf{x}) \quad (3)$$

where $\mathcal{P}(\mathbf{y})$ is the **precover** of \mathbf{y} , with respect to f , defined as $\mathcal{P}(\mathbf{y}) \stackrel{\text{def}}{=} \{\mathbf{x} \in \mathcal{X}^* : \mathbf{y} \preceq f(\mathbf{x})\}$.⁷

Prefix probabilities yield a conditional factorization of string probability (see §2), enabling efficient left-to-right autoregressive generation. We develop a method in §4 that allows us to compute the sum in Eq. (3) in *finite* time for a general class of mappings, such as those mentioned in the introduction (i.e., normalizing text, inserting orthographic word boundaries, or converting DNA to amino-acid sequences). In §5, we present algorithms to compute these quantities.

4 DECOMPOSING THE PRECOVER

In §3, we saw that if we can sum over the precover of \mathbf{y} , we can calculate $\vec{p}_{\mathcal{Y}}(\mathbf{y})$ (Eq. (3)), unlocking an autoregressive interface to the transduced language model. The following two examples illustrate how we can often compute this infinite sum by exploiting structural properties of the transducer.

Example 1. *The transducer below lowercases a string. For the target string \mathbf{ab} , the precover is the infinite set $\mathcal{P}(\mathbf{ab}) = \langle \{\mathbf{AB}, \mathbf{Ab}, \mathbf{aB}, \mathbf{ab}\} \rangle$. Given a model $p_{\mathcal{X}}$ over the input language, the derivation on the right (4a–4c) applies Eq. (3) to express $\vec{p}_{\mathcal{Y}}(\mathbf{ab})$ as a sum of four source-language prefix probabilities:*

$$\vec{p}_{\mathcal{Y}}(\mathbf{ab}) = \sum_{\mathbf{x} \in \mathcal{P}(\mathbf{ab})} p_{\mathcal{X}}(\mathbf{x}) \quad (4a)$$

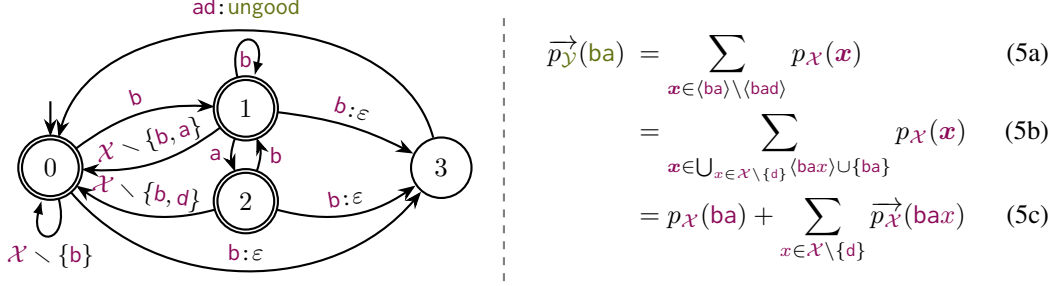
$$= \sum_{\mathbf{x}' \in \{\mathbf{AB}, \mathbf{Ab}, \mathbf{aB}, \mathbf{ab}\}} \sum_{\mathbf{x} \in \langle \mathbf{x}' \rangle} p_{\mathcal{X}}(\mathbf{x}) \quad (4b)$$

$$= \vec{p}_{\mathcal{X}}(\mathbf{AB}) + \vec{p}_{\mathcal{X}}(\mathbf{Ab}) + \vec{p}_{\mathcal{X}}(\mathbf{aB}) + \vec{p}_{\mathcal{X}}(\mathbf{ab}) \quad (4c)$$

In Example 1, each input symbol maps to exactly one output symbol, so the precover decomposes neatly into cylinders. The next example shows what happens when some source strings cover the target string, while their extensions do not.

⁷Note that the precover depends on f ; we suppress this dependency when it is clear from context.

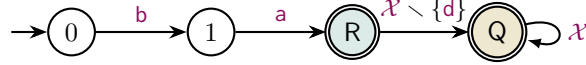
Example 2. The transducer below implements a newspeak⁸ rewrite rule: the word **bad** is replaced by **ungood**. For the target string **ba**, the precover does not decompose neatly into cylinders: since **bad** does not map to a string prefixed by **ba**, the cylinder $\langle \text{bad} \rangle$ does not contribute to $\vec{p}_{\mathcal{Y}}(\text{ba})$. The derivation on the right (5–5c) shows how this cylinder is excluded.⁹



Because $\text{bad} \in \langle \text{ba} \rangle$ but $\text{bad} \notin \mathcal{P}(\text{ba})$, the precover cannot be decomposed entirely into cylinders. Instead, we decompose it into two disjoint parts: a maximal cylindrical subset and its complement in the precover. The *quotient* collects the shortest element of each cylinder; the complement is the *remainder*. The final step (5c) illustrates a **computational shortcut**; for any \mathbf{y} we can decompose $\vec{p}_{\mathcal{Y}}(\mathbf{y})$:

$$\vec{p}_{\mathcal{Y}}(\mathbf{y}) = \underbrace{\sum_{\mathbf{x} \in \mathcal{Q}(\mathbf{y})} \vec{p}_{\mathcal{X}}(\mathbf{x})}_{\text{Quotient}} + \underbrace{\sum_{\mathbf{x} \in \mathcal{R}(\mathbf{y})} p_{\mathcal{X}}(\mathbf{x})}_{\text{Remainder}} \quad (6)$$

The precover can also be represented as an FSA, as shown below for $\mathcal{P}(\text{ba})$. The single string accepted at R (teal node) marks the remainder element **ba** while the state Q (yellow node) accepts $\langle \text{ba} \cdot (\mathcal{X} \setminus \{d\}) \rangle$ and marks the cylinder over the quotient.



We now formalize the remainder, quotient, and decomposition for any string-to-string function f .

The prefix decomposition of the precover. Let $f: \mathcal{X}^* \rightarrow \mathcal{Y}^*$ be a map. For each $\mathbf{y} \in \mathcal{Y}^*$, define $\mathcal{C}(\mathbf{y}) \stackrel{\text{def}}{=} \{\mathbf{x} \in \mathcal{X}^* : \langle \mathbf{x} \rangle \subseteq \mathcal{P}(\mathbf{y})\}$; this set is a cylinder—if $\mathbf{x} \in \mathcal{C}(\mathbf{y})$ then every extension of \mathbf{x} also belongs to $\mathcal{C}(\mathbf{y})$ —making it the largest cylinder contained in $\mathcal{P}(\mathbf{y})$. We define the **quotient** and **remainder** of \mathbf{y} with respect to f as

$$\mathcal{Q}(\mathbf{y}) \stackrel{\text{def}}{=} \text{pf}(\mathcal{C}(\mathbf{y})) \quad \text{and} \quad \mathcal{R}(\mathbf{y}) \stackrel{\text{def}}{=} \mathcal{P}(\mathbf{y}) \setminus \mathcal{C}(\mathbf{y}) \quad (7)$$

We call the pair $(\mathcal{Q}(\mathbf{y}), \mathcal{R}(\mathbf{y}))$ the **optimal prefix decomposition** of $\mathcal{P}(\mathbf{y})$, characterized by three conditions: (i) $\mathcal{Q}(\mathbf{y})$ is *prefix-free*, (ii) $\mathcal{P}(\mathbf{y}) = \langle \mathcal{Q}(\mathbf{y}) \rangle \sqcup \langle \mathcal{R}(\mathbf{y}) \rangle$ (*validity*), and (iii) $\langle \mathcal{Q}(\mathbf{y}) \rangle = \mathcal{C}(\mathbf{y})$ (*maximality*)— $\mathcal{Q}(\mathbf{y})$ identifies the largest cylinder in $\mathcal{P}(\mathbf{y})$. This decomposition (indeed, any valid one) lets us compute prefix probabilities using the shortcut:

$$\vec{p}_{\mathcal{Y}}(\mathbf{y}) = \sum_{\mathbf{x} \in \mathcal{P}(\mathbf{y})} p_{\mathcal{X}}(\mathbf{x}) = \sum_{\mathbf{x} \in \mathcal{C}(\mathbf{y}) \sqcup \mathcal{R}(\mathbf{y})} p_{\mathcal{X}}(\mathbf{x}) = \sum_{\substack{\mathbf{x} \in \mathcal{Q}(\mathbf{y}) \\ \mathbf{x}' \in \mathcal{X}^*}} p_{\mathcal{X}}(\mathbf{x}\mathbf{x}') + \sum_{\mathbf{x} \in \mathcal{R}(\mathbf{y})} p_{\mathcal{X}}(\mathbf{x}) = \sum_{\mathbf{x} \in \mathcal{Q}(\mathbf{y})} \vec{p}_{\mathcal{X}}(\mathbf{x}) + \sum_{\mathbf{x} \in \mathcal{R}(\mathbf{y})} p_{\mathcal{X}}(\mathbf{x}) \quad (8a)$$

§5 provides an algorithm for computing the prefix decomposition; §6 identifies when it is finite.

5 ALGORITHMS

We now present an algorithm for computing prefix decompositions by exploiting the explicit structure of a transducer that encodes the function. Combined with the computational shortcut (Eq. (6)), this gives an autoregressive interface to transduced language models. We first describe the algorithm abstractly, then instantiate its checks using a transducer, and finally discuss optimizations.

⁸*Newspeak* is the controlled language from Orwell’s *1984* (Orwell, 1949); the example $\text{bad} \rightarrow \text{ungood}$ is canonical. A complete Newspeak transducer is left as an exercise for the Party.

⁹Arcs labeled by a single symbol are *copy transitions*, e.g., \mathbf{b} is shorthand for $\mathbf{b} : \mathbf{b}$; a set label such as $\mathcal{X} \setminus \{\mathbf{b}\}$ denotes one copy-transition arc per symbol in the set.

Fig. 2 gives the decomposition algorithm (`decompose`), which maintains a queue of candidate source strings and explores them by breadth-first search (BFS), optionally pruning low-probability candidates at each step (described below).¹⁰ Each dequeued string x undergoes three checks, defined in terms of the precover $\mathcal{P}(y)$:

1. *Cylinder*: `is_cylinder`(x, y) $\iff \langle x \rangle \subseteq \mathcal{P}(y)$, i.e., every extension of x covers y . x is added to the quotient set Q and not explored further (line 12).
2. *Member*: `is_member`(x, y) $\iff x \in \mathcal{P}(y)$, i.e., x itself covers y . When `is_cylinder` is false but `is_member` is true, x is added to the remainder set R ; its extensions are still explored (line 15).
3. *Live*: `is_live`(x, y) $\iff \exists x'' \in \mathcal{X}^* : xx'' \in \mathcal{P}(y)$, i.e., some extension of x belongs to the precover. Only live extensions are enqueued (line 18).

Because strings are processed shortest-first, if any prefix of the current string had already entered the quotient, the current string would never have been enqueued. Once the queue is exhausted, the algorithm returns the prefix decomposition. We instantiate these checks concretely in §5.1.

Theorem 5.1 (Correctness of `decompose`). *If $\mathcal{P}(y)$ admits a finite decomposition and the three checks exactly implement the conditions above with no pruning, then `decompose`(y) terminates and its output $\langle Q, R \rangle$ is the optimal prefix decomposition (Eq. (7)).*

Proof. We verify the three conditions of the optimal prefix decomposition (Eq. (7)).

1. *Prefix-freeness* (Q is prefix-free): When `is_cylinder` succeeds for x (line 12), the `continue` (line 14) skips the extension loop, so no xx' is enqueued. Since strings enter the queue only as single-symbol extensions of dequeued strings, no extension of x is ever enqueued or dequeued, and thus no two elements of Q share a prefix.
2. *Validity* ($\mathcal{P}(y) = \langle Q \rangle \sqcup R$): Let $x \in \mathcal{P}(y)$; we first show that $x \in \langle Q \rangle \sqcup R$. We show by induction on prefix length that either a prefix of x enters Q or x itself is dequeued and added to Q or R . The base case holds: ε is enqueued. If $x_{<k}$ is dequeued and not placed in Q , then $x_{<k+1}$ is enqueued by the extension loop: since $x_{<k+1} \preceq x$ and $x \in \mathcal{P}(y)$, we have `is_live`($x_{<k+1}, y$) (line 18). By induction, either some prefix $x_{<j}$ enters Q —giving $x \in \langle x_{<j} \rangle \subseteq \langle Q \rangle$ —or x itself is dequeued, the cylinder check fails, and $x \in \mathcal{P}(y)$ gives $x \in R$ via `is_member` (line 15). The reverse direction is clear since elements of Q pass the exact `is_cylinder` check, so $\langle Q \rangle \subseteq \mathcal{P}(y)$. Similarly, elements of R pass `is_member`, so $R \subseteq \mathcal{P}(y)$. What remains is to show that $\langle Q \rangle$ and R are disjoint. If $x \in R$, then x was dequeued and `is_cylinder` failed, so $x \notin Q$. No proper prefix of x is in Q either—otherwise x would never have been enqueued (prefix-freeness). Hence $x \notin \langle Q \rangle$.
3. *Maximality* ($\langle Q \rangle = \mathcal{C}(y)$): shortest-first processing ensures no proper prefix of a quotient element satisfies `is_cylinder` (line 12), so Q is the *minimal* prefix-free set of cylinders. Together with the exact cylinder check, the earliest qualifying prefix is always found, as required by Eq. (7). It remains to show $\mathcal{C}(y) \subseteq \langle Q \rangle$. By validity, $\mathcal{P}(y) = \langle Q \rangle \sqcup R$. Every element of R fails `is_cylinder`, so $R \cap \mathcal{C}(y) = \emptyset$. Hence $\mathcal{C}(y) \subseteq \langle Q \rangle$.

Termination: `is_live` (line 18) ensures only viable extensions are enqueued; finiteness of the decomposition guarantees the queue empties. ■

Conservative checks and suboptimality. If the checks used by `decompose` are conservative approximations, the algorithm may produce *suboptimal* decompositions—valid but with a smaller quotient than the optimal one. A conservative liveness check (false positives) enqueues unnecessary extensions but does not affect classification: every dequeued string is still correctly classified by `is_cylinder` and `is_member`, so the result remains optimal. A conservative cylinder check (false negatives) may fail to recognize some quotient elements, placing them in R instead. The decomposition

```

1 def decompose(y): # memoize
2   N ← |y|
3   if N = 0:
4     q ← QUEUE({ε})
5   else:
6     (Q', R') ← decompose(y_{<N})
7     q ← QUEUE(Q' ∪ R')
8   (Q, R) ← (∅, ∅)
9   while |q| > 0:
10    q' ← ∅
11    for x ∈ q:
12      if is_cylinder(x, y):
13        Q.add(x)
14        continue
15      if is_member(x, y):
16        R.add(x)
17      for x' ∈ X:
18        if is_live(xx', y):
19          q'.add(xx')
20    q ← prune(q')
21  return (Q, R)

```

Figure 2: Decomposition algorithm.

¹⁰For efficiency, `decompose` should be memoized. For $|y| > 0$, the recursive call `decompose`($y_{<N}$) seeds the queue with the previous decomposition $Q' \cup R'$ rather than enumerating from ε .

remains valid, but because a successful cylinder check terminates exploration of that subtree (line 14), missing a cylinder means the BFS continues exploring extensions that would otherwise have been cut off, potentially inflating the remainder and increasing the computation. By contrast, the membership check must be exact to preserve validity.

Approximation via pruning. When the prefix decomposition becomes large, exhaustively enumerating and scoring can become infeasible. In these cases, we use a pruning strategy (`prune`) that sorts candidates by prefix probability and removes those whose cumulative probability mass falls below a specified threshold τ . This discards low-probability candidates to keep decomposition tractable. Since pruning only removes candidates from the queue, every element found is correct— $\langle Q \rangle \sqcup R \subseteq \mathcal{P}(y)$ —but the decomposition is no longer valid in general (coverage may be incomplete), so the computed prefix probability is a lower bound on the true value. Our strategy is detailed in §C.3.

5.1 GETTING STARTED: INSTANTIATING THE CHECKS WITH THE PRECOVER MACHINE

We now show how to instantiate the three checks (Fig. 2) using a finite-state transducer. This serves as a pedagogical introduction; §C describes a more detailed, but faster algorithm.

We represent the transformation f with a transducer f (see §2 and §B). Given a target prefix y , $\text{proj}_x(f \circ y\mathcal{Y}^*)$ is an NFA that accepts exactly $\mathcal{P}(y)$. To enable the efficient state-based checks below, we determinize and trim this NFA to obtain a DFA: $P_y \stackrel{\text{def}}{=} \text{trim}(\text{determinize}(\text{proj}_x(f \circ y\mathcal{Y}^*)))$. Let S_y , I_y , F_y , and T_y denote the components of P_y . Since P_y is deterministic, scanning a source string $x = x_1 \cdots x_N$ yields a unique state, which we denote by $\text{run}_y(x)$. We now describe how to implement the three checks using P_y (pseudocode in Fig. 3).

- *Cylinder:* We need to check whether $\langle x \rangle \subseteq \mathcal{P}(y)$ to decide if $x \in Q(y)$. Let $S = \text{run}_y(x)$ be the unique state reached after scanning x . Since P_y is deterministic, $\langle x \rangle \subseteq \mathcal{P}(y)$ if and only if S is **universal**: $\llbracket P_y[S] \rrbracket = \mathcal{X}^*$, meaning every continuation of x is accepted. The `is_cylinder` check (Fig. 3) tests universality via breadth-first search (BFS) from S .
- *Member:* When the `is_cylinder` check fails for x with $S = \text{run}_y(x)$, we need to determine whether the scanned string x is in $\mathcal{R}(y)$. Here it suffices to check if $S \in F_y$, i.e., if P_y accepts x .
- *Live:* We construct P_y as a *trimmed* automaton accepting x where $y \preceq f(x)$.¹¹ Trimming ensures that every reachable state lies on some accepting path, so liveness reduces to $\text{run}_y(x) \neq \emptyset$.

Although `decompose` is written in terms of source strings, each check internally computes the state $S = \text{run}_y(x)$ reached by scanning x in the deterministic P_y , and reduces to a state property.

5.2 OPTIMIZATIONS

The algorithm above is correct but impractical for large transducers. In §C, we describe several optimizations; we summarize the key ideas here.

Lazy determinization. Eagerly determinizing P_y is often computationally expensive. Instead, we track *frontiers*: sets of transducer states reachable after scanning a source prefix, paired with the output emitted so far. Frontiers lazily perform the subset construction (the standard NFA-to-DFA conversion; Rabin & Scott, 1959) and the composition with $y\mathcal{Y}^*$ simultaneously, avoiding both eager determinization and eager composition. The three checks—cylinder, member, and liveness—are now defined in terms of the frontier rather than a single DFA state (§C.2).

Incremental next-symbol decomposition. To efficiently compute $\vec{p}_y(y' | y)$ for all $y' \in \mathcal{Y}$, we introduce `decompose_next` (§C.4), which derives the decomposition of each extension yy' from the decomposition of y . It operates in a single BFS pass that handles each $y' \in \mathcal{Y}$ simultaneously.

Decomposition shortcuts. Many structural properties of the decomposition allow the BFS to skip work: non-cylinder monotonicity (Prop. C.3), cylinder uniqueness (Prop. C.4), input-projection universality (§C.6), combined universality (Prop. C.5), and an all-universal fast path (Fig. 14).

Lazier enumeration. Rather than explicitly composing the transducer with the copy transducer $y\mathcal{Y}^*$, the frontier-based algorithms track output buffers directly, performing the composition lazily and avoiding the materialization cost. Additionally, we precompute states whose input projection

¹¹This can also be expressed as $\mathcal{P}(y) = f^{-1}(y\mathcal{Y}^*) = \llbracket \text{proj}_x(f \circ y\mathcal{Y}^*) \rrbracket$.

```

22 def stepy(s, x):
23     return Ty(s, x) # deterministic
24 def runy(x1 ... xN):
25     if N = 0: return ly # unique
26     return stepy(runy(x<N), xN)
27 def is_member(x, y):
28     return runy(x) ∈ Fy
29 def is_live(x, y):
30     # not in failure state
31     return runy(x) ≠ ∅
32 def is_cylinder(x, y):
33     # Run BFS to find a counterexample:
34     # a nonaccepting or incomplete state
35     S ← runy(x); V ← {S}; q ← QUEUE({S})
36     while q:
37         S' ← q.pop()
38         if S' ∉ Fy: return False
39         for x' ∈ X:
40             S' ← stepy(S, x')
41             if S' = ∅: return False
42             if S' ∉ V: q.add(S'); V.add(S')
43     return True # No counterexamples

```

Figure 3: State-based instantiation of the checks from Fig. 2 on the precover DFA P_y . Helper functions `step` and `run` advance through the DFA; `is_member` and `is_live` are single-state lookups; `is_cylinder` performs a BFS to verify universality.

accepts all of \mathcal{X}^* (§C.6). When a frontier reaches such a state with a buffer that already covers y , the cylinder check succeeds immediately, bypassing the expensive check.

Label pushing. As a standard preprocessing step (see, e.g., Oncina et al., 1993; Mohri, 2003; 2009), we push output labels toward the initial state of f : when every path through a state s emits output beginning with y , that y is shifted to the incoming arc so it is produced one step earlier. This ensures that output is committed as early as possible, speeding up the frontier-based cylinder check.

6 SUFFICIENT CONDITIONS FOR FINITE DECOMPOSITIONS

The decomposition algorithms in §5 enumerate strings by breadth-first search. For the enumeration to terminate, the quotient $Q(y)$ and remainder $R(y)$ need to be finite for a given target string $y \in \mathcal{Y}^*$. Previous work (Vieira et al., 2025a, Props 1 and 3; also in §D.2) showed that strict-prefix monotonicity guarantees an empty remainder and a bounded quotient. This ensures that $\overline{p}_y^{\rightarrow}(y)$ is computable.

For functions that are not strict-prefix monotone, however, the decomposition may be infinite. In this section, we give additional conditions for finite decomposition. We first give function-level properties that guarantee an empty remainder and bounded quotient, and then transducer-level conditions for when the quotient and remainder are finite.

We say that a map $f: \mathcal{X}^* \rightarrow \mathcal{Y}^*$ is **strict-prefix monotone** if and only if $x \prec x' \implies f(x) \prec f(x')$. Similarly f is **prefix monotone** if and only if $x \preceq x' \implies f(x) \preceq f(x')$. We say that a map f is **prefix-continuous** if, for every $y \in \mathcal{Y}^*$, the set $\mathcal{P}(y)$ is cylindrical, i.e., $R(y) = \emptyset$. The following proposition shows that prefix monotonicity implies prefix-continuity:

Proposition 6.1. *The following are equivalent: (i) f is prefix monotone (ii) $f(\langle x \rangle) \subseteq \langle f(x) \rangle$ for all $x \in \mathcal{X}^*$ (iii) $\mathcal{P}(f(x)) = \mathcal{C}(f(x))$ for all $x \in \mathcal{X}^*$ (iv) f is prefix-continuous. [Proof: §D.1]*

Proposition 6.1 shows how we generalize Vieira et al. (2025a). First, by relaxing strict-prefix monotonicity to prefix monotonicity, we support multi-symbol lookahead in the quotient. Ex. (6) is an example of this: it is prefix monotone and requires two-symbol lookahead before committing to an output. Second, by introducing the remainder, we can handle functions that are not prefix monotone, meaning that there can be source strings that cover the target, but not all of their extensions do (e.g., Example 2).

Lemma 6.1 gives sufficient conditions on a transducer that guarantee a finite decomposition for every target string, even when the underlying function is not prefix monotone. The key notion is *safety*: a state is safe if it is IP-universal, has **finite closure** (i.e., $\|\llbracket f_{[s]} \rrbracket\| < \infty$), or all its successors are safe.

Lemma 6.1. *Let $f: \mathcal{X}^* \rightarrow \mathcal{Y}^*$ be a function realized by a transducer f . The decomposition $(Q(y), R(y))$ is finite for every $y \in \mathcal{Y}^*$ if:*

- (i) No ε -output cycles: f contains no cycle in which every arc outputs ε .
- (ii) Safety: Every state of f is **safe**, defined inductively as the smallest set such that s is safe if: (a) s is IP-universal; (b) $\|\llbracket f_{[s]} \rrbracket\| < \infty$ (finite closure); or (c) for all transitions $s \xrightarrow{x:y} s'$, s' is safe.

Proof: See §D.3.

The conditions in Lemma 6.1 guarantee exact computation. In particular, these are satisfied by the transducers introduced in the experiments section (§7): the token-to-byte transducer f_α and the DNA-to-amino-acid transducer f_{dna2aa} , whose quotients are finite and remainders empty, but not by the PTB transducer f_{ptb} , whose quotients are infinite.

The finiteness of decomposition is a property of the function f , not of any particular transducer encoding it. The lemma’s conditions are sufficient but not necessary: safety tests each state individually, whereas the decomposition algorithm tests universality of frontiers (sets of state/string pairs), which can succeed even when individual states are not safe. There are many cases where the prefix decomposition is infinite, or otherwise prohibitively large; in these cases, we let the source language model determine which prefix decomposition members carry the most significant mass and prune others (§5). This lets us greedily approximate the probabilities of the transduced language model by enumerating a high-mass subset of the decomposition.

7 EXPERIMENTS

We now consider three examples of transduced language models. For each use case, we follow the approach in Vieira et al. (2025a) and measure the Jensen–Shannon divergence (JSD) between the distributions obtained using the approximation via probability mass pruning mentioned in §C.3 and a reference distribution we get by choosing a pruning threshold τ . We also report cross-entropy loss (§G.4), reflecting the cost of scoring specific sequences rather than full distributions. Experiments use GPT-2 Large (p_{gpt2}) (Radford et al., 2019), LLaMA 3.2-1B (p_{llama1B}) and LLaMA 3.1-8B (p_{llama8B}) (Team, 2024), Phi-4 (p_{phi4}) (14B; Abdin et al., 2024), and a DNA model trained on the human genome (p_{dna}).¹² For the experiments in §7, we use `genlm-bytes`¹³ to convert token-level models to byte-level models. See §F for details on the training and evaluation setup, and §F.5 for transducer details.

Recall that a transduced language model p_Y is characterized by a source model p_X and a transducer f encoding some function f (§3). To make this dependency explicit, we write $p_X \circ f \stackrel{\text{def}}{=} p_Y$ and refer to the operation as composing. All experiments compute next-symbol distributions using the more efficient algorithm (§C.8), which reuses cached decompositions across target positions and exploits structural shortcuts (§C.5). Probability mass pruning (§C.3) retains the most likely decomposition elements such that the discarded probability mass does not exceed the pruning threshold.

Our experiments span the prefix-monotonicity spectrum (Proposition 6.1): token-to-byte (T2B) is strict-prefix monotone, DNA-to-amino-acid is prefix monotone with multi-symbol lookahead, and PTB tokenization is not prefix monotone.

From tokens to bytes. We revisit the algorithm for converting models from tokens to bytes, as in Vieira et al. (2025a). This transformation can be realized by a simple transducer f_α , with $\mathcal{O}(|\mathcal{X}|)$ states. Specifically, the transducer contains a chain for each token present in the input vocabulary \mathcal{X} . This structure allows us to use a shortcut (see Fig. 14) that resolves each quotient element with a single LM call. An example of such a machine is given in Fig. 4. We benchmark the algorithms in §5 using the transducers $p_{\text{gpt2}} \circ f_\alpha$, $p_{\text{llama1B}} \circ f_\alpha$, $p_{\text{llama8B}} \circ f_\alpha$, and $p_{\text{phi4}} \circ f_\alpha$ on the first ten paragraphs of the `wikitext-2-raw-v1` dataset (Merity et al., 2017) (corresponding to the first 7684 bytes). As shown in Fig. 6 (left) and Tab. 8 in §G, lower pruning thresholds (τ) give lower JSD values against a reference distribution ($\tau = 1e-5$) at the cost of throughput, measured in bytes per second. We confirm that the JSD values are similar to those achieved by Vieira et al. (2025a) in §G.1, Tab. 6. Their method is limited to strict-prefix monotone transformations, which enables a specialized trie-based algorithm that achieves higher throughput while maintaining comparable accuracy.

From tokens to orthographic word boundaries. The next transformation we consider is converting language models over tokens to language models over *orthographic* words. The precise definition of what constitutes such a word varies depending on the application. In some settings, contractions such as “wouldn’t” should be treated as a single unit. In other settings, however, a more natural segmentation would be “would” and “n’t”. We can accommodate any FST-based definition. Linguistic tokenizers, such as the PTB tokenizer (Marcus et al., 1993), use contextual information to

¹²Links to models: <https://huggingface.co/openai-community/gpt2-large>, <https://huggingface.co/meta-llama/Llama-3.2-1B>, <https://huggingface.co/meta-llama/Llama-3.1-8B>, <https://huggingface.co/microsoft/phi-4> and <https://huggingface.co/vesteinn/gpt2-dna>.

¹³`genlm-bytes` is an implementation of Vieira et al. (2025a); see <https://github.com/genlm/genlm-bytes>.

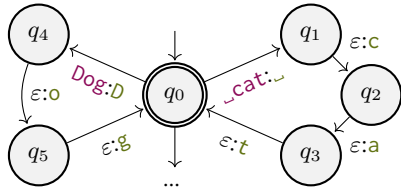


Figure 4: An FST for converting a token model into a character model. Paths for `_cat` and `Dog`.

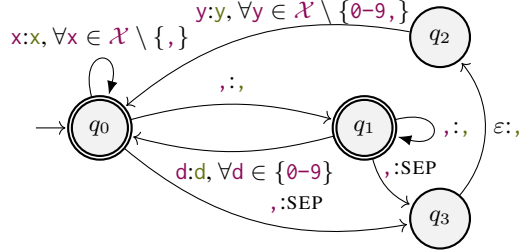


Figure 5: An FST that inserts a separator (SEP) before commas followed by non-digit characters.

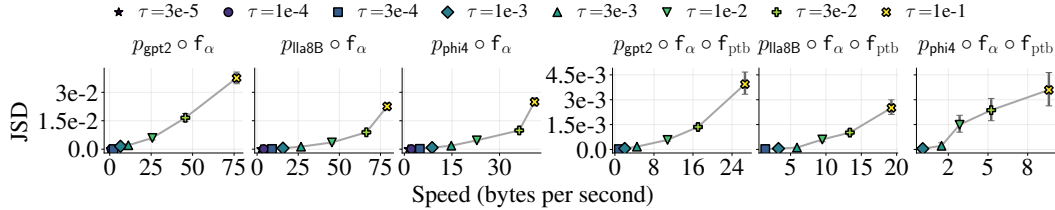


Figure 6: Average Jensen–Shannon divergence (JSD) and throughput (bytes/sec) across thresholds τ . Left: $p_{\mathcal{X}} \circ f_{\alpha}$ (reference: $\tau = 1e-5$). Right: $p_{\mathcal{X}} \circ f_{\alpha} \circ f_{\text{ptb}}$ (reference: $\tau = 1e-4$; $3e-4$ for p_{phi4}). Bars show 95% bootstrapped CIs. At the tightest thresholds, large decomposition sizes prevent some models from completing all paragraphs; see §G.2.

segment raw English text into linguistically meaningful units suitable for downstream NLP tasks. We construct an FST that encodes the PTB tokenizer, f_{ptb} ; details are in §F.5. An example of a rule in the transducer is given in Fig. 5, which inserts `SEP` before a comma if a digit does not follow. Composing $p_{\mathcal{X}} \circ f_{\alpha} \circ f_{\text{ptb}}$ yields a transduced language model, mapping subword tokens to PTB tokens. To reduce the state count of the composed FST and improve efficiency, we represent $p_{\mathcal{X}} \circ f_{\alpha}$ using the byte-transformed models from `genlm-bytes`.¹⁴ In Fig. 6 (right), we plot the average JSD against the throughput for different thresholds τ , using the same dataset as in §7. The reference distribution uses $\tau = 1e-4$ ($3e-4$ for p_{phi4}). As with the experiments in §7, we observe lower JSD at lower thresholds, albeit at the cost of throughput. For experiments using higher thresholds, see §G, Tab. 9.

Converting DNA models to models over amino acids. We use a transducer that converts sequences of the four DNA nucleotides to sequences over the twenty-two amino acids.¹⁵ Let $p_{\text{dna}} \circ f_{\text{dna2aa}}$ denote the transduced model that converts DNA nucleotides into amino acids. To evaluate our approach, we sample 65 human proteins.¹⁶ In Tab. 10, we show the average JSD and throughput for different thresholds τ . Note that this transducer is particularly challenging since the set of candidates in the decomposed precover grows exponentially with the sequence length. To mitigate the combinatorial blow-up, we cap the candidate-set and report throughput and JSD while varying the cap.

8 CONCLUSION

We have introduced a general framework for transforming language models using transducers. Empirically, we have shown that our beam-summing approximation efficiently transduces token-based LLMs into models over bytes, words, and even amino acids, without requiring retraining. Our theoretical analysis characterizes the conditions under which such mappings can be performed exactly. The proposed approach is an effective way to repurpose existing language models and to accurately compute probabilities for any unit and transformation defined by a transducer. By reducing the problem to transducer decomposition, the framework opens the door to leveraging future advances in finite-state methods for language model adaptation. (Future work and limitations are discussed in §J.)

¹⁴<https://github.com/genlm/genlm-bytes> that implements Vieira et al.’s (2025a) method.

¹⁵I.e., $\mathcal{X} = \{A, C, G, T\}$ and $\mathcal{Y} = \{A, R, N, D, C, Q, E, G, H, I, L, K, M, F, P, S, T, V, W, Y, B, Z, *\}$.

¹⁶Sampled from <https://www.uniprot.org/uniprotkb?query=Human>, see Tab. 1 for the accession numbers.

ACKNOWLEDGMENTS

The authors thank Ben LeBrun, Brian DuSell, Clemente Pasti, Juan Luis Gastaldi, Mario Giulianelli, and Yahya Emara for useful feedback and discussions that greatly improved this work. Vésteinn Snæbjarnarson is supported by the Pioneer Centre for AI, DNRG grant number P1.

REFERENCES

- Marah Abidin, Jyoti Aneja, Harkirat Behl, Sébastien Bubeck, Ronen Eldan, Suriya Gunasekar, Michael Harrison, Russell J. Hewett, Mojan Javaheripi, Piero Kauffmann, James R. Lee, Yin Tat Lee, Yuanzhi Li, Weishung Liu, Caio C. T. Mendes, Anh Nguyen, Eric Price, Gustavo de Rosa, Olli Saarikivi, Adil Salim, Shital Shah, Xin Wang, Rachel Ward, Yue Wu, Dingli Yu, Cyril Zhang, and Yi Zhang. Phi-4 technical report, 2024. URL <https://arxiv.org/abs/2412.08905>.
- Cyril Allauzen, Bill Byrne, Adria de Gispert, Gonzalo Iglesias, and Michael Riley. Pushdown Automata in Statistical Machine Translation. *Computational Linguistics*, 2014. URL <https://aclanthology.org/J14-3008/>.
- Lisa Beinborn and Yuval Pinter. Analyzing Cognitive Plausibility of Subword Tokenization. In *Proceedings of the Conference on Empirical Methods in Natural Language Processing*, 2023. URL <https://aclanthology.org/2023.emnlp-main.272/>.
- Martin Berglund and Brink van der Merwe. Formalizing BPE tokenization. In *Proceedings of the International Workshop on Non-Classical Models of Automata and Applications*, volume 388, 2023. URL <https://cgi.cse.unsw.edu.au/~eptcs/paper.cgi?NCMA2023.4.pdf>.
- Martin Berglund, Willeke Martens, and Brink van der Merwe. Constructing a BPE Tokenization DFA. In *Implementation and Application of Automata*, 2024. ISBN 978-3-031-71112-1. URL https://link.springer.com/chapter/10.1007/978-3-031-71112-1_5.
- Jean Berstel. *Transductions and Context-Free Languages*, volume 38. Teubner, Stuttgart, Germany, 1979. URL <https://www.worldcat.org/oclc/06364613>.
- Harry E. Blanchard, Alexander Pollatsek, and Keith Rayner. The acquisition of parafoveal word information in reading. *Perception & Psychophysics*, 46(1), 1989. ISSN 0031-5117. URL <https://link.springer.com/content/pdf/10.3758/BF03208078.pdf>.
- Filippo Bonchi and Damien Pous. Hacking nondeterminism with induction and coinduction. *Communications of the ACM*, 2015. URL <https://doi.org/10.1145/2713167>.
- Christian Choffrut. Une caractérisation des fonctions séquentielles et des fonctions sous-séquentielles en tant que relations rationnelles. *Theoretical Computer Science*, 5(3), 1977. ISSN 0304-3975. URL [https://doi.org/10.1016/0304-3975\(77\)90049-4](https://doi.org/10.1016/0304-3975(77)90049-4).
- Marco Cognetta, David Pohl, Junyoung Lee, and Naoaki Okazaki. Pitfalls, subtleties, and techniques in automata-based subword-level constrained generation. In *Tokenization Workshop*, 2025. URL <https://openreview.net/forum?id=DFyb0GeGDS>.
- M. De Wulf, L. Doyen, T. A. Henzinger, and J. F. Raskin. Antichains: A New Algorithm for Checking Universality of Finite Automata. In *Proceedings of the International Conference on Computer Aided Verification*, 2006. URL https://doi.org/10.1007/11817963_5.
- Edo Dotan, Gal Jaschek, Tal Pupko, and Yonatan Belinkov. Effect of tokenization on transformers for biological sequences. *Bioinformatics*, 40(4), 2024. ISSN 1367-4811. URL <https://doi.org/10.1093/bioinformatics/btae196>.
- Philip Gage. A new algorithm for data compression. *The C Users Journal Archive*, 12, 1994. URL <https://api.semanticscholar.org/CorpusID:59804030>.
- Renato Geh, Honghua Zhang, Kareem Ahmed, Benjie Wang, and Guy Van Den Broeck. Where is the signal in tokenization space? In *Proceedings of the Conference on Empirical Methods in Natural Language Processing*, 2024. URL <https://aclanthology.org/2024.emnlp-main.230/>.

- Marjan Ghazvininejad, Xing Shi, Yejin Choi, and Kevin Knight. Generating Topical Poetry. In *Proceedings of the Conference on Empirical Methods in Natural Language Processing*, 2016. URL <https://aclanthology.org/D16-1126/>.
- Mario Giulianelli, Luca Malagutti, Juan Luis Gastaldi, Brian DuSell, Tim Vieira, and Ryan Cotterell. On the Proper Treatment of Tokenization in Psycholinguistics. In *Proceedings of the Conference on Empirical Methods in Natural Language Processing*, 2024. URL <https://aclanthology.org/2024.emnlp-main.1032>.
- Kyle Gorman. Pynini: A Python library for weighted finite-state grammar compilation. In *Proceedings of the SIGFSM Workshop on Statistical NLP and Weighted Automata*, 2016. URL <https://aclanthology.org/W16-2409/>.
- Jonathan Hayase, Alisa Liu, Noah A. Smith, and Sewoong Oh. Sampling from Your Language Model One Byte at a Time. In *Tokenization Workshop*, 2025. URL <https://openreview.net/forum?id=DM8D9Nq9u0>.
- John E. Hopcroft, Rajeev Motwani, and Jeffrey D. Ullman. *Introduction to Automata Theory, Languages, and Computation*. Addison-Wesley, 2nd edition, 2001. ISBN 0201441241. URL <https://openlibrary.org/books/OL6795097M>.
- Yanrong Ji, Zhihan Zhou, Han Liu, and Ramana V Davuluri. DNABERT: Pre-trained bidirectional encoder representations from transformers model for DNA-language in genome. *Bioinformatics*, 37(15), 2021. ISSN 1367-4803. URL <https://doi.org/10.1093/bioinformatics/btab083>.
- Arthur B. Kahn. Topological sorting of large networks. *Communications of the ACM*, 5(11), 1962. URL <https://dl.acm.org/doi/10.1145/368996.369025>.
- Terry Koo, Frederick Liu, and Luheng He. Automata-based constraints for language model decoding. In *Conference on Language Modeling*, 2024. URL <https://openreview.net/forum?id=BDBdbLmyzY>.
- Taku Kudo. Subword Regularization: Improving Neural Network Translation Models with Multiple Subword Candidates. In *Proceedings of the Annual Meeting of the Association for Computational Linguistics*, 2018. URL <https://aclanthology.org/P18-1007/>.
- Woosuk Kwon, Zhuohan Li, Siyuan Zhuang, Ying Sheng, Lianmin Zheng, Cody Hao Yu, Joseph Gonzalez, Hao Zhang, and Ion Stoica. Efficient memory management for large language model serving with PagedAttention. In *SOSP*, 2023. URL <https://doi.org/10.1145/3600006.3613165>.
- Alexander K. Lew, Tan Zhi-Xuan, Gabriel Grand, and Vikash Mansinghka. Sequential Monte Carlo Steering of Large Language Models using Probabilistic Programs. In *ICML Workshop: Sampling and Optimization in Discrete Space*, 2023. URL <https://openreview.net/forum?id=U12K0qXxY>.
- Chu-Cheng Lin, Hao Zhu, Matthew R. Gormley, and Jason Eisner. Neural Finite-State Transducers: Beyond Rational Relations. In *Proceedings of the Conference of the North American Chapter of the Association for Computational Linguistics: Human Language Technologies*, 2019. URL <https://aclanthology.org/N19-1024/>.
- Mitchell P. Marcus, Beatrice Santorini, and Mary Ann Marcinkiewicz. Building a large annotated corpus of English: The Penn Treebank. *Computational Linguistics*, 1993. URL <https://aclanthology.org/J93-2004/>.
- Stephen Merity, Caiming Xiong, James Bradbury, and Richard Socher. Pointer Sentinel Mixture Models. In *International Conference on Learning Representations*, 2017. URL <https://openreview.net/forum?id=Byj72udxe>.
- A. R. Meyer and L. J. Stockmeyer. The equivalence problem for regular expressions with squaring requires exponential space. In *Proceedings of the Annual Symposium on Switching and Automata Theory*, 1972. URL <https://doi.org/10.1109/SWAT.1972.29>.
- Mehryar Mohri. Finite-State Transducers in Language and Speech Processing. *Computational Linguistics*, 1997. URL <https://aclanthology.org/J97-2003/>.

- Mehryar Mohri. Edit-Distance of Weighted Automata: General Definitions and Algorithms. *International Journal of Foundations of Computer Science*, 14(06), 2003. doi: 10.1142/S0129054103002114. URL <https://doi.org/10.1142/S0129054103002114>.
- Mehryar Mohri. *Weighted Automata Algorithms*, chapter 5. Springer Berlin Heidelberg, Berlin, Heidelberg, 2009. ISBN 978-3-642-01492-5. URL https://doi.org/10.1007/978-3-642-01492-5_6.
- Sathvik Nair and Philip Resnik. Words, subwords, and morphemes: What really matters in the surprisal-reading time relationship? In *Findings of the Association for Computational Linguistics: EMNLP*, 2023. URL <https://aclanthology.org/2023.findings-emnlp.752/>.
- Eric Nguyen, Michael Poli, Marjan Faizi, Armin W Thomas, Michael Wornow, Callum Birch-Sykes, Stefano Massaroli, Aman Patel, Clayton M. Rabideau, Yoshua Bengio, Stefano Ermon, Christopher Re, and Stephen Baccus. HyenaDNA: Long-range genomic sequence modeling at single nucleotide resolution. In *Proceedings of the Conference on Neural Information Processing Systems*, 2023. URL <https://openreview.net/forum?id=ubzNoJj0Kj>.
- Byung-Doh Oh and William Schuler. Leading whitespaces of language models’ subword vocabulary pose a confound for calculating word probabilities. In *Proceedings of the Conference on Empirical Methods in Natural Language Processing*, 2024. URL <https://aclanthology.org/2024.emnlp-main.202/>.
- J. Oncina, P. Garcia, and E. Vidal. Learning subsequential transducers for pattern recognition interpretation tasks. *IEEE Transactions on Pattern Analysis and Machine Intelligence*, 15(5), 1993. URL <https://ieeexplore.ieee.org/document/211465>.
- OpenAI. Tiktoken: A fast BPE tokeniser for OpenAI’s models, 2024. URL <https://github.com/openai/tiktoken>.
- George Orwell. *Nineteen Eighty-Four*. Secker & Warburg, 1949. URL https://en.wikipedia.org/wiki/Nineteen_Eighty-Four.
- Buu Phan, Marton Havasi, Matthew Muckley, and Karen Ullrich. Understanding and Mitigating Tokenization Bias in Language Models, 2024. URL <https://arxiv.org/abs/2406.16829>.
- Tiago Pimentel and Clara Meister. How to compute the probability of a word. In *Proceedings of the Conference on Empirical Methods in Natural Language Processing*, 2024. URL <https://aclanthology.org/2024.emnlp-main.1020/>.
- Jean-Éric Pin. *Mathematical Foundations of Automata Theory*. Lecture notes LIAFA, Université Paris, 2025. URL <https://www.irif.fr/~jep/PDF/MPRI/MPRI.pdf>.
- Jean-Éric Pin. *Handbook of Automata Theory*. European Mathematical Society Publishing House, 2021. ISBN 978-3-98547-006-8. URL <https://doi.org/10.4171/Automata>.
- Lifeng Qiao, Peng Ye, Yuchen Ren, Weiqiang Bai, chaoqi liang, Xinzhu Ma, Nanqing Dong, and Wanli Ouyang. Model decides how to tokenize: Adaptive DNA sequence tokenization with MxDNA. In *The Annual Conference on Neural Information Processing Systems*, 2024. URL <https://openreview.net/forum?id=AQ1umQL7dZ>.
- Michael O. Rabin and Dana Scott. Finite automata and their decision problems. *IBM Journal of Research and Development*, 3(2), 1959. URL <https://ieeexplore.ieee.org/document/5392601>.
- Alec Radford, Jeff Wu, Rewon Child, David Luan, Dario Amodei, and Ilya Sutskever. Language Models are Unsupervised Multitask Learners. *OpenAI Blog*, 2019. URL https://cdn.openai.com/better-language-models/language_models_are_unsupervised_multitask_learners.pdf.
- Pushpendre Rastogi, Ryan Cotterell, and Jason Eisner. Weighting Finite-State Transductions With Neural Context. In *Proceedings of the Conference of the North American Chapter of the Association for Computational Linguistics: Human Language Technologies*, 2016. doi: 10.18653/v1/N16-1076. URL <https://aclanthology.org/N16-1076/>.

- Keith Rayner, Arnold D. Well, Alexander Pollatsek, and James H. Bertera. The availability of useful information to the right of fixation in reading. *Perception & Psychophysics*, 31(6), 1982. URL <https://doi.org/10.3758/BF03204186>.
- Rico Sennrich, Barry Haddow, and Alexandra Birch. Neural Machine Translation of Rare Words with Subword Units. In *Proceedings of the Annual Meeting of the Association for Computational Linguistics*, 2016. URL <https://aclanthology.org/P16-1162/>.
- Xinying Song, Alex Salcianu, Yang Song, Dave Dopson, and Denny Zhou. Fast WordPiece tokenization. In *Proceedings of the Conference on Empirical Methods in Natural Language Processing*, 2021. URL <https://aclanthology.org/2021.emnlp-main.160/>.
- Felix Stahlberg, Christopher Bryant, and Bill Byrne. Neural grammatical error correction with finite state transducers. In *Proceedings of the Conference of the North American Chapter of the Association for Computational Linguistics: Human Language Technologies*, 2019. URL <https://aclanthology.org/N19-1406/>.
- Llama Team. The Llama 3 herd of models, 2024. URL <https://arxiv.org/abs/2407.21783>.
- Tim Vieira, Benjamin LeBrun, Mario Giulianelli, Juan Luis Gastaldi, Brian DuSell, John Terilla, Timothy J. O’Donnell, and Ryan Cotterell. From Language Models over Tokens to Language Models over Characters. In *Forty-second International Conference on Machine Learning*, 2025a. URL <https://openreview.net/forum?id=sQS0roNQZR>.
- Tim Vieira, Tianyu Liu, Clemente Pasti, Yahya Emar, Brian DuSell, Benjamin LeBrun, Mario Giulianelli, Juan Luis Gastaldi, John Terilla, Timothy J. O’Donnell, and Ryan Cotterell. Language Models over Canonical Byte-Pair Encodings. In *International Conference on Machine Learning*, 2025b. URL <https://openreview.net/forum?id=eCVrfVDNSY>.
- Ning Wang, Jiang Bian, Yuchen Li, Xuhong Li, Shahid Mumtaz, Linghe Kong, and Haoyi Xiong. Multi-purpose RNA language modelling with motif-aware pretraining and type-guided fine-tuning. *Nature Machine Intelligence*, 6(5), 2024. URL <https://doi.org/10.1038/s42256-024-00836-4>.
- Xuezhi Wang, Jason Wei, Dale Schuurmans, Quoc V Le, Ed H. Chi, Sharan Narang, Aakanksha Chowdhery, and Denny Zhou. Self-Consistency Improves Chain of Thought Reasoning in Language Models. In *The International Conference on Learning Representations*, 2023. URL <https://openreview.net/forum?id=1PL1NIMMrw>.
- Brandon T. Willard and Rémi Louf. Efficient guided generation for large language models, 2023. URL <https://arxiv.org/abs/2307.09702>.
- Thomas Wolf, Lysandre Debut, Victor Sanh, Julien Chaumond, Clement Delangue, Anthony Moi, Pierric Cistac, Tim Rault, Remi Louf, Morgan Funtowicz, Joe Davison, Sam Shleifer, Patrick von Platen, Clara Ma, Yacine Jernite, Julien Plu, Canwen Xu, Teven Le Scao, Sylvain Gugger, Mariama Drame, Quentin Lhoest, and Alexander Rush. Transformers: State-of-the-art natural language processing. In *Proceedings of the Conference on Empirical Methods in Natural Language Processing: System Demonstrations*, 2020. URL <https://aclanthology.org/2020.emnlp-demos.6>.
- Yonghui Wu, Mike Schuster, Zhifeng Chen, Quoc V. Le, Mohammad Norouzi, Wolfgang Macherey, Maxim Krikun, Yuan Cao, Qin Gao, Klaus Macherey, Jeff Klingner, Apurva Shah, Melvin Johnson, Xiaobing Liu, Łukasz Kaiser, Stephan Gouws, Yoshikiyo Kato, Taku Kudo, Hideto Kazawa, Keith Stevens, George Kurian, Nishant Patil, Wei Wang, Cliff Young, Jason Smith, Jason Riesa, Alex Rudnick, Oriol Vinyals, Greg Corrado, Macduff Hughes, and Jeffrey Dean. Google’s Neural Machine Translation System: Bridging the Gap between Human and Machine Translation, 2016. URL <https://arxiv.org/abs/1609.08144>.
- Vicky Xeferi, Tim Vieira, Ryan Cotterell, and Afra Amini. Syntactic Control of Language Models by Posterior Inference. In Wanxiang Che, Joyce Nabende, Ekaterina Shutova, and Mohammad Taher Pilehvar (eds.), *Findings of the Association for Computational Linguistics: ACL 2025*, pp. 25350–25365, Vienna, Austria, July 2025. Association for Computational Linguistics. ISBN 979-8-89176-256-5. doi: 10.18653/v1/2025.findings-acl.1300. URL <https://aclanthology.org/2025.findings-acl.1300/>.

APPENDIX CONTENTS

A	Notation Glossary	17
B	Background on Transducers	18
C	Efficient Algorithms	19
C.1	The Goal: An Efficient Implementation of the Autoregressive Interface	19
C.2	Frontier-Based Checks (<code>is_cylinder</code> , <code>is_member</code> , <code>is_live</code>)	21
C.3	Pruning (<code>prune</code>)	22
C.4	Fast Next-Symbol Decomposition (<code>decompose_next</code>)	23
C.5	Next-Symbol Decomposition Shortcuts	25
C.6	Input-Projection Universality Shortcut (<code>fast_univ_filter</code>)	26
C.7	Memoization and Batching of $p_{\mathcal{X}}$	26
C.8	Realizing the Autoregressive Interface	27
C.9	All-Universal Fast Path	28
D	Proofs for Finiteness Conditions	30
D.1	Properties of Prefix Monotone Maps	30
D.2	Quotient Bound for Strict-Prefix Monotone Maps	31
D.3	Sufficient Conditions for Finite Quotients and Remainders	32
E	Example Decompositions	34
F	Experimental Setup	36
F.1	Datasets	36
F.2	Models	36
F.3	Parameters	36
F.4	GPU Usage	36
F.5	Details on Transducers Used in Experiments	37
G	Additional Experimental Results	39
G.1	Comparison to Vieira et al. (2025a)	39
G.2	Jensen–Shannon Divergence	40
G.3	Decomposition Size	43
G.4	Cross-Entropy	45
G.5	Benchmarking the Computational Shortcut	46
H	State-Based Decomposition	47
I	Related Work	48

J Limitations

50

A NOTATION GLOSSARY

Notation	Gloss
ε	Empty string
EOS	End-of-string symbol
$x, x' \in \mathcal{X}$	Symbols in the source alphabet \mathcal{X}
$\mathbf{x}, \mathbf{x}' \in \mathcal{X}^*$	Source strings
\mathcal{X}^*	Set of all source strings
$Z, Z' \subseteq \mathcal{X}^*$	Sets of source strings
\mathbf{xx}'	Concatenation (strings)
ZZ'	Concatenation (sets of strings)
$y, y' \in \mathcal{Y}$	Symbols in the target alphabet
$\mathbf{y}, \mathbf{y}' \in \mathcal{Y}^*$	Target strings
\mathcal{Y}^*	Set of all target strings
$f: \mathcal{X}^* \rightarrow \mathcal{Y}^*$	Transformation from source strings \mathcal{X}^* to target strings \mathcal{Y}^*
$\mathbf{x} \preceq \mathbf{x}'$	\mathbf{x} is a prefix of \mathbf{x}'
$\mathbf{x} \prec \mathbf{x}'$	\mathbf{x} is a strict-prefix of \mathbf{x}'
$\langle Z \rangle$	Cylinder set spanned by Z
$\text{pf}(Z)$	Prefix-base of Z
$p_{\mathcal{X}}$	Language model over source strings \mathcal{X}^*
X	\mathcal{X}^* -valued random variable $X \sim p_{\mathcal{X}}$
$\overrightarrow{p_{\mathcal{X}}}$	Prefix probability of $p_{\mathcal{X}}$
$p_{\mathcal{Y}}$	Language model over target strings \mathcal{Y}^*
$f(X)$	\mathcal{Y}^* -valued random variable $f(X) \sim p_{\mathcal{Y}}$
$\overrightarrow{p_{\mathcal{Y}}}$	Prefix probability of $p_{\mathcal{Y}}$
f	Transducer implementation of f
$\hookrightarrow \mathcal{X}$	Input alphabet
$\hookrightarrow \mathcal{Y}$	Output alphabet
$\hookrightarrow S$	Set of states
$\hookrightarrow I \subseteq S$	Set of initial states
$\hookrightarrow F \subseteq S$	Set of accepting states
$\hookrightarrow T$	Set of transitions
$\hookrightarrow U \subseteq S$	Set of IP-universal states (§C.6)
$s, s' \in S$	States
$(s \xrightarrow{x:y} s') \in T$	Transition from s to s' that scans x and emits y
$T(s) \subseteq T$	Outgoing transitions from state s
$f \circ f'$	Transducer composition
$f \circ f'$	Relation composition
$\text{proj}_{\mathcal{X}}(f)$	Input projection
$f_{[s]}$	Force-start f in state s
$\mathbf{y}\mathcal{Y}^*$	Either a copy-transducer that accepts $\mathbf{y}\mathcal{Y}^*$ or the corresponding relation.
$f \circ \mathbf{y}\mathcal{Y}^*$	A transducer whose paths are restricted to those that accept $\mathbf{y}\mathcal{Y}^*$.
$f^{-1}(\mathbf{y})$	Preimage of the target string \mathbf{y} (§3)
$f^{-1}(\mathcal{Y})$	The preimage of a set \mathcal{Y} , $\{f^{-1}(\mathbf{y}) \mid \mathbf{y} \in \mathcal{Y}\}$ (§3)
$\mathcal{P}(\mathbf{y})$	Precover of the target string \mathbf{y} (§3)
$\mathcal{C}(\mathbf{y})$	The largest cylinder set contained in $\mathcal{P}(\mathbf{y})$ (§4)
$\mathcal{Q}(\mathbf{y})$	Quotient (§4)
$\mathcal{R}(\mathbf{y})$	Remainder (§4)

Notation conventions. **Color** encodes domain: **magenta** denotes source-domain objects (e.g., $\mathbf{x}, \mathcal{X}, \mathcal{P}, \mathcal{Q}, \mathcal{R}$) and **olive green** denotes target-domain objects (e.g., $\mathbf{y}, \mathcal{Y}, f$). **Font** encodes type: lowercase italic for symbols (x, y), bold italic for strings (\mathbf{x}, \mathbf{y}), calligraphic for alphabets and sets ($\mathcal{X}, \mathcal{Y}, \mathcal{P}, \mathcal{Q}, \mathcal{R}$), sans-serif for transducer components (S, T, I, F, U), and typewriter for the transducer itself (f) and for concrete strings in examples (abc, xyz). The overrightarrow $\overrightarrow{}$ marks prefix probabilities: $\overrightarrow{p_{\mathcal{X}}}$ is the prefix probability of $p_{\mathcal{X}}$.

B BACKGROUND ON TRANSDUCERS

This section introduces additional information on transducers, complementing §2.

Transducer variants. We say a transducer is **functional** if it defines a function, and **partially functional** if it defines a partial function. A transducer is **input-deterministic** if for every state $s \in S$, $|\mathbb{T}(s, \varepsilon)| = 0$ and $|\mathbb{T}(s, x)| \leq 1$ for all $x \in \mathcal{X}$ ¹⁷. For input-deterministic transducers, each source string $x \in \mathcal{X}^*$ has at most one accepting path that scans x and, therefore, can emit at most one target string $y \in \mathcal{Y}^*$. Thus, every input-deterministic transducer defines a (partial) function. A **copy-transducer** is one where every transition emits the same symbol as it scans, i.e., every transition is of the form $s \xrightarrow{x:x} s'$. We abbreviate copy transitions as $s \xrightarrow{x} s'$.¹⁸ Copy-transducers define partial identity functions: they map each string in a designated subset to itself, and drop all others. In the same way that we abbreviate copy transitions, we may implicitly map them to a set of strings via $(x, x) \mapsto x$.

Operations. Transducers support **composition**: given transducers f and f' , their composition $f \circ f'$ is a transducer denoting $\llbracket f \circ f' \rrbracket \stackrel{\text{def}}{=} \llbracket f \rrbracket \circ \llbracket f' \rrbracket$.^{19,20} We denote a transducer that encodes the relationship $\llbracket f \rrbracket \circ \{(y', y') \mid y' \in \langle y \rangle\}$ with $f \circ y\mathcal{Y}^*$. We freely coerce between these representations when the intent is clear from context. We define the **input projection** operation encoding the relationship $\llbracket \text{proj}_{\mathcal{X}}(f) \rrbracket = \{(x, x) \mid \exists y: (x, y) \in \llbracket f \rrbracket\}$ as $\text{proj}_{\mathcal{X}}(f) \stackrel{\text{def}}{=} (S, \mathcal{X}, \mathcal{X}, l, F, \{(s \xrightarrow{x:x} s') \mid s \xrightarrow{x:y} s' \in \mathbb{T}\})$, which is a copy-transducer. Let $f_{[s]}$ denote the operation of **force-starting** f in state s , $f_{[s]} \stackrel{\text{def}}{=} (S, \mathcal{X}, \mathcal{Y}, \{s\}, F, \mathbb{T})$; this operation yields a machine defining the set of source–target suffix pairs that are generated by paths starting at a given s and ending in an accepting state. We say that a state s is **IP-universal (input-projection universal)** if $\llbracket \text{proj}_{\mathcal{X}}(f_{[s]}) \rrbracket = \mathcal{X}^*$, i.e., no matter what input follows, the transducer can still produce output. Let $U \subseteq S$ denote the set of IP-universal states; this set can be precomputed for each transducer (§C.6).

Our algorithms use an **input-determinization** transformation $\text{determinize}(f)$ that maps a (partially) functional transducer f to an equivalent one that is input-deterministic. In general, such a mapping is not always realizable with a finite number of states.²¹ However, in the special case of copy-transducers, input-determinization is always possible, but may result in exponential blowup in the worst case.²² We use $\text{trim}(f)$ to denote a **trimming** operation that removes all states and edges that do not appear on any accepting path. These are standard operations that are implemented in any FST library; more details can be found in (Pin, 2021; 2025).

Visual notation. We use diagrams like those shown in §E to represent transducers. Transitions without source states denote initial states; double-lined states indicate accepting states. Transitions $s \xrightarrow{x:y} s'$ are shown as arrows between states.

Limitations. Finite-state transducers define the class of *rational relations* (Berstel, 1979, Ch. III). Because FSTs only have finitely many states, they are inherently limited in the relations they can represent. For example, FSTs cannot perform transformations that require unbounded matching or counting. In contrast, transducers with unbounded memory extend beyond the rational class, offering greater expressive power, but come with increased complexity and often undecidability of key properties, such as *universality*.

¹⁷The more general notion of a *subsequential transducer* additionally includes a final output function; this distinction does not arise for copy-transducers.

¹⁸For readers familiar with finite-state automata, every copy-transducer is isomorphic to an *acceptor*.

¹⁹Here, **relation composition** is given by $f \circ g \stackrel{\text{def}}{=} \{(x, z) \mid (x, y) \in f, (y, z) \in g\}$ where f and g are relations.

²⁰Pin (2025, Ch. XIX, sec. 2) gives an efficient method for constructing $f \circ f'$.

²¹Choffrut (1977) gives such an algorithm, by using a power set construction on the input side as in the determinization of nondeterministic finite automata. He shows it yields a finite machine if and only if the automaton has *bounded variation*, the constraint that for any two strings whose prefix distance (the combined length of the strings with the longest shared prefix removed) is bounded, then the output prefix distance is also bounded. He also provides a testable condition for determinization, known as the *twinning condition*: once two runs have read the same input prefix (i.e., we cut the input at the same point), then for every common continuation, they append the same further output.

²²For readers familiar with finite-state automata, input-determinization of a copy-transducer is isomorphic to the determinization of an equivalent finite-state automaton, see §B.

C EFFICIENT ALGORITHMS

The decomposition algorithm of §5 operates on a determinized, trimmed precover machine $\mathbf{P} = \text{trim}(\text{determinize}(\text{proj}_{\mathcal{X}}(\mathbf{f} \circ \mathbf{y}\mathcal{Y}^*)))$. In practice, both the composition with $\mathbf{y}\mathcal{Y}^*$ and the explicit determinization are expensive and must be repeated for each target \mathbf{y} . The algorithms in this section perform both steps lazily, operating directly on the original transducer \mathbf{f} and avoiding explicit materialization. This requires careful bookkeeping of partial outputs via *frontiers* (§C.1.1), but enables precomputation of IP-universal states and incremental reuse across targets.

We begin by stating the algorithmic goal (§C.1), then introduce the frontier data structure (§C.1.1) and show how each check reduces to a frontier query (§C.2). We write $(S, \mathcal{X}, \mathcal{Y}, l, F, T) = \mathbf{f}$ throughout and omit the dependency on $\overrightarrow{p_{\mathcal{X}}}$ since it is clear from context.

C.1 THE GOAL: AN EFFICIENT IMPLEMENTATION OF THE AUTOREGRESSIVE INTERFACE

We seek efficient algorithms for the prefix probabilities $\overrightarrow{p_{\mathcal{Y}}}(\mathbf{y})$, string probabilities $p_{\mathcal{Y}}(\mathbf{y})$, and next-token distributions $\overrightarrow{p_{\mathcal{Y}}}(\cdot | \mathbf{y})$ of transduced language models. Specifically, we want efficient implementations of the following methods, which constitute the interface to the transduced language model (§2).

```

44 def prefix_prob(y):
45     (Q,R) ← decompose(y)
46     return  $\sum_{\mathbf{x} \in Q} \overrightarrow{p_{\mathcal{X}}}(\mathbf{x}) + \sum_{\mathbf{x} \in R} p_{\mathcal{X}}(\mathbf{x})$ 
47 def prob(y):
48     return prefix_prob(y) · next_dist(y)[EOS]
49 def next_dist(y):
50      $\overline{p} \leftarrow \{\}$ 
51     Z ← prefix_prob(y)
52     for y' ∈  $\mathcal{Y}$ :
53          $\overline{p}[y'] \leftarrow \text{prefix\_prob}(\mathbf{y}\mathbf{y}') / Z$ 
54      $\overline{p}[\text{EOS}] \leftarrow 1 - \sum_{y' \in \mathcal{Y}} \overline{p}[y']$ 
55     return  $\overline{p}$ 

```

The primitive operation above is `prefix_prob`, which requires a single call to `decompose`. Both `next_dist` and `prob` are derived from it: `next_dist` computes $|\mathcal{Y}|$ additional prefix probabilities and obtains $\overrightarrow{p_{\mathcal{Y}}}(\text{EOS} | \mathbf{y})$ by complement; `prob` is a one-line product. In an implementation, $\overrightarrow{p_{\mathcal{X}}}$ and $p_{\mathcal{X}}$ should be memoized so that extending $\overrightarrow{p_{\mathcal{X}}}(\mathbf{x})$ to $\overrightarrow{p_{\mathcal{X}}}(\mathbf{x}\mathbf{x})$ requires only a single conditional evaluation rather than replaying the entire history (see §C.7). In §C.4, we show how to compute `next_dist` with a more efficient, joint decomposition, rather than $|\mathcal{Y}|+1$ separate calls to `prefix_prob`.

The three checks in Fig. 2—`is_cylinder`, `is_member`, and `is_live`—all require determining which transducer states are reachable after reading a source string \mathbf{x} , and what output each has produced relative to \mathbf{y} . We capture this information in a single data structure: the *frontier* (§C.1.1). In §C.2, we show how each check reduces to a simple query on the frontier. In practice, the quotient and remainder may be large or infinite, so we introduce pruning (§C.3) to obtain practical approximations.

C.1.1 FRONTIER COMPUTATION

Since \mathbf{f} can be nondeterministic even if it is functional, the transducer \mathbf{f} may reach many states simultaneously for a given source string \mathbf{x} and target \mathbf{y} . Each of these paths may have produced a different output buffer. The **frontier** $\mathcal{F} = \text{run}_{\mathbf{y}}(\mathbf{x})$ collects this information: it is the set of (s, \mathbf{b}) pairs—where $s \in S$ is a transducer state and $\mathbf{b} \in \mathcal{Y}^*$ is the output produced so far—reachable by reading \mathbf{x} from the initial states, filtered to buffers \mathbf{b} compatible with \mathbf{y} .²³ The frontier encodes all information needed for the three checks: `is_cylinder`, `is_member`, and `is_live` can each be evaluated from \mathcal{F} alone, without retaining the full path history (§C.2; Fig. 8). The pseudocode in Fig. 7 describes how to compute the frontier using the three functions `runy`, `stepy`, and `closurey`.

The frontier replaces the explicit precover machine $\mathbf{P} = \text{trim}(\text{determinize}(\text{proj}_{\mathcal{X}}(\mathbf{f} \circ \mathbf{y}\mathcal{Y}^*)))$ used in §5. Rather than materializing \mathbf{P} , the frontier tracks the same information directly on \mathbf{f} , avoiding both the composition with $\mathbf{y}\mathcal{Y}^*$ and the explicit determinization. The design reflects a two-phase structure: before a path’s buffer covers the target, the frontier tracks per-state output buffers (s, \mathbf{b}) filtered by target compatibility; once the buffer reaches or passes \mathbf{y} , the frontier can be truncated for universality checking (§C.2). The frontier unifies the two phases into a single lazy data structure.

²³A buffer \mathbf{b} is compatible with \mathbf{y} if and only if $\mathbf{b} \preceq \mathbf{y} \vee \mathbf{y} \preceq \mathbf{b}$, i.e., the buffer has either covered the target or has yet to diverge from it.

```

56 def runy(x1 ... xN): # memoize
57   if N = 0: return closurey(l × {ε})
58   return stepy(runy(x<N), xN)

59 def stepy(F, x):
60   F' ← ∅
61   for (s, b) in F:
62     for (⊖  $\xrightarrow{x:y}$  s') ∈ T(s, x):
63       b' ← by
64       if b' ≤ y ∨ y ≤ b':
65         F'.add((s', b'))
66   return closurey(F')

67 def closurey(F):
68   F' ← F
69   q ← QUEUE(F)
70   while |q| > 0:
71     (s, b) ← q.pop()
72     for (⊖  $\xrightarrow{\varepsilon:y'}$  s') ∈ T(s, ε):
73       b' ← by'
74       if b' ≤ y ∨ y ≤ b':
75         if (s', b') ∉ F':
76           F'.add((s', b'))
77           q.add((s', b'))
78   return F'

```

Figure 7: Frontier-based state machine

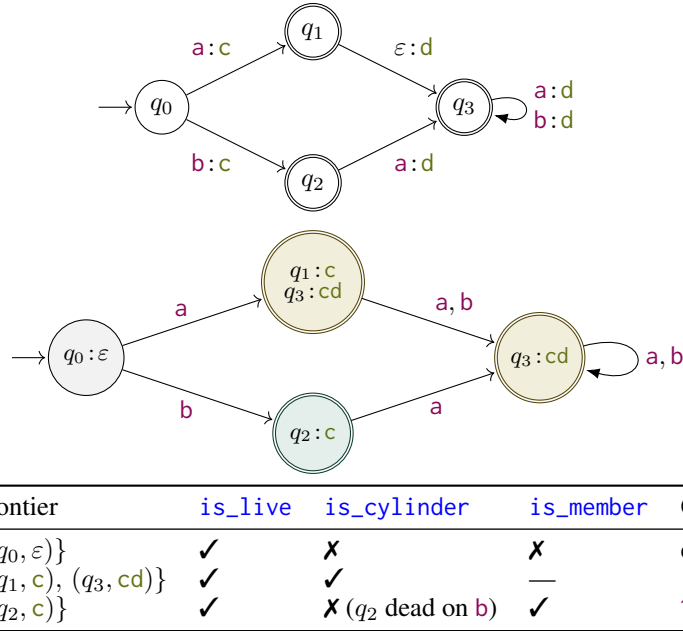


Figure 8: Truncated frontier example for the target $y = c$. **Top:** the transducer f . **Middle:** the frontier graph run_c , whose nodes are sets of (s, b) pairs and whose edges are input symbols. Buffers are truncated to length $|y|+1 = 2$: advancing (q_3, cd) by any input produces cdd , truncated back to cd , yielding the self-loop. Truncation keeps the state space finite while preserving whether the buffer has reached the target and which next output symbol it commits to. Reading $x = a$ reaches two states via ε -closure: q_1 (buffer = y) and q_3 (buffer $\succ y$). Yellow nodes are universal—every input leads to a non-empty accepting successor—placing a in $\mathcal{Q}(c)$. The teal node q_2 has no arc on b , so the BFS fails and b enters $\mathcal{R}(c)$.

The frontier enjoys a useful monotonicity property: extending the target by one symbol can only remove elements from the frontier, never add new ones. This means we can compute the frontier incrementally—filtering rather than rebuilding—as the target grows.

Proposition C.1 (Frontier containment). *For any source string x , target string $y_1 \dots y_N$ with $N > 0$:*

$$\text{run}_{y_1 \dots y_N}(x) = \{(s, b) \in \text{run}_{y_1 \dots y_{N-1}}(x) : |b| < N \vee b_N = y_N\} \quad (9)$$

Proof. Buffer filtering in `step` and `closure` keeps only (s, b) pairs where b and the target agree on their shared prefix. Since FST arcs only append to the buffer, once b is long enough to have an N^{th} symbol and $b_N \neq y_N$, then all descendant buffers would be filtered out by the $y_1 \dots y_N$ -compatibility filter. Therefore, filtering $\text{run}_y(x)$ at the end is equivalent to filtering at each step.

To see this, note that the (\supseteq) direction holds because $y_1 \dots y_N$ -compatible elements are also $y_1 \dots y_{N-1}$ -compatible (the former is strictly more restrictive). The (\subseteq) direction holds because elements that are $y_1 \dots y_{N-1}$ -compatible but *not* $y_1 \dots y_N$ -compatible (i.e., $|b| \geq N$ and $b_N \neq y_N$) cannot produce descendants that become $y_1 \dots y_N$ -compatible, since buffers only grow. ■

Proposition C.2. *Prop. C.1 generalizes beyond single-symbol extensions: for any $y' \preceq y$:*

$$\text{run}_y(x) = \{(s, b) \in \text{run}_{y'}(x) : b \preceq y \vee b \succeq y\} \quad (10)$$

Proof. By induction on $|y| - |y'|$. The base case $y = y'$ is immediate. For the inductive step, write $y = y'y_N$ with $y' \preceq y'$. By Prop. C.1, $\text{run}_y(x) = \{(s, b) \in \text{run}_{y'}(x) : |b| < N \vee b_N = y_N\}$. By the induction hypothesis, $\text{run}_{y'}(x) = \{(s, b) \in \text{run}_{y'}(x) : b \preceq y' \vee b \succeq y'\}$. Substituting, $(s, b) \in \text{run}_y(x)$ survives both filters iff b agrees with y on all positions up to $\min(|b|, N)$, i.e., $b \preceq y \vee b \succeq y$. ■

Prop. C.2 is the key property that enables warm-starting `decompose_next` (§C.4) from any target prefix’s cached frontiers.

C.2 FRONTIER-BASED CHECKS (`is_cylinder`, `is_member`, `is_live`)

Recall that the decomposition algorithm (Fig. 2) relies on three checks (`is_cylinder`, `is_member`, `is_live`). This section describes how to compute them in terms of the frontier.

```

79 def is_cylinder(x, y): # memoize
80     N ← |y|
81     F ← trunc_buf_y(run_y(x))
82     V ← {F}; q ← QUEUE({F})
83     while q:
84         F ← q.pop()
85         # Accepting: some pair has matched
86         # target and is accepting
87         if ¬∃(s, b) ∈ F: b ⪰ y ∧ s ∈ F:
88             return False
89         # Complete: every input leads to a
90         # non-empty successor
91         for x' ∈ X:
92             F' ← trunc_buf_y(step_y(F, x'))
93             if F' = ∅: return False
94             if F' ∉ V: V.add(F'); q.push(F')
95     return True

96 def is_member(x, y):
97     return ∃(s, b) ∈ run_y(x):
98         b ⪰ y ∧ s ∈ F
99 def is_live(x, y):
100    return run_y(x) ≠ ∅
101 def trunc_buf_y(F):
102    N ← |y|
103    return {(s, b_{≤N}) | (s, b) ∈ F,
104            b ⪰ y ∨ y ⪰ b}

```

Figure 9: Frontier-based checks. `is_cylinder`(x, y) verifies universality via powerset BFS over projected frontiers. `is_member` checks for an accepting covering state; `is_live` checks whether the frontier is non-empty.

To check whether $\langle x \rangle \subseteq \mathcal{P}(y)$, the frontier-based `is_cylinder` applies `trunc_buf` to the frontier $\text{run}_y(x)$, which truncates buffers to length $|y|$, yielding a **truncated frontier**—a set of (s, b) pairs whose buffers are compatible with y . It then verifies universality via BFS over truncated frontiers: each successor frontier is obtained by applying `step_y` followed by `trunc_buf`. Unlike the ordinary frontier, where buffers can grow without bound, truncated buffers must be prefixes of y , so at most $|y|+1$ distinct buffers exist, making the truncated frontier state space finite. Each truncated frontier corresponds to a state of the determinized precover machine \mathcal{P} , so the BFS terminates. The BFS checks that every truncated frontier is both accepting (some pair has $b \succeq y$ and $s \in F$) and complete (every input symbol leads to a non-empty successor). Without this exploration, two nondeterministic paths may yield the same string yet end in different states s_1 and s_2 , where neither is universal on its own, although $\llbracket f_{[s_1]} \rrbracket \cup \llbracket f_{[s_2]} \rrbracket = \mathcal{X}^*$.²⁴ The precomputation of IP-universal states and a cylinder check shortcut are discussed in §C.6.

²⁴Universality is decidable for finite-state automata; efficient algorithms include antichain-based simulation (De Wulf et al., 2006), bisimulation up to congruence (Bonchi & Pous, 2015), and classical equivalence checking (Meyer & Stockmeyer, 1972).

When the cylinder check fails, membership reduces to checking whether the frontier contains a covering accepting pair ($\mathbf{b} \succeq \mathbf{y}$ and $s \in F$): if so, $\mathbf{x} \in \mathcal{P}(\mathbf{y})$ and \mathbf{x} enters $\mathcal{R}(\mathbf{y})$.

Liveness is non-emptiness of the frontier. Since frontier pairs are already filtered to target-compatible buffers, a non-empty frontier witnesses that some extension of \mathbf{x} can reach the precover.

C.3 PRUNING (prune)

Even when the decomposition is finite, the quotient and remainder can be very large. Enumerating all of them is often impractical, so pruning is essential for scalability.²⁵ At minimum, `prune` drops source strings with zero prefix probability, since these cannot contribute any mass:

```

105 def prune(q'):
106     return {x ∈ q' : p_x(x) > 0}

```

This simplistic filter drops only strings with zero probability. In practice, we use a probability-mass pruning strategy: given candidates q' with total mass $Z = \sum_{\mathbf{x} \in q'} p_{\mathbf{x}}(\mathbf{x})$, we sort by descending $p_{\mathbf{x}}$ and greedily retain candidates until their cumulative mass reaches $(1 - \tau) \cdot Z$ or the capacity n_{\max} is reached, whichever comes first. The resulting decomposition is approximate: discarded candidates contribute at most $\tau \cdot Z$ mass per step, but the error vanishes as $\tau \rightarrow 0$.

```

107 def prune_prob_mass(τ, n_max):
108     def prune(q'):
109         M ← |q'|
110         q' ← sort_descending(q', key=p_x)
111         w ← [p_x(x) for x ∈ q'] # w_1 ≥ ... ≥ w_M
112         W ← cumulative_sum(w)
113         Z ← W_M
114         q ← ∅
115         for m ∈ {1, ..., min(n_max, M)}:
116             q.add(q'_m)
117             if W_m ≥ (1 - τ)Z: break
118         return q
119     return prune

```

Approximation bound. At each step, the discarded mass is at most $\tau \cdot Z$. As $\tau \rightarrow 0$ and $n_{\max} \rightarrow \infty$, the algorithm converges to the exact decomposition.

Finite termination. Even when the decomposition is finite, its size can be enormous. Pruning makes the algorithm tractable by bounding the queue at n_{\max} candidates per step, and also guarantees termination for transducers whose decomposition is infinite (§D.3).

Backtracking. Pruning may occasionally lead to dead ends where no valid extension remains. When this occurs while scoring an observed sequence, the next symbol \mathbf{y} receives zero conditional probability under the approximate $p_{\mathbf{y}}(\cdot | \mathbf{y})$. We recover using the procedure in Fig. 10, which takes the current target string \mathbf{y} , the next symbol \mathbf{y} , the current pruning threshold τ , and hyperparameters: maximum retries R , threshold floor τ_{\min} , and maximum eviction depth D_{\max} . On each retry, τ is halved (floored at τ_{\min} to prevent unlimited q growth), and cached decompositions for prefixes of \mathbf{y} are evicted at exponentially increasing depth $D = \min(2^{i-1}, D_{\max})$, forcing `decompose` to recompute with the relaxed threshold. The original threshold is restored afterward. The procedure is heuristic: there is no guarantee that a fixed number of retries with halved thresholds will recover. Frequent backtracking signals that the pruning threshold is overly aggressive; in such cases, the overhead of repeated eviction and recomputation can dominate runtime. In our experiments, we use $R = 20$, $\tau_{\min} = 10^{-10}$, $D_{\max} = 32$. Backtracking is infrequent in practice: for $\tau \leq 1e-3$, zero fallbacks occur across all experiments. At the coarsest threshold ($\tau = 1e-1$), the mean number of fallbacks per paragraph reaches at most 96 for $p_{\text{gpt2}} \circ f_{\alpha}$ (max 159), 5.1 for $p_{\text{gpt2}} \circ f_{\alpha} \circ f_{\text{ptb}}$ (max 18), and 0.4 for $p_{\text{dna}} \circ f_{\text{dna2aa}}$ (max 5).

²⁵An alternative to deterministic pruning is importance sampling with a proposal distribution over source strings; we leave this direction to future work.

```

120 def backtrack( $\mathbf{y}, y, \tau, R, \tau_{\min}, D_{\max}$ ):
121      $\tau_0 \leftarrow \tau$ 
122     for  $i \in 1, \dots, R$ :
123          $\tau \leftarrow \max(\tau/2, \tau_{\min})$ 
124          $D \leftarrow \min(2^{i-1}, D_{\max})$ 
125         for  $d \in 0, \dots, D-1$ :
126             if  $d > |\mathbf{y}|$ : break
127             evict cached decompose( $\mathbf{y}_{<|\mathbf{y}|-d}$ )
128              $\bar{p} \leftarrow \text{next\_dist}(\mathbf{y})$ 
129             if  $\bar{p}[y] > 0$ :
130                  $\tau \leftarrow \tau_0$ 
131             return  $\bar{p}$ 
132      $\tau \leftarrow \tau_0$ 
133     raise DeadEnd

```

Figure 10: Backtracking. On each retry, halve τ (floored at τ_{\min}) and evict cached decompositions for progressively longer prefixes of \mathbf{y} (depth $D = \min(2^{i-1}, D_{\max})$), then recompute `next_dist`. Restore τ afterward.

C.4 FAST NEXT-SYMBOL DECOMPOSITION (`decompose_next`)

Since $\langle \mathcal{Q}(\mathbf{y}y) \rangle \subseteq \langle \mathcal{Q}(\mathbf{y}) \rangle$, we have $\mathcal{P}(\mathbf{y}y) = (\langle \mathcal{Q}(\mathbf{y}) \rangle \cap \langle \mathcal{Q}(\mathbf{y}y) \rangle) \sqcup \mathcal{R}(\mathbf{y}y)$. The decomposition for $\mathbf{y}y$ can therefore be obtained with incremental work starting from $\mathcal{Q}(\mathbf{y}) \cup \mathcal{R}(\mathbf{y})$. The structural reason is monotonicity: the precover for \mathbf{y} and $\mathbf{y}y$ share the same alphabet and initial states; only the accepting states differ, as acceptability depends on which buffers cover the target. This is formalized by the frontier containment property (Prop. C.1).

The `decompose_next` method computes $\mathcal{Q}(\mathbf{y}y)$ and $\mathcal{R}(\mathbf{y}y)$ for all $y \in \mathcal{Y}$ simultaneously, as well as the exact preimage $f^{-1}(\mathbf{y})$. This is the key efficiency improvement over calling `decompose`($\mathbf{y}y$) independently for each y .

The BFS is seeded with $\mathcal{Q}(\mathbf{y}) \cup \mathcal{R}(\mathbf{y})$ (line 152). For each source string \mathbf{x} in the queue, we first check whether `is_exact_member`(\mathbf{x}, \mathbf{y}) (line 156) and, if so, record \mathbf{x} in the preimage set. Next, for each $y \in \text{reachable_outputs}(\mathbf{x}, \mathbf{y})$ (defined below; line 159), we classify \mathbf{x} as a cylinder or member for $\mathbf{y}y$; by functionality of `f`, at most one y can be a cylinder (Prop. C.4). If a cylinder was found for some y , the entire subtree rooted at \mathbf{x} is absorbed—we skip extension for *all* symbols (line 164). Otherwise, we extend by all reachable source symbols (line 165).

The `decompose_next` algorithm relies on two mechanisms described next: target recursion for cheap frontier computation, and three frontier-based helpers. We now introduce these.

Target recursion. The call `is_cylinder`($\mathbf{x}, \mathbf{y}y$) internally triggers `runyy`(\mathbf{x}). Target recursion is used opportunistically when the parent frontier `runy`(\mathbf{x}) is already cached: the frontier for the extended target is derived by filtering rather than recomputing the entire source-string chain (Prop. C.1). This is the typical case in `decompose_next`, where `decompose`(\mathbf{y}) has already populated the cache. This optimization is transparent: `is_cylinder` is called unchanged; the logic lives entirely inside `run`.

Per-symbol frontier helpers. The BFS loop uses three frontier-based helpers.

- `is_exact_member`(\mathbf{x}, \mathbf{y}) checks whether \mathbf{x} maps to \mathbf{y} exactly, i.e., `is_exact_member`(\mathbf{x}, \mathbf{y}) \iff ($f(\mathbf{x}) = \mathbf{y}$).
- `reachable_inputs`(\mathbf{x}, \mathbf{y}) conservatively approximates the set of source symbols \mathbf{x}' such that extending \mathbf{x} by \mathbf{x}' remains compatible with \mathbf{y} , i.e., $\{\mathbf{x}' \in \mathcal{X} : \langle \mathbf{x}\mathbf{x}' \rangle \cap \mathcal{P}(\mathbf{y}) \neq \emptyset\}$. The pseudocode checks for transitions from frontier states whose extended buffer is prefix-compatible with \mathbf{y} ; this may over-report when the resulting state cannot reach acceptance.
- `reachable_outputs`(\mathbf{x}, \mathbf{y}) conservatively approximates the set of target symbols y' such that some extension of \mathbf{x} can produce $\mathbf{y}y'$ as an output prefix, i.e., $\{y' \in \mathcal{Y} : \langle \mathbf{x} \rangle \cap \mathcal{P}(\mathbf{y}y') \neq \emptyset\}$. The pseudocode checks single-step transitions from frontier states, which may over-report (a transition from a frontier state that cannot reach acceptance) because the frontier is not cotrimmed. Symbols requiring multiple transitions to extend past \mathbf{y} are handled by the expansion loop.

All three are computed directly from the frontier $\text{run}_y(\mathbf{x})$:

```

134 def is_exact_member(x, y):
135     return  $\exists (s, \mathbf{b}) \in \text{run}_y(\mathbf{x})$ :
136          $\mathbf{b} = \mathbf{y} \wedge s \in \mathbf{F}$ 
137 def reachable_inputs(x, y):
138     return  $\{x' \mid (s, \mathbf{b}) \in \text{run}_y(\mathbf{x}),$ 
139          $(s \xrightarrow{x':y'} s') \in \mathbf{T}, \mathbf{b}y' \preceq \mathbf{y} \vee \mathbf{y} \preceq \mathbf{b}y'\}$ 
140 def reachable_outputs(x, y):
141      $\mathcal{F} \leftarrow \text{run}_y(\mathbf{x})$ 
142     #  $y'$  is read from  $\mathbf{b}$  (committed)
143     # or  $\mathbf{y}$  (boundary)
144     return  $\{y' \mid (s, \mathbf{b}) \in \mathcal{F},$ 
145          $(s \xrightarrow{-:y'} s') \in \mathbf{T}(s), \mathbf{y}y' \preceq \mathbf{b}y'\}$ 

```

Expansion loop. The following algorithm combines the seeding, shortcuts, and helpers above into a single BFS that computes the per-symbol quotients and remainders for every $y \in \mathcal{Y}$ simultaneously.

```

146 def decompose_next(y):
147      $(\mathbf{Q}, \mathbf{R}) \leftarrow \text{decompose}(y)$ 
148      $qs \leftarrow \{\}$ ;  $rs \leftarrow \{\}$  # map  $y \mapsto \text{set of } \mathbf{x}$ 
149      $ps \leftarrow \emptyset$ 
150     # Remainders were not cylinders for  $\mathbf{y}$ , hence not for any  $\mathbf{y}y$  (Prop. C.3)
151      $\text{non\_cyl} \leftarrow \mathbf{R}$ 
152      $q \leftarrow \mathbf{Q} \cup \mathbf{R}$ 
153     while  $|q| > 0$ :
154          $q' \leftarrow \emptyset$ 
155         for  $\mathbf{x}$  in  $q$ :
156             if  $\text{is\_exact\_member}(\mathbf{x}, \mathbf{y})$ :  $ps.add(\mathbf{x})$  #  $f(\mathbf{x}) = \mathbf{y}$  exactly
157             # Check reachable  $\mathbf{y}$ ; at most one  $\mathbf{y}$  can have  $\mathbf{x}$  as a cylinder (Prop. C.4).
158              $\hat{\mathbf{y}} \leftarrow \perp$ 
159             for  $\mathbf{y}$  in  $\text{reachable\_outputs}(\mathbf{x}, \mathbf{y})$ :
160                 if  $\hat{\mathbf{y}} = \perp$  and  $\mathbf{x} \notin \text{non\_cyl}$  and  $\text{is\_cylinder}(\mathbf{x}, \mathbf{y}y)$ :
161                      $qs[\mathbf{y}].add(\mathbf{x})$ ;  $\hat{\mathbf{y}} \leftarrow \mathbf{y}$ ; continue
162                 if  $\text{is\_member}(\mathbf{x}, \mathbf{y}y)$ :
163                      $rs[\mathbf{y}].add(\mathbf{x})$ 
164             if  $\hat{\mathbf{y}} \neq \perp$ : continue # absorbed  $\Rightarrow$  skip extension for all  $\mathbf{y}$ 
165             for  $x' \in \text{reachable\_inputs}(\mathbf{x}, \mathbf{y})$ :
166                  $q'.add(\mathbf{x}x')$ 
167          $q \leftarrow \text{prune}(q')$ 
168     return  $(qs, rs, ps)$ 

```

Figure 11: Fast next-token decomposition algorithm.

$\text{decompose_next}(y)$ computes $\mathcal{Q}(yy)$ and $\mathcal{R}(yy)$ for all $y \in \mathcal{Y}$ in a single BFS pass. The $\text{is_cylinder}(\mathbf{x}, \mathbf{y}y)$ call triggers $\text{run}_{yy}(\mathbf{x})$, which is computed cheaply via target recursion (Prop. C.1) since the parent frontier $\text{run}_y(\mathbf{x})$ is already cached. The non-cylinder shortcut avoids the universality check entirely for seeds in $\mathcal{R}(y)$. After the BFS, the cache is populated so that subsequent $\text{decompose}(yy)$ calls are free. The exact preimage is collected as a byproduct: if \mathbf{x} is a cylinder for some $\mathbf{y}y$, every extension produces output strictly longer than \mathbf{y} , so no extension can be an exact preimage of \mathbf{y} .

Cache population. After the BFS, the computed $\mathcal{Q}(yy)$ and $\mathcal{R}(yy)$ should be written into decompose 's memoization cache. A subsequent $\text{decompose}(yy)$ call (e.g., from $\text{decompose_next}(yy)$) hits the cache instead of re-running its own BFS.

```

169 def decompose_next(y):
170     ...
171     # Populate decompose's cache for all children
172     for  $y \in qs.keys() \cup rs.keys()$ :
173          $\text{cache}[\text{decompose}, \mathbf{y}y] \leftarrow (qs[\mathbf{y}], rs[\mathbf{y}])$ 
174     return ...

```

C.5 NEXT-SYMBOL DECOMPOSITION SHORTCUTS

The `decompose_next` algorithm (Fig. 11) shares work across all output symbols by making a single BFS pass for all output symbols at once instead of calling the decomposition for each symbol as in `decompose` (Fig. 2). By starting with the decomposition from the prior step and using target recursion, the overall frontier computations are reused. The remaining bottleneck is the per-symbol cylinder check `is_cylinder` (Fig. 9). Three shortcuts avoid or reduce this cost, each justified by a proposition about the structure of the precovers. *Non-cylinder monotonicity* and *cylinder uniqueness* enable skipping BFS for some settings. *Combined universality* resolves additional symbols by examining how a frontier partitions into committed and boundary elements.

(1) Non-cylinder shortcut. Strings in $\mathcal{R}(\mathbf{y})$ cannot be quotient elements for \mathbf{y} . And since $\langle \mathcal{Q}(\mathbf{y}\mathbf{y}') \rangle \subseteq \langle \mathcal{Q}(\mathbf{y}) \rangle$, they are not quotient elements for the strictly more restrictive $\mathbf{y}\mathbf{y}'$ either. The expensive cylinder check (line 160) is thus skipped for these seeds (line 151).

Proposition C.3 (Non-cylinder monotonicity). *If $\mathbf{x} \in \mathcal{R}(\mathbf{y})$ then $\mathbf{x} \notin \mathcal{Q}(\mathbf{y}\mathbf{y}')$ for all $\mathbf{y}' \in \mathcal{Y}$.*

Proof. We have that $\mathbf{x} \in \mathcal{R}(\mathbf{y})$ implies $\langle \mathbf{x} \rangle \not\subseteq \mathcal{P}(\mathbf{y})$. Since $\mathcal{P}(\mathbf{y}\mathbf{y}') \subseteq \mathcal{P}(\mathbf{y})$, and thus $\langle \mathbf{x} \rangle \not\subseteq \mathcal{P}(\mathbf{y}\mathbf{y}')$, so $\mathbf{x} \notin \mathcal{Q}(\mathbf{y}\mathbf{y}')$. ■

(2) Cylinder uniqueness shortcut. Since the transformations we consider are functions, at most one output symbol \mathbf{y} can have \mathbf{x} as a cylinder element. Once a cylinder element is found, the cylinder check is skipped for the remaining output symbols (line 159).

Proposition C.4 (Cylinder uniqueness). *For a function f and target prefix \mathbf{y} , $\mathbf{x} \in \mathcal{Q}(\mathbf{y}\mathbf{y}') \cap \mathcal{Q}(\mathbf{y}\mathbf{y}'') \implies \mathbf{y} = \mathbf{y}' = \mathbf{y}''$.*

Proof. Suppose $\mathbf{y} \neq \mathbf{y}'$ and $\mathbf{x} \in \mathcal{Q}(\mathbf{y}\mathbf{y}') \cap \mathcal{Q}(\mathbf{y}\mathbf{y}'')$. Then $\langle \mathbf{x} \rangle \subseteq \mathcal{P}(\mathbf{y}\mathbf{y}') \cap \mathcal{P}(\mathbf{y}\mathbf{y}'') = f^{-1}(\mathbf{y}\mathbf{y}'\mathcal{Y}^*) \cap f^{-1}(\mathbf{y}\mathbf{y}''\mathcal{Y}^*) = \emptyset$, where the last equality holds because f is a function and $\mathbf{y}\mathbf{y}'\mathcal{Y}^* \cap \mathbf{y}\mathbf{y}''\mathcal{Y}^* = \emptyset$. This contradicts $\langle \mathbf{x} \rangle \neq \emptyset$. ■

(3) Combined universality shortcut. Given $\mathbf{x} \in \mathcal{Q}(\mathbf{y})$ and $\hat{\mathbf{y}} \in \mathcal{Y}$, we want to determine whether $\mathbf{x} \in \mathcal{Q}(\mathbf{y}\hat{\mathbf{y}})$ using the covering frontier at \mathbf{y} without running a full powerset BFS. The frontier `run`(\mathbf{x}, \mathbf{y}) partitions into *committed* elements (s, \mathbf{b}) with $\mathbf{b} \succeq \mathbf{y}\hat{\mathbf{y}}$ (the accumulated output already extends past \mathbf{y} with symbol $\hat{\mathbf{y}}$) and *boundary* elements (s, \mathbf{b}) with $\mathbf{b} = \mathbf{y}$ (the next output symbol is undetermined). The committed states alone may not be universal—some input symbols may lack outgoing transitions from committed states. Boundary states can fill the gaps, provided every transition from a boundary state produces $\hat{\mathbf{y}}$ as its next output symbol.

Proposition C.5 (Combined universality). *Let $\mathbf{x} \in \mathcal{Q}(\mathbf{y})$, $\hat{\mathbf{y}} \in \mathcal{Y}$, and define*

$$\begin{aligned} S_c &= \{s \mid (s, \mathbf{b}) \in \text{run}(\mathbf{x}, \mathbf{y}), \mathbf{b} \succeq \mathbf{y}\hat{\mathbf{y}}\}, \\ S_b &= \{s \mid (s, \mathbf{b}) \in \text{run}(\mathbf{x}, \mathbf{y}), \mathbf{b} = \mathbf{y}\} \end{aligned}$$

If the union $S_c \cup S_b$ is universal (i.e., $\llbracket \text{proj}_{\mathcal{X}}(\mathbf{f}_{[S_c \cup S_b]}) \rrbracket = \mathcal{X}^$), $S_c \cap F \neq \emptyset$, and every transition from a boundary state produces $\hat{\mathbf{y}}$, except that ε -input transitions may produce ε (i.e., $s \in S_b$ and $s \xrightarrow{\varepsilon} s' \in \mathbb{T}$ implies $\mathbf{y} = \hat{\mathbf{y}}$ or $(\mathbf{x} = \varepsilon \wedge \mathbf{y} = \varepsilon)$), then $\mathbf{x} \in \mathcal{Q}(\mathbf{y}\hat{\mathbf{y}})$.*

Proof. Let $\mathbf{x}' \in \mathcal{X}^*$ be arbitrary. By universality of $S_c \cup S_b$, there exists $(s, \mathbf{b}) \in \text{run}(\mathbf{x}, \mathbf{y})$ with $s \in S_c \cup S_b$ such that s has an accepting run on \mathbf{x}' in the input projection. If $s \in S_c$, then $\mathbf{b} \succeq \mathbf{y}\hat{\mathbf{y}}$, so the output of the corresponding path in \mathbf{f} already begins with $\mathbf{y}\hat{\mathbf{y}}$, giving $\mathbf{x}\mathbf{x}' \in \mathcal{P}(\mathbf{y}\hat{\mathbf{y}})$. If $s \in S_b$, then $\mathbf{b} = \mathbf{y}$. By the exclusivity hypothesis, every non- ε -input transition from s produces output $\hat{\mathbf{y}}$, and ε -input transitions produce $\hat{\mathbf{y}}$ or ε . States reachable from s via ε -arcs are also in S_b (since the frontier is ε -closed and the buffer is unchanged), so they satisfy the same constraint. Therefore the first non- ε output along any path from s is $\hat{\mathbf{y}}$, and the output begins with $\mathbf{y}\hat{\mathbf{y}}$, giving $\mathbf{x}\mathbf{x}' \in \mathcal{P}(\mathbf{y}\hat{\mathbf{y}})$. Since \mathbf{x}' was arbitrary, $\langle \mathbf{x} \rangle \subseteq \mathcal{P}(\mathbf{y}\hat{\mathbf{y}})$, i.e., $\mathbf{x} \in \mathcal{Q}(\mathbf{y}\hat{\mathbf{y}})$. ■

This shortcut is complementary to the IP-universality shortcut (Prop. C.6): IP-universality is a per-state property, while combined universality is a set-level property that leverages partial coverage from both committed and boundary states.

The proposition requires set-level universality of $S_c \cup S_b$ (the input-projection NFA started from those states accepts \mathcal{X}^*). In practice, we use a stronger but cheaper sufficient condition: we require every individual state in $S_c \cup S_b$ to be in the precomputed U. This runs in $O(|\mathcal{F}|)$ time, whereas the set-level check requires a powerset BFS that may be as expensive as the full `is_cylinder` check this shortcut is meant to avoid.

```

175 def combined_universal( $\mathcal{F}, \mathbf{y}\hat{\mathbf{y}}$ ):
176    $S_c \leftarrow \{s \mid (s, \mathbf{b}) \in \mathcal{F}, \mathbf{b} \succeq \mathbf{y}\hat{\mathbf{y}}\}$  # covered
177    $S_b \leftarrow \{s \mid (s, \mathbf{b}) \in \mathcal{F}, \mathbf{b} = \mathbf{y}\}$  # boundary
178   if  $\exists s \in S_c \cup S_b: s \notin U$ : return False
179   # Non- $\varepsilon$  input must produce  $\hat{\mathbf{y}}$ ;  $\varepsilon$  input may produce  $\varepsilon$ 
180   for  $s \in S_b$ :
181     for  $(\_ \xrightarrow{x:y} s') \in T(s)$ :
182       if not  $(y = \hat{\mathbf{y}}$  or  $(x = \varepsilon \wedge y = \varepsilon))$ ):
183         return False
184   return  $S_c \cap F \neq \emptyset$ 

```

C.6 INPUT-PROJECTION UNIVERSALITY SHORTCUT (`fast_univ_filter`)

Recall that the cylinder check `is_cylinder` verifies whether every extension of a source prefix maps through the target prefix, using a powerset BFS that can be expensive. A cheap sufficient condition avoids it in many cases: a state $s \in S$ is **input-projection universal** if the input projection of the transducer started from s accepts all of \mathcal{X}^* —intuitively, no matter what input follows, the transducer can still produce output. Let $U \subseteq S$ be the set of all input-projection universal states.

Proposition C.6 (IP-universality shortcut). *If some covering frontier state of \mathbf{x} with respect to \mathbf{y} is IP-universal, then \mathbf{x} is a cylinder: $(\exists (s, \mathbf{b}) \in \text{run}(\mathbf{x}, \mathbf{y}) : \mathbf{b} \succeq \mathbf{y} \wedge s \in U) \implies \mathbf{x} \in \mathcal{Q}(\mathbf{y})$.*

Proof. Let $(s, \mathbf{b}) \in \text{run}(\mathbf{x}, \mathbf{y})$ with $\mathbf{b} \succeq \mathbf{y}$ and $s \in U$ be the witness from the antecedent. Then $\llbracket \text{proj}_{\mathcal{X}}(f_{[s]}) \rrbracket = \mathcal{X}^*$, so for any $\mathbf{x}' \in \mathcal{X}^*$, there exists an accepting run of f on $\mathbf{x}\mathbf{x}'$ passing through s with output prefix \mathbf{y} . Hence $\mathbf{x}\mathbf{x}' \in \mathcal{P}(\mathbf{y})$. Since \mathbf{x}' was arbitrary, $\langle \mathbf{x} \rangle \subseteq \mathcal{P}(\mathbf{y})$, i.e., $\mathbf{x} \in \mathcal{Q}(\mathbf{y})$. ■

Fig. 12 shows how to efficiently precompute the set of input-projection universal states. We first input-project the transducer and remove ε -transitions (replacing each path $s \xrightarrow{\varepsilon} \dots \xrightarrow{\varepsilon} s' \xrightarrow{x} s''$ with a direct transition $s \xrightarrow{x} s''$; see, e.g., Hopcroft et al. 2001, Ch. 2) to obtain an ε -free NFA \mathbf{A} over \mathcal{X} . Both operations preserve the state set: input projection drops output labels, and ε -removal modifies only transitions (adding shortcuts through ε -closures), so $S_{\mathbf{A}} = S$ and states in U correspond directly to transducer states in the frontier. A state s of \mathbf{A} is input-projection universal iff it is accepting and, for every $x \in \mathcal{X}$, has at least one x -successor that is also input-projection universal—a greatest-fixpoint condition. We compute the fixpoint in linear time using an algorithm analogous to Kahn’s algorithm for topological sorting (Kahn, 1962): initialize the candidate set U to the accepting states of \mathbf{A} and maintain per-state, per-symbol successor counts. When a count reaches zero, remove the state and propagate the change to its predecessors via a reverse transition index. Each transition is processed at most once, yielding $\mathcal{O}(|T_{\mathbf{A}}|)$ time.

The shortcut can be integrated into `is_cylinder` (Fig. 9) as a fast path in `is_cylinder`:

```

205 def is_cylinder( $\mathbf{x}, \mathbf{y}$ ): # memoize
206   if fast_univ_filter( $\mathbf{x}, \mathbf{y}$ ): return True # fast path
207    $N \leftarrow |\mathbf{y}|$ 
208   ... # continue BFS as before

```

For transducers in which most accepting states are input-projection universal, this shortcut avoids the universality BFS in `is_cylinder` for the vast majority of cylinder checks. In BPE, where all states are input-projection universal, the universality BFS is never needed.

C.7 MEMOIZATION AND BATCHING OF $p_{\mathcal{X}}$

The source LM is queried in two places: first during decomposition, where probability-mass pruning calls $\overrightarrow{p_{\mathcal{X}}}(\mathbf{x})$ to rank candidates, and then during scoring, where `prefix_prob` and `next_dist` sum $\overrightarrow{p_{\mathcal{X}}}(\mathbf{x})$ and $p_{\mathcal{X}}(\mathbf{x})$ over the quotient and remainder. These calls involve many overlapping source prefixes. Naïvely, each call recomputes the entire chain $\overrightarrow{p_{\mathcal{X}}}(x_1) \cdot \overrightarrow{p_{\mathcal{X}}}(x_2 \mid x_1) \dots$ from scratch. Memoizing the conditional $\overrightarrow{p_{\mathcal{X}}}(\cdot \mid \mathbf{x})$ avoids this: given a cached state for \mathbf{x} , extending by one symbol x requires a single conditional evaluation rather than replaying the entire history.

For transformer language models, the cached state is the *key-value (KV) cache*: the accumulated key and value tensors from the self-attention layers. Extending by one token reuses the cached KV entries and runs a single forward pass for the new position. Moreover, most LMs return the complete next-symbol distribution $\overrightarrow{p_{\mathcal{X}}}(\cdot \mid \mathbf{x})$ in a single call, so we cache the full distribution rather than

```

185 # Preprocess: input-project and  $\varepsilon$ -remove
186  $A \leftarrow \text{eps-remove}(\text{proj}_{\mathcal{X}}(f))$ 
187 # queue-based greatest fixpoint
188  $U \leftarrow F_A$ ;  $q \leftarrow \emptyset$ 
189  $\text{count}[:, :] \leftarrow 0$ 
190 for  $(s \xrightarrow{x} s') \in T_A$  with  $s' \in U$ :
191    $\text{count}[s, x] += 1$ 
192 for  $s \in U$ :
193   if  $\exists x \in \mathcal{X}$ :  $\text{count}[s, x] = 0$ :
194      $q.\text{add}(s)$ 
195 while  $q \neq \emptyset$ :
196    $s' \leftarrow q.\text{pop}()$ 
197    $U \leftarrow U \setminus \{s'\}$ 
198 for  $(s, x)$  with  $(s \xrightarrow{x} s') \in T_A$ :
199    $\text{count}[s, x] -= 1$ 
200   if  $\text{count}[s, x] = 0$  and  $s \in U$ :
201      $q.\text{add}(s)$ 
202 def  $\text{fast\_univ\_filter}(x, y)$ :
203   # Does any covering frontier state have a universal input projection?
204   return  $\exists (s, b) \in \text{run}(x, y)$ :  $b \succeq y \wedge s \in U$ 

```

Figure 12: Efficient computation of input-projection universal states and the `fast_univ_filter` method that uses them.

individual values. When the extension loop generates children $\mathbf{x}x_1, \dots, \mathbf{x}x_k$, their prefix probabilities are read directly from the cached distribution without additional LM calls.²⁶

Batching while pruning. The `prune` step (§ C.3) needs $\vec{p}_{\mathcal{X}}(\mathbf{x})$ for every string \mathbf{x} in the queue. Many of these strings share a common prefix but extend by different symbols. We group the queue by parent: for each parent $\mathbf{x}_{<N}$ whose next-symbol distribution $\vec{p}_{\mathcal{X}}(\cdot | \mathbf{x}_{<N})$ is not yet cached, we issue a single batched LM call. Each call returns the full distribution, from which $\vec{p}_{\mathcal{X}}(\mathbf{x}_{<N}\mathbf{x}) = \vec{p}_{\mathcal{X}}(\mathbf{x}_{<N}) \cdot \vec{p}_{\mathcal{X}}(\mathbf{x} | \mathbf{x}_{<N})$ is read off for all children simultaneously. On GPU-based LMs, batching these parent contexts into a single forward pass amortizes the per-call overhead.

C.8 REALIZING THE AUTOREGRESSIVE INTERFACE

Given the decomposition, the transduced LM interface from § C.1 is implemented as follows. The prefix probability $\vec{p}_{\mathcal{Y}}(\mathbf{y})$ sums LM prefix probabilities over \mathcal{Q} and LM string probabilities over \mathcal{R} . The string probability $p_{\mathcal{Y}}(\mathbf{y})$ sums over the exact preimage. The next-symbol distribution $\vec{p}_{\mathcal{Y}}(\cdot | \mathbf{y})$ is computed via `decompose_next`, which provides the per-symbol decompositions and exact preimage in a single BFS pass; the computational cost is dominated by `decompose_next`, and once the per-symbol quotients, remainders, and preimage are available, the scoring reduces to lookups into the memoized source LM (§ C.7).

```

209 def  $\text{prefix\_prob}(\mathbf{y})$ :
210    $(Q, R) \leftarrow \text{decompose}(\mathbf{y})$ 
211   return  $\sum_{\mathbf{x} \in Q} \vec{p}_{\mathcal{X}}(\mathbf{x}) + \sum_{\mathbf{x} \in R} p_{\mathcal{X}}(\mathbf{x})$ 
212 def  $\text{prob}(\mathbf{y})$ :
213    $(\_, \_, \text{ps}) \leftarrow \text{decompose\_next}(\mathbf{y})$ 
214   return  $\sum_{\mathbf{x} \in \text{ps}} p_{\mathcal{X}}(\mathbf{x})$ 
215 def  $\text{next\_dist}(\mathbf{y})$ :
216    $(\text{qs}, \text{rs}, \text{ps}) \leftarrow \text{decompose\_next}(\mathbf{y})$ 
217    $\bar{p} \leftarrow \{\}$ ;  $Z \leftarrow \text{prefix\_prob}(\mathbf{y})$ 
218   for  $\mathbf{x} \in \text{ps}$ :  $\bar{p}[\text{EOS}] += p_{\mathcal{X}}(\mathbf{x})/Z$ 
219   for  $y \in \text{qs.keys()} \cup \text{rs.keys}()$ :
220     for  $\mathbf{x} \in \text{qs}[y]$ :  $\bar{p}[y] += \vec{p}_{\mathcal{X}}(\mathbf{x})/Z$ 
221     for  $\mathbf{x} \in \text{rs}[y]$ :  $\bar{p}[y] += p_{\mathcal{X}}(\mathbf{x})/Z$ 
222   return  $\bar{p}$ 

```

Figure 13: Fast implementation of the autoregressive interface using `decompose_next`.

²⁶Our implementation uses `genlm` (<https://github.com/genlm/genlm-backend>) for its seamless caching and auto-batching interface.

For reference, the naïve next-symbol distribution computes `prefix_prob(yy)` independently for each y (see §C.1). The reference implementation is correct, but inefficient because it does not share work: each `prefix_prob(yy')` call triggers its own `decompose` BFS, and it does not benefit from the non-cylinder shortcut, target recursion, or cache population described in §C.4.

C.9 ALL-UNIVERSAL FAST PATH

When every transducer state is IP-universal, the remainder is always empty and every newly discovered element is immediately a quotient element, so decomposition terminates in a single BFS round. If, additionally, every non- ε -input arc produces at least one output symbol, then boundary frontier elements can be resolved in closed form via a precomputed first-output table. Together, these two conditions let `next_dist` (Fig. 13) simplify into `all_universal_next_dist` (Fig. 14). We describe the simplifications below (normalization is unchanged).

Decompose (simplified). Because every state is IP-universal, $\mathcal{R}(y) = \emptyset$ for all y : every source prefix in the precover is in the quotient. The call to `decompose(y)` (Fig. 2) terminates in a single BFS round—every newly discovered element is immediately classified as a quotient element. This makes `decompose_next` unnecessary: the per-symbol classification is absorbed into the scoring below.

Score (simplified). For each $(\mathcal{F}, \mathbf{x}) \in \mathcal{Q}$, the frontier partitions into *committed* elements (s, \mathbf{b}) with $\mathbf{b} \succ \mathbf{y}$ and *boundary* elements with $\mathbf{b} = \mathbf{y}$, as in the combined universality shortcut (§C.5). Committed elements have already determined their next output symbol $\hat{y} = \mathbf{b}_{N+1}$; because all states are IP-universal, each contributes $\vec{p}_{\mathcal{X}}(\mathbf{x})$ directly to $\vec{p}[\hat{y}]$; thus, no expansion is needed.

Boundary elements $(\mathbf{b} = \mathbf{y})$ need one more source symbol to commit to an output. The no- ε -output precondition ensures that each non- ε -input arc produces at least one output symbol, so a precomputed *first-output table* $\mathbf{fo}(S, \mathbf{x})$ (defined in the pseudocode) maps each input symbol to the unique output it produces from a given powerstate. This symbol is unique: functionality of f requires that all transitions on x from states in S produce the same output, since IP-universality guarantees each successor has an accepting continuation (so both outputs would be realized). Each boundary element is thus resolved with a single batched LM call: $\ell = \vec{p}_{\mathcal{X}}(\cdot | \mathbf{x})$ is queried once per quotient element, and for each $x \in \mathcal{X}$, the mass $\vec{p}_{\mathcal{X}}(\mathbf{x}) \cdot \ell(x)$ is attributed to $\mathbf{fo}(S, \mathbf{x})$. If any boundary state is accepting, the LM’s EOS probability contributes $\vec{p}_{\mathcal{X}}(\mathbf{x}) \cdot \ell(\text{EOS})$ to $\vec{p}[\text{EOS}]$.

The f_{α} transducers satisfy both preconditions (Tab. 4: all states IP-universal, no ε -output on non- ε -input arcs), explaining their substantially higher throughput (§7). The DNA transducer f_{dna2aa} has all states IP-universal but uses ε -output arcs (the first two bases of each codon emit no amino acid), so the fast path does not apply.

```

223 def all_universal_next_dist(y):
224     (Q, _) ← decompose(y) # R = ∅ always
225     p̄ ← {}; Z ← prefix_prob(y)
226     for (F, x) in Q:
227         # Committed: output past target
228         for ŷ ∈ {bN+1 | (s, b) ∈ F, b ≻ y}:
229             p̄[ŷ] += px(x)
230         # Boundary: output = target
231         Sb ← {s | (s, b) ∈ F, b = y}
232         if Sb ≠ ∅:
233             ℓ ← px(· | x) # one LM call
234             for x ∈ X:
235                 ŷ ← fo(Sb, x)
236                 if ŷ ≠ ⊥:
237                     p̄[ŷ] += px(x) · ℓ(x)
238             if ∃ s ∈ Sb: s ∈ F:
239                 p̄[EOS] += px(x) · ℓ(EOS)
240     return p̄/Z

```

```

241 def fo(S, x):
242     for (x →y s') ∈ T(S, x):
243         # Unique if functional &
244         # all states IP-universal
245         return y
246     return ⊥

```

Figure 14: `all_universal_next_dist`: specialization of `next_dist` (Fig. 13) when all states are IP-universal and every non- ε -input arc produces output. $R = \emptyset$ always, so only Q contributes. Boundary elements are resolved via `fo`, requiring one LM call per quotient element.

D PROOFS FOR FINITENESS CONDITIONS

D.1 PROPERTIES OF PREFIX MONOTONE MAPS

Proposition 6.1. *The following are equivalent: (i) f is prefix monotone (ii) $f(\langle \mathbf{x} \rangle) \subseteq \langle f(\mathbf{x}) \rangle$ for all $\mathbf{x} \in \mathcal{X}^*$ (iii) $\mathcal{P}(f(\mathbf{x})) = \mathcal{C}(f(\mathbf{x}))$ for all $\mathbf{x} \in \mathcal{X}^*$ (iv) f is prefix-continuous.*

Proof. (1) \Rightarrow (2): Prefix monotonicity means that for any $\mathbf{x}, \mathbf{x}' \in \mathcal{X}^*$, if we have that $\mathbf{x} \preceq \mathbf{x}\mathbf{x}'$ then $f(\mathbf{x}) \preceq f(\mathbf{x}\mathbf{x}')$ and thus that there exists a $\mathbf{y} \in \mathcal{Y}^*$ such that $f(\mathbf{x}\mathbf{x}') = f(\mathbf{x})\mathbf{y}$. And since \mathbf{x}' was chosen arbitrarily (2) holds.

(2) \Rightarrow (3): Let $\mathbf{x} \in \mathcal{X}^*$. Suppose $f(\langle \mathbf{x} \rangle) \subseteq \langle f(\mathbf{x}) \rangle$. Then, $\langle \mathbf{x} \rangle \subseteq f^{-1}(f(\langle \mathbf{x} \rangle)) \subseteq \mathcal{P}(f(\mathbf{x}))$. Note that, for any $\mathbf{x}' \in \mathcal{P}(f(\mathbf{x}))$, $\mathcal{P}(f(\mathbf{x}')) \subseteq \mathcal{P}(f(\mathbf{x}))$. Therefore, $\langle \mathbf{x}' \rangle \subseteq \mathcal{P}(f(\mathbf{x}')) \subseteq \mathcal{P}(f(\mathbf{x}))$ and so $\mathbf{x}' \in \mathcal{C}(f(\mathbf{x}))$. This shows that $\mathcal{P}(f(\mathbf{x})) = \mathcal{C}(f(\mathbf{x}))$.

(3) \Rightarrow (4): By assumption, any element in the precover is an extension of a quotient element, and thus a member in the cylinder over quotient elements.

(4) \Rightarrow (1): Assume f is prefix-continuous, i.e., $\mathcal{P}(\mathbf{y})$ is cylindrical for all \mathbf{y} . Let $\mathbf{x} \preceq \mathbf{x}'$. Since $f(\mathbf{x}) \preceq f(\mathbf{x}')$, we have $\mathbf{x} \in \mathcal{P}(f(\mathbf{x}'))$. By prefix-continuity, $\mathcal{P}(f(\mathbf{x}'))$ is cylindrical, so $\langle \mathbf{x} \rangle \subseteq \mathcal{P}(f(\mathbf{x}'))$. In particular, $\mathbf{x}' \in \mathcal{P}(f(\mathbf{x}'))$, which gives $f(\mathbf{x}) \preceq f(\mathbf{x}')$. ■

D.2 QUOTIENT BOUND FOR STRICT-PREFIX MONOTONE MAPS

The following proposition bounds the size of the quotient when the map is strict-prefix monotone.

Proposition D.1. *Let $f: \mathcal{X}^* \rightarrow \mathcal{Y}^*$ be a strict-prefix monotone map. Then, for every $\mathbf{y} \in \mathcal{Y}^*$:*

1. $f^{-1}(\mathbf{y}) = \mathcal{Q}(\mathbf{y}) \setminus \bigsqcup_{y \in \mathcal{Y}} \mathcal{Q}(\mathbf{y}y)$
2. $\bigsqcup_{y \in \mathcal{Y}} \mathcal{Q}(\mathbf{y}y) \subseteq \mathcal{Q}(\mathbf{y})(\mathcal{X} \sqcup \{\varepsilon\})$
3. $|\mathcal{Q}(\mathbf{y})| \leq (|\mathcal{X}| + 1)^{|\mathbf{y}|}$

Proof. (1) Observe that (using Proposition 6.1) for every $\mathbf{y} \in \mathcal{Y}^*$

$$\mathcal{C}(\mathbf{y}) = \mathcal{P}(\mathbf{y}) = f^{-1}(\mathbf{y}) \sqcup \bigsqcup_{y \in \mathcal{Y}} \mathcal{P}(\mathbf{y}y) = f^{-1}(\mathbf{y}) \sqcup \bigsqcup_{y \in \mathcal{Y}} \mathcal{C}(\mathbf{y}y) \quad (11)$$

In particular, the minimality of $\mathcal{Q}(\mathbf{y})$ in $\mathcal{P}(\mathbf{y})$ implies that

$$\mathcal{Q}(\mathbf{y}) \cap \bigsqcup_{y \in \mathcal{Y}} \mathcal{Q}(\mathbf{y}y) = \mathcal{Q}(\mathbf{y}) \cap \bigsqcup_{y \in \mathcal{Y}} \langle \mathcal{Q}(\mathbf{y}y) \rangle \quad (12)$$

Consequently, we obtain the identity $f^{-1}(\mathbf{y}) = \mathcal{C}(\mathbf{y}) \setminus \bigsqcup_{y \in \mathcal{Y}} \mathcal{C}(\mathbf{y}y) = \langle \mathcal{Q}(\mathbf{y}) \rangle \setminus \bigsqcup_{y \in \mathcal{Y}} \langle \mathcal{Q}(\mathbf{y}y) \rangle$, which in turn yields the inclusion

$$\mathcal{Q}(\mathbf{y}) \setminus \bigsqcup_{y \in \mathcal{Y}} \mathcal{Q}(\mathbf{y}y) = \mathcal{Q}(\mathbf{y}) \setminus \bigsqcup_{y \in \mathcal{Y}} \langle \mathcal{Q}(\mathbf{y}y) \rangle \subseteq f^{-1}(\mathbf{y}) \quad (13)$$

For the reverse inclusion, let $\mathbf{x}' \in f^{-1}(\mathbf{y})$. Then there exists a unique $\mathbf{x}_q \in \mathcal{Q}(\mathbf{y})$ such that $\mathbf{x}_q \preceq \mathbf{x}'$, by definition of the quotient set. Since f is strict-prefix monotone and $f(\mathbf{x}_q) \preceq f(\mathbf{x}') = \mathbf{y}$, we must have $\mathbf{x}_q = \mathbf{x}'$. This shows that $f^{-1}(\mathbf{y}) \subseteq \mathcal{Q}(\mathbf{y})$, and completes the proof of (1).

(2) Fix $y \in \mathcal{Y}$, $\mathbf{y} \in \mathcal{Y}^*$ and let $\mathbf{x} \in \mathcal{Q}(\mathbf{y}y)$. There exists a unique $\mathbf{x}_y \in \mathcal{Q}(\mathbf{y})$ such that $\mathbf{x}_y \preceq \mathbf{x}$. Intersecting $\langle \mathbf{x}_y \rangle$ with both sides of (11), one obtains

$$\langle \mathbf{x}_y \rangle = (\langle \mathbf{x}_y \rangle \cap f^{-1}(\mathbf{y})) \sqcup \bigsqcup_{y' \in \mathcal{Y}} (\langle \mathbf{x}_y \rangle \cap \mathcal{C}(\mathbf{y}y')) \quad (14)$$

$$= (\langle \mathbf{x}_y \rangle \cap f^{-1}(\mathbf{y})) \sqcup \langle \mathbf{x} \rangle \sqcup C_{\mathbf{x}} \quad (15)$$

where $C_{\mathbf{x}} \stackrel{\text{def}}{=} \bigsqcup_{y' \in \mathcal{Y}} (\langle \mathbf{x}_y \rangle \cap \mathcal{C}(\mathbf{y}y')) \setminus \langle \mathbf{x} \rangle$. Note that this set is cylindrical. By strict monotonicity we have $|\langle \mathbf{x}_y \rangle \cap f^{-1}(\mathbf{y})| \leq 1$. Hence either: (i) $\langle \mathbf{x}_y \rangle \cap f^{-1}(\mathbf{y}) = \emptyset$, in which case

$$\mathbf{x} = \mathbf{x}_y \in \mathcal{Q}(\mathbf{y}) \cap \mathcal{Q}(\mathbf{y}y),$$

or (ii) $\langle \mathbf{x}_y \rangle \cap f^{-1}(\mathbf{y}) = \{\mathbf{x}_y\}$. Then there exists a word $z \in \mathcal{X}^*$ such that $\mathbf{x} = \mathbf{x}_y z$. Let $z' \prec z$. If $z' \neq \varepsilon$, then $\mathbf{x}_y z' \in C_{\mathbf{x}}$. Since $C_{\mathbf{x}}$ is cylindrical, it contains $\langle \mathbf{x}_y z' \rangle$ and in particular it must contain $\langle \mathbf{x} \rangle$ contradicting the definition of $C_{\mathbf{x}}$. Therefore no non-empty proper prefix $z' \prec z$ exists, so z is a single symbol $x \in \mathcal{X}$ and

$$\mathbf{x} = \mathbf{x}_y x \in \mathcal{Q}(\mathbf{y})\mathcal{X}.$$

(3) For any $\mathbf{y} \in \mathcal{Y}^*$ and any $y \in \mathcal{Y}$, we have from (2),

$$|\mathcal{Q}(\mathbf{y}y)| \leq (|\mathcal{X}| + 1)|\mathcal{Q}(\mathbf{y})| \quad (16)$$

Iterating this bound along any string $\mathbf{y} \in \mathcal{Y}^*$, we have:

$$|\mathcal{Q}(\mathbf{y})| \leq (|\mathcal{X}| + 1)^{|\mathbf{y}|} |\mathcal{Q}(\varepsilon)| = (|\mathcal{X}| + 1)^{|\mathbf{y}|} \quad \blacksquare$$

D.3 SUFFICIENT CONDITIONS FOR FINITE QUOTIENTS AND REMAINDERS

Lemma 6.1 below gives sufficient conditions for when one can derive a finite precover decomposition. An example of such a transducer is given in Example 3.

Lemma 6.1. *Let $f: \mathcal{X}^* \rightarrow \mathcal{Y}^*$ be a function realized by a transducer \mathbf{f} . The decomposition $(\mathcal{Q}(\mathbf{y}), \mathcal{R}(\mathbf{y}))$ is finite for every $\mathbf{y} \in \mathcal{Y}^*$ if:*

- (i) No ε -output cycles: \mathbf{f} contains no cycle in which every arc outputs ε .
- (ii) Safety: Every state of \mathbf{f} is **safe**, defined inductively as the smallest set such that s is safe if: (a) s is IP-universal; (b) $\|\llbracket \mathbf{f}_{[s]} \rrbracket\| < \infty$ (finite closure); or (c) for all transitions $s \xrightarrow{x:y} s'$, s' is safe.

Proof. Fix $\mathbf{y} \in \mathcal{Y}^*$; we show that $\mathcal{Q}(\mathbf{y})$ and $\mathcal{R}(\mathbf{y})$ are finite. Let $\Pi_{\mathbf{y}}$ be the set of all paths in \mathbf{f} that emit exactly \mathbf{y} , i.e., $\Pi_{\mathbf{y}} \stackrel{\text{def}}{=} \{s_0 \xrightarrow{x_1:y_1} s_1 \cdots s_{N-1} \xrightarrow{x_N:y_N} s_N \mid s_0 \in I, y_1 \cdots y_N = \mathbf{y}\}$. By condition (i), the ε -output subgraph of \mathbf{f} is acyclic, so any sub-path that emits no output has length at most $|S|$. Since the total output is \mathbf{y} , each path has bounded length, and $\Pi_{\mathbf{y}}$ is finite. Let $\Pi_{\succeq \mathbf{y}}$ be the set of all valid paths formed by extending the roots in $\Pi_{\mathbf{y}}$ until they reach a state satisfying a safety base case. By condition (ii), every state of \mathbf{f} is safe—in particular, the end states of paths in $\Pi_{\mathbf{y}}$. This implies that no extension path can continue indefinitely without satisfying a base case (IP-universality or finite closure). Since a finite-state transducer has finite branching and no infinite valid extension paths, König’s Lemma implies that the tree of extensions is finite.²⁷ Thus, $\Pi_{\succeq \mathbf{y}}$ is a finite set.

Let $S_U \stackrel{\text{def}}{=} \{s \in S : s \text{ is IP-universal}\}$ and $S_C \stackrel{\text{def}}{=} \{s \in S : \|\llbracket \mathbf{f}_{[s]} \rrbracket\| < \infty\}$ be the sets of states satisfying conditions (a) and (b), respectively, and let $S_S \stackrel{\text{def}}{=} S_U \cup S_C$. We can decompose the set of extended paths disjointly based on their end state:

$$\Pi_{\succeq \mathbf{y}} = \{\rho \in \Pi_{\succeq \mathbf{y}} : \rho_{|\rho} \in S_U\} \sqcup \{\rho \in \Pi_{\succeq \mathbf{y}} : \rho_{|\rho} \in S_C\} \quad (17)$$

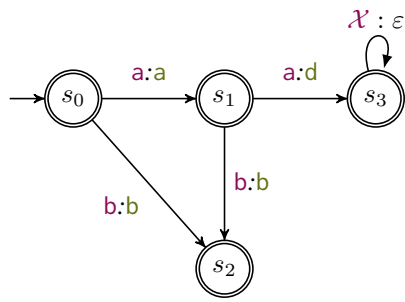
$$\begin{aligned} &= \{\pi \cdot s_{|\pi} \xrightarrow{\quad} s_N \mid \pi \in \Pi_{\mathbf{y}}, s_N \in S_U, \{s_{|\pi}, \dots, s_{N-1}\} \cap S_S = \emptyset\} \\ &\quad \sqcup \{\pi \cdot s_{|\pi} \xrightarrow{\quad} s_N \mid \pi \in \Pi_{\mathbf{y}}, s_N \in S_C, \{s_{|\pi}, \dots, s_{N-1}\} \cap S_S = \emptyset\} \end{aligned} \quad (18)$$

The first term corresponds to $\mathcal{Q}(\mathbf{y})$ by definition. Since $\Pi_{\succeq \mathbf{y}}$ is finite, this set is finite. The second term collects paths leading to states $s \in S_C$. The remainder $\mathcal{R}(\mathbf{y})$ consists of the input strings from these paths, concatenated with the finite language accepted by s . Since the number of paths is finite and the closure of each stopping state is finite, $\mathcal{R}(\mathbf{y})$ is finite. ■

Example 3. Consider the transducer below over $\mathcal{X} = \{a, b\}$, $\mathcal{Y} = \{a, b, d\}$, encoding a (partial) function f . The four states illustrate all cases of safety. State s_3 is universal: it is accepting and loops on every input symbol with ε -output, so $L(s_3) = \mathcal{X}^*$ (base case a). State s_2 has finite closure: it is accepting with no outgoing transitions, so $L(s_2) = \{\varepsilon\}$ (base case b). State s_1 is neither universal nor finite closure, but is safe by the recursive step (c): its successors s_3 (via **a**) and s_2 (via **b**) are both safe. Similarly, s_0 is safe because its successors s_1 (via **a**) and s_2 (via **b**) are both safe.

For target $\mathbf{y} = a$, the path set $\Pi_a = \{s_0 \xrightarrow{a:a} s_1\}$ is finite (condition i), with terminal state s_1 safe (condition ii). Extending from s_1 : input **a** reaches the universal state s_3 , contributing **aa** to $\mathcal{Q}(a)$; input **b** reaches the finite-closure state s_2 , contributing **ab** to $\mathcal{R}(a)$. The root string **a** is also in $\mathcal{R}(a)$: s_1 is accepting with $f(a) = a \succeq a$, but **a** is not cylindrical since **ab** cannot be further extended (stuck at s_2). Thus $\mathcal{Q}(a) = \{aa\}$ and $\mathcal{R}(a) = \{a, ab\}$.

²⁷König’s Lemma states that every infinite tree with finite branching must have an infinite path. Since our alphabet is finite (finite branching) and the Safety condition forbids cycles among non-base-case states (no infinite paths), the resulting tree of extensions must be finite.



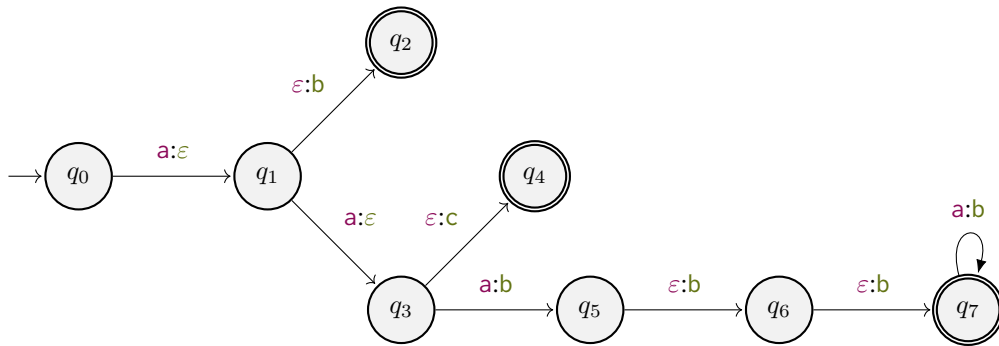


Figure 15: An FST that maps n occurrences of 'a' to the same number of 'b's, except when the input is exactly two 'a's, which are mapped to 'c'.

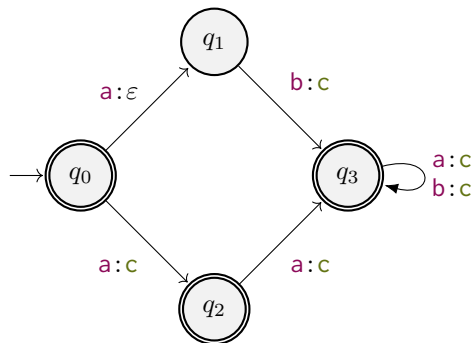


Figure 16: An FST where the ε -output arc $q_0 \xrightarrow{a:\varepsilon} q_1$ creates a frontier element whose output has not yet reached the target. For target $y = c$ and source prefix $x = a$, the frontier is $\mathcal{F} = \{(q_1, \varepsilon), (q_2, c)\}$. The covering states $\{q_2\}$ are not input-projection universal (q_2 has no arc on b), so `fast_univ_filter(a, c)` fails and a would be misclassified as non-quotient. However, q_1 handles input b and produces c , matching the target. The BFS in `is_cylinder` confirms universality over the full frontier, correctly placing a in $Q(c)$.

F EXPERIMENTAL SETUP

Here we detail the experimental setup for reproducing the experiments in §7 and §G.5.

F.1 DATASETS

For the tokens-to-byte and PTB experiments in §7, we choose the first 10 paragraphs (excluding headers) of the test split in the `wikitext-2-raw-v1` dataset (Merity et al., 2017) (corresponding to the first 7684 bytes) from the 🤗 Hugging Face datasets library. We use the first 256 bytes of the same dataset and split to run the experiments in §G.5. For the DNA experiments in §7, we sample 65 human proteins²⁸, each consisting of 4-12 amino acids, with their accession numbers given in Tab. 1.

Table 1: Accession numbers used in this study.

C0HLZ5	P01858	P0DPI4	P0DUS0	P84464
P84465	P0DOY5	P67857	P67858	P67859
P81826	P23210	P85003	P84071	P86168
C0HJF1	C0HJG0	P02729	P81010	P86909
P86922	B3EWE5	P0DMM6	P0DQM6	P0DQM7
P12481	P85002	B3EWR3	P01358	P02728
P0C005	P0DKX2	P0DMM7	P0DQM9	P0DX30
P22103	P84200	P84785	P84868	P86600
A8C8X2	B3A0L6	B3EUR5	C0HJM6	C0HLK7
P0DJC3	P0DJF4	P69208	P85444	P85870
P86942	A0A0A0MT89	B3EWS0	C0HJB6	C0HL84
C0HL88	P0C8I8	P0DQH7	P0DQH8	P0DQX4
P0DQX5	P58805	P69437	P82820	P83127

F.2 MODELS

We conduct experiments using GPT-2 Large (Radford et al., 2019), Llama 3.2-1B, Llama 3.1-8B and Phi-4 (14B; Abdin et al., 2024)²⁹ from the 🤗 Hugging Face hub (Wolf et al., 2020). We use the `GenLM` library³⁰ and the `vLLM` (Kwon et al., 2023) backend to efficiently evaluate the models.

For the PTB experiments we use `GenLM.bytes`³¹ to convert token-level models into byte-level models and compose them with f_{ptb} . For `GenLM.bytes` we use a beam size of $K=5$ and a pruning threshold of 0.001. For the DNA experiments we train a custom GPT-2 Small model³² on a human DNA dataset³³. The token set of the model is $\mathcal{X} = \{A, C, G, T\}$, eliminating the need for composing the model with a transducer f_{α} that maps from subword tokens to bytes. For training parameters, see Tab. 2, for training and validation metrics, see Tab. 3.

F.3 PARAMETERS

For all experiments, we use the pruning heuristic described in §C.3. For the experiments in §7 we report the results for different values of $n_{\max} \in \{5000, 10000, 15000, 20000, 25000, 30000\}$. For all other experiments, we set $n_{\max} = \infty$.

F.4 GPU USAGE

All experiments in §7 use a single NVIDIA GeForce RTX 4090 (24 GB), except Phi-4, which requires two. The benchmarks in §G.5 use an NVIDIA GeForce RTX 3090.

²⁸<https://www.uniprot.org/uniprotkb?query=Human>

²⁹Available under `openai/gpt2-large`, `meta-llama/Llama-3.2-1B`, `meta-llama/Llama-3.1-8B` and `microsoft/phi-4` at <https://huggingface.co>.

³⁰<https://github.com/genlm/genlm-backend>

³¹<https://github.com/genlm/genlm-bytes>

³²<https://huggingface.co/vesteinn/gpt2-dna>

³³https://huggingface.co/datasets/simecek/Human_DNA_v0.

Table 2: Training parameters for the GPT-2 small model, trained on a human DNA.

Parameter	Value
Learning Rate	0.0003
Optimizer	AdamW
	$\beta_1 = 0.9, \beta_2 = 0.999,$
	$\epsilon = 1e-8$
Learning Rate Scheduler	Linear
Warm-up Steps	1000
Train Batches (per device)	64
Eval Batches (per device)	8
Total Train Batches	256 (262,144 tokens)
Total Eval Batches	32
Epochs	10
Seed	42
Distributed Training	Multi-GPU (4 devices)
Mixed Precision	Native AMP

Table 3: Training and validation metrics for the GPT-2 small model, trained on a human DNA.

Step	Epoch	Train Loss	Val Loss	Acc (%)
5k	0.69	1.1252	1.1206	47.45
10k	1.38	1.0835	1.0814	49.91
15k	2.07	1.0641	1.0639	51.03
20k	2.76	1.0563	1.0547	51.63
25k	3.45	1.0504	1.0486	52.04
30k	4.14	1.0439	1.0439	52.33
35k	4.84	1.0425	1.0407	52.54
40k	5.53	1.0365	1.0380	52.71
45k	6.22	1.0325	1.0361	52.84
50k	6.91	1.0322	1.0341	52.96
55k	7.60	1.0307	1.0328	53.05
60k	8.29	1.0267	1.0316	53.13
65k	8.98	1.0273	1.0306	53.20
70k	9.67	1.0270	1.0299	53.24

F.5 DETAILS ON TRANSDUCERS USED IN EXPERIMENTS

Tab. 4 contains the number of states, IP-universal states, and transitions for the transducers described in §7. We construct all finite-state transducers using Pynini (Gorman, 2016). Note that for experiments using the Penn Treebank FST (f_{ptb}), we realize $p_{\mathcal{X}} \circ f_{\alpha}$ using **GenLM.bytes**, thereby keeping the number of states and arcs constant.

Table 4: Number of states, IP-universal states, and transitions.

Model	States	IP-Univ. States	Transitions
Tokens to Bytes			
$p_{\text{gpt2}} \circ f_{\alpha}$	75,723	75,723	125,979
$p_{\text{llama1B}} \circ f_{\alpha}$	176,990	176,990	305,244
$p_{\text{llama8B}} \circ f_{\alpha}$	176,990	176,990	305,244
$p_{\text{phi4}} \circ f_{\alpha}$	115,244	115,244	215,593
Tokens to Words			
$p_{\text{gpt2}} \circ f_{\alpha} \circ f_{\text{ptb}}$	479	56	26,962
$p_{\text{llama1B}} \circ f_{\alpha} \circ f_{\text{ptb}}$	479	56	26,962
$p_{\text{llama8B}} \circ f_{\alpha} \circ f_{\text{ptb}}$	479	56	26,962
$p_{\text{phi4}} \circ f_{\alpha} \circ f_{\text{ptb}}$	479	56	26,962
DNA to amino acids			
$p_{\text{dna}} \circ f_{\text{dna2aa}}$	21	21	84

Constructing the PTB transducer. We construct the PTB FST by encoding each tokenizer rule³⁴ as an FST that segments character sequences by inserting a distinguished separator symbol $\text{SEP} \notin \mathcal{Y}$. Specifically, the transducer inserts SEP at punctuation and clitic boundaries, and collapses whitespace characters (spaces, tabs, newlines, etc.) into SEP . Note that the resulting transduced language model is thus not a true distribution over PTB tokens, but over characters and separators corresponding to the same boundaries that the PTB tokens would have. This is a pragmatic decision, as the PTB tokenizer can tokenize any sentence into orthographic words. In other words, it would accept an infinite vocabulary. Such a transducer can be built on the fly and would be equivalent to one with infinitely many states. In this paper, we only use the finite version. An example of such a rule is given in Fig. 5, which inserts SEP before a comma if it is not followed by a digit. We then compose

³⁴See https://www.nltk.org/_modules/nltk/tokenize/treebank.html#TreebankWordTokenizer for the full specification.

these FSTs into a single transducer (f_{ptb}). Note that context-dependent rules, such as the one given in Fig. 5, introduce non-IP-universal states. For example, state q_2 only accepts $x \in \mathcal{X} \setminus \{0-9\}$. In fact, of the 479 states in f_{ptb} , just 56 are IP-universal.

The DNA to amino acid transducer. The DNA to amino-acid transducer, described in §7, is partially shown in Fig. 17.

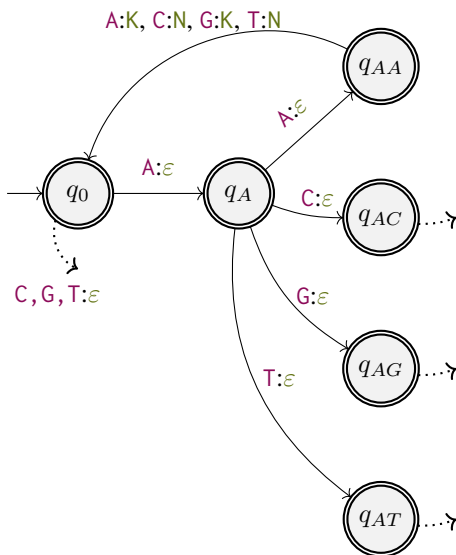


Figure 17: An FST for converting DNA sequences to amino acids. Each triplet of nucleobases maps to one of 20 different amino acids. We only show a proportion of the machine.

G ADDITIONAL EXPERIMENTAL RESULTS

Here we provide complementary results to the experiments presented in §7, using the algorithms described in §C. First, in §G.1 we compare our transducer-based method using f_α to **GenLM.bytes** (Vieira et al., 2025a), then give full JSD (§G.2) comparisons for f_α , f_{ptb} , and f_{dna2aa} . In §G.4 we report cross-entropy comparisons for f_α , and finally ablate the importance of IP-universal states (§G.5).

G.1 COMPARISON TO VIEIRA ET AL. (2025A)

Vieira et al. (2025a) convert token-level models to byte-level models using a beam-search algorithm parameterized by a beam size K . We compare our transducer-based approach with their method by computing the JSD between the two resulting distributions over the paragraphs from WikiText (§F). Tab. 6 uses genlm-bytes ($K = 32$, pruning threshold of 0.0) as a reference and varies our pruning threshold τ . As τ decreases, JSD drops, and our distributions converge to the baseline. At moderate thresholds ($\tau \leq 1e-3$), JSD is already below $1.5e-3$ for all models, confirming that the two methods produce closely matching distributions.

To verify that the two methods compute the same underlying distribution in the exact setting, we compare them with no pruning: $\tau = 0$ (no pruning) for our method and exact inference for genlm-bytes ($K = \infty$). Tab. 5 shows the per-position JSD and maximum absolute difference for the first 10 bytes of the WikiText evaluation data using $p_{\text{gpt2}} \circ f_\alpha$. The JSD values are on the order of $1e-14$ – $1e-15$, and the maximum absolute probability difference is at most $3.4e-6$, confirming that both methods give the same distribution within floating-point precision.

Tab. 7 reports the JSD and throughput of the baseline itself at $K \in \{8, 16, 32\}$, showing the accuracy–speed trade-off within their method. Reducing K from 32 to 8 substantially increases throughput while introducing only modest changes in JSD, indicating that the baseline’s approximation error at $K = 32$ is small. Note that the method of Vieira et al.

(2025a) is designed specifically for strictly prefix monotone transformations, a property that f_α satisfies. This specialization enables a trie-based algorithm that achieves a better accuracy–speed trade-off than our more general-purpose approach on this class of transformations.

Table 5: Exact comparison: our method ($\tau = 0$) vs. genlm-bytes (exact) for $p_{\text{gpt2}} \circ f_\alpha$.

Pos	Byte	JSD	max $ \Delta p $
0	R	3.9e-15	7.9e-7
1	o	6.5e-16	1.2e-6
2	b	3.5e-15	1.2e-6
3	e	4.4e-14	1.7e-6
4	r	4.5e-15	3.4e-6
5	t	1.8e-15	2.4e-6
6	_	1.1e-14	1.4e-6
7	B	1.9e-15	1.8e-6
8	o	6.1e-15	1.2e-6
9	u	1.3e-14	1.5e-6

Table 6: Average Jensen–Shannon divergence (JSD) and bytes/sec for various thresholds τ using $p_{\mathcal{X}} \circ f_{\alpha}$ against a reference distribution from Vieira et al. (2025a) with a beam size of $K=32$. 95% confidence intervals are given in parentheses.

τ	$p_{\text{gpt2}} \circ f_{\alpha}$		$p_{\text{llama1B}} \circ f_{\alpha}$	
	average JSD / byte	bytes / sec	average JSD / byte	bytes / sec
1e-1	4.0e-2 (3.7e-2, 4.2e-2)	70.95 (64.14, 79.65)	2.8e-2 (2.5e-2, 3.0e-2)	84.21 (71.77, 99.54)
3e-2	1.9e-2 (1.8e-2, 2.1e-2)	44.68 (40.59, 48.66)	1.2e-2 (1.1e-2, 1.4e-2)	72.23 (65.87, 78.10)
1e-2	6.7e-3 (5.8e-3, 7.8e-3)	25.13 (23.83, 26.69)	4.2e-3 (3.5e-3, 4.9e-3)	40.45 (37.60, 43.43)
3e-3	2.5e-3 (1.9e-3, 3.3e-3)	10.48 (9.89, 11.12)	1.1e-3 (8.4e-4, 1.3e-3)	22.09 (20.94, 23.51)
1e-3	1.4e-3 (9.3e-4, 1.9e-3)	6.21 (5.89, 6.59)	4.0e-4 (2.9e-4, 5.6e-4)	11.86 (11.27, 12.49)
3e-4	7.6e-5 (6.0e-5, 9.9e-5)	1.97 (1.84, 2.11)	1.3e-4 (1.1e-4, 1.5e-4)	5.90 (5.60, 6.22)
1e-4	3.7e-5 (3.0e-5, 4.7e-5)	0.65 (0.61, 0.71)	8.8e-5 (8.1e-5, 9.5e-5)	2.15 (2.04, 2.26)
3e-5	2.5e-5 (2.4e-5, 2.7e-5)	0.21 (0.19, 0.22)	7.8e-5 (7.3e-5, 8.3e-5)	1.20 (1.15, 1.27)
1e-5	2.5e-5 (2.3e-5, 2.7e-5)	0.19 (0.17, 0.21)	7.4e-5 (6.9e-5, 7.7e-5)	0.62 (0.59, 0.66)

τ	$p_{\text{llama8B}} \circ f_{\alpha}$		$p_{\text{phi4}} \circ f_{\alpha}$	
	average JSD / byte	bytes / sec	average JSD / byte	bytes / sec
1e-1	2.2e-2 (2.0e-2, 2.4e-2)	79.03 (71.08, 87.28)	2.5e-2 (2.3e-2, 2.7e-2)	41.04 (36.96, 45.33)
3e-2	8.8e-3 (7.7e-3, 1.0e-2)	66.41 (62.69, 70.69)	9.7e-3 (8.6e-3, 1.1e-2)	36.20 (33.26, 38.87)
1e-2	3.5e-3 (2.9e-3, 4.2e-3)	45.47 (43.10, 47.91)	4.6e-3 (3.8e-3, 5.4e-3)	22.85 (21.14, 24.77)
3e-3	1.3e-3 (9.3e-4, 1.8e-3)	26.71 (25.11, 28.34)	1.8e-3 (1.4e-3, 2.4e-3)	14.80 (13.70, 15.83)
1e-3	5.1e-4 (2.9e-4, 8.4e-4)	15.73 (14.88, 16.60)	8.5e-4 (5.0e-4, 1.3e-3)	8.75 (8.30, 9.27)
3e-4	1.3e-4 (1.1e-4, 1.5e-4)	9.08 (8.68, 9.57)	1.9e-4 (1.4e-4, 2.5e-4)	4.87 (4.60, 5.16)
1e-4	9.1e-5 (8.0e-5, 1.0e-4)	4.03 (3.84, 4.23)	1.0e-4 (8.8e-5, 1.2e-4)	2.19 (2.07, 2.33)
3e-5	7.5e-5 (6.8e-5, 8.3e-5)	2.38 (2.27, 2.49)	7.6e-5 (6.8e-5, 8.4e-5)	1.30 (1.23, 1.37)
1e-5	7.3e-5 (6.6e-5, 8.1e-5)	1.40 (1.33, 1.47)	7.9e-5 (7.2e-5, 8.8e-5)	0.74 (0.70, 0.79)

Table 7: Throughput and Jensen–Shannon divergence (JSD) of Vieira et al. (2025a) at beam sizes $K \in \{8, 16, 32\}$. JSD is measured against $K = 32$. 95% confidence intervals are given in parentheses.

K	$p_{\text{gpt2}} \circ f_{\alpha}$		$p_{\text{llama1B}} \circ f_{\alpha}$	
	JSD vs $K = 32$	bytes / sec	JSD vs $K = 32$	bytes / sec
8	3.0e-5 (2.5e-5, 3.9e-5)	37.81 (37.59, 37.98)	7.1e-5 (6.7e-5, 7.6e-5)	46.94 (45.69, 47.97)
16	2.4e-5 (2.3e-5, 2.7e-5)	28.83 (28.53, 29.13)	7.1e-5 (6.7e-5, 7.5e-5)	28.76 (28.42, 29.08)
32	(not applicable)	18.12 (17.87, 18.36)	(not applicable)	5.34 (4.21, 7.19)

K	$p_{\text{llama8B}} \circ f_{\alpha}$		$p_{\text{phi4}} \circ f_{\alpha}$	
	JSD vs $K = 32$	bytes / sec	JSD vs $K = 32$	bytes / sec
8	6.8e-5 (6.3e-5, 7.4e-5)	18.30 (18.17, 18.43)	4.6e-5 (4.3e-5, 4.9e-5)	11.59 (11.29, 11.80)
16	6.9e-5 (6.2e-5, 7.8e-5)	10.55 (10.45, 10.65)	5.3e-5 (4.9e-5, 5.6e-5)	7.90 (7.84, 7.96)
32	(not applicable)	5.85 (5.79, 5.91)	(not applicable)	4.51 (4.44, 4.56)

G.2 JENSEN–SHANNON DIVERGENCE

We benchmark how well the algorithm given in §C approximates the exact distribution when using high pruning thresholds τ in the probability mass pruning described in §C.3. Across all three settings—token-to-byte, PTB tokenization, and DNA-to-amino-acid—JSD decreases as τ decreases, at the cost of throughput (bytes/sec).

Tab. 8 reports the token-to-byte results ($p_{\mathcal{X}} \circ f_{\alpha}$) for all four models. JSD drops by two to three orders of magnitude from $\tau = 1e-1$ to $\tau = 3e-5$, with the tightest thresholds reaching JSD below $1e-4$ for all models.

Tab. 9 gives the corresponding results for PTB tokenization ($p_{\mathcal{X}} \circ f_{\alpha} \circ f_{\text{ptb}}$), complementing Fig. 6 (right). Although f_{ptb} has fewer states than the token-to-byte transducers, only 56 of its 479 states are IP-universal, making lower thresholds computationally expensive; the reference is therefore $\tau = 1e-4$ ($3e-4$ for p_{phi4}) rather than $1e-5$. Despite this, JSD converges quickly, reaching the order of $1e-5$ at $\tau = 3e-4$ for p_{gpt2} , p_{llama1B} , and p_{llama8B} , while p_{phi4} converges more slowly.

Tab. 10 reports the DNA-to-amino-acid results ($p_{\text{dna}} \circ f_{\text{dna2aa}}$), where we additionally vary the candidate-set cap n_{max} to mitigate the combinatorial blow-up inherent in the three-to-one nucleotide-to-amino-acid mapping. Tighter thresholds generally reduce JSD. However, the interaction between τ and n_{max} is less uniform, as both the evaluated and reference distributions depend on the cap.

Incomplete runs. As shown in §G.3, the decomposition size grows rapidly at tight thresholds—mean $|Q|$ exceeds 35,000 at $\tau = 1\text{e-}5$ for f_{α} . For some model–threshold combinations, this growth prevents calculating the full distribution at each position in all ten evaluation paragraphs. Specifically, $p_{\text{gpt2}} \circ f_{\alpha}$ in Tab. 8 completed only 7 of 10 paragraphs at $\tau = 1\text{e-}5$. In Tab. 9, $p_{\text{phi4}} \circ f_{\alpha} \circ f_{\text{ptb}}$ completed 7 of 10 paragraphs at its reference threshold of $\tau = 3\text{e-}4$, and $p_{\text{lama1B}} \circ f_{\alpha} \circ f_{\text{ptb}}$ completed 9 of 10 at $\tau = 1\text{e-}4$. Additionally, $p_{\text{phi4}} \circ f_{\alpha} \circ f_{\text{ptb}}$ completed only 9 of 10 paragraphs at $\tau = 1\text{e-}1$ due to an unrecoverable backtracking failure (Fig. 10). In these cases, JSD and throughput are computed over the paragraphs shared across all thresholds for that model–transducer combination.

Table 8: Average Jensen–Shannon divergence (JSD) and bytes/sec for various thresholds τ using $p_{\mathcal{X}} \circ f_{\alpha}$ against a reference distribution ($\tau = 1\text{e-}5$). 95% confidence intervals are given in parentheses.

τ	$p_{\text{gpt2}} \circ f_{\alpha}$		$p_{\text{lama1B}} \circ f_{\alpha}$	
	average JSD / byte	bytes / sec	average JSD / byte	bytes / sec
1e-1	3.8e-2 (3.4e-2, 4.1e-2)	76.50 (66.94, 89.01)	2.8e-2 (2.6e-2, 3.0e-2)	84.21 (72.49, 99.24)
3e-2	1.7e-2 (1.5e-2, 1.9e-2)	45.61 (39.82, 51.46)	1.2e-2 (1.1e-2, 1.4e-2)	72.23 (66.25, 78.94)
1e-2	5.9e-3 (4.8e-3, 7.1e-3)	25.71 (24.08, 27.89)	4.2e-3 (3.5e-3, 5.0e-3)	40.45 (37.65, 43.43)
3e-3	2.1e-3 (1.4e-3, 2.9e-3)	11.22 (10.44, 12.07)	1.1e-3 (8.5e-4, 1.3e-3)	22.09 (20.90, 23.34)
1e-3	1.5e-3 (9.1e-4, 2.3e-3)	6.49 (6.02, 6.99)	4.0e-4 (2.8e-4, 5.4e-4)	11.86 (11.25, 12.54)
3e-4	5.5e-5 (4.7e-5, 6.7e-5)	2.28 (2.09, 2.48)	1.2e-4 (1.1e-4, 1.4e-4)	5.90 (5.59, 6.23)
1e-4	3.6e-5 (2.9e-5, 4.8e-5)	1.00 (0.92, 1.09)	7.4e-5 (6.9e-5, 8.0e-5)	2.15 (2.03, 2.26)
3e-5	2.4e-5 (2.2e-5, 2.7e-5)	0.44 (0.40, 0.49)	5.2e-5 (4.9e-5, 5.6e-5)	1.20 (1.14, 1.26)
1e-5	(not applicable)	0.19 (0.17, 0.21)	(not applicable)	0.62 (0.59, 0.65)

τ	$p_{\text{lama8B}} \circ f_{\alpha}$		$p_{\text{phi4}} \circ f_{\alpha}$	
	average JSD / byte	bytes / sec	average JSD / byte	bytes / sec
1e-1	2.3e-2 (2.1e-2, 2.5e-2)	79.03 (71.62, 87.24)	2.5e-2 (2.3e-2, 2.7e-2)	41.04 (36.75, 45.30)
3e-2	8.9e-3 (7.8e-3, 1.0e-2)	66.41 (61.96, 70.51)	9.9e-3 (8.7e-3, 1.1e-2)	36.20 (33.36, 38.85)
1e-2	3.5e-3 (2.9e-3, 4.4e-3)	45.47 (43.16, 48.08)	4.7e-3 (3.8e-3, 5.6e-3)	22.85 (21.06, 24.55)
3e-3	1.3e-3 (9.4e-4, 1.8e-3)	26.71 (25.17, 28.24)	1.8e-3 (1.3e-3, 2.4e-3)	14.80 (13.74, 15.78)
1e-3	5.2e-4 (3.0e-4, 8.4e-4)	15.73 (14.89, 16.61)	8.3e-4 (4.8e-4, 1.2e-3)	8.75 (8.30, 9.27)
3e-4	1.2e-4 (1.1e-4, 1.4e-4)	9.08 (8.64, 9.60)	1.9e-4 (1.1e-4, 2.9e-4)	4.87 (4.61, 5.19)
1e-4	8.3e-5 (7.3e-5, 9.6e-5)	4.03 (3.83, 4.26)	7.4e-5 (6.1e-5, 9.2e-5)	2.19 (2.05, 2.33)
3e-5	5.9e-5 (5.3e-5, 6.6e-5)	2.38 (2.27, 2.49)	3.7e-5 (3.4e-5, 4.0e-5)	1.30 (1.23, 1.37)
1e-5	(not applicable)	1.40 (1.34, 1.47)	(not applicable)	0.74 (0.70, 0.79)

Table 9: Average Jensen–Shannon divergence (JSD) and bytes/sec for various thresholds τ using $p_{\mathcal{X}} \circ f_{\alpha} \circ f_{\text{ptb}}$ against a reference distribution ($\tau = 1\text{e-}4; 3\text{e-}4$ for p_{phi4}). 95% confidence intervals are given in parentheses.

τ	$p_{\text{gpt2}} \circ f_{\alpha} \circ f_{\text{ptb}}$		$p_{\text{llama1B}} \circ f_{\alpha} \circ f_{\text{ptb}}$	
	average JSD / byte	bytes / sec	average JSD / byte	bytes / sec
1e-1	3.9e-3 (3.3e-3, 4.7e-3)	26.65 (25.79, 27.48)	3.0e-3 (2.6e-3, 3.5e-3)	30.44 (28.31, 32.19)
3e-2	1.4e-3 (1.2e-3, 1.5e-3)	17.03 (16.42, 17.66)	1.1e-3 (9.3e-4, 1.3e-3)	17.45 (16.67, 18.27)
1e-2	5.7e-4 (5.0e-4, 6.7e-4)	10.79 (10.23, 11.36)	3.7e-4 (3.4e-4, 4.0e-4)	10.54 (10.03, 11.09)
3e-3	1.7e-4 (1.5e-4, 1.9e-4)	4.52 (4.29, 4.79)	1.3e-4 (1.2e-4, 1.4e-4)	8.30 (7.98, 8.67)
1e-3	5.5e-5 (5.1e-5, 6.1e-5)	2.01 (1.88, 2.15)	6.1e-5 (5.8e-5, 6.5e-5)	4.13 (3.91, 4.36)
3e-4	2.0e-5 (1.7e-5, 2.4e-5)	0.81 (0.77, 0.85)	3.3e-5 (3.1e-5, 3.5e-5)	1.67 (1.59, 1.76)
1e-4	(not applicable)	0.20 (0.16, 0.25)	(not applicable)	0.70 (0.66, 0.74)

τ	$p_{\text{llama8B}} \circ f_{\alpha} \circ f_{\text{ptb}}$		$p_{\text{phi4}} \circ f_{\alpha} \circ f_{\text{ptb}}$	
	average JSD / byte	bytes / sec	average JSD / byte	bytes / sec
1e-1	2.5e-3 (2.1e-3, 3.0e-3)	19.25 (18.79, 19.76)	4.6e-3 (3.2e-3, 6.5e-3)	10.07 (9.53, 10.67)
3e-2	1.0e-3 (8.6e-4, 1.2e-3)	13.38 (12.99, 13.83)	3.8e-3 (2.6e-3, 5.1e-3)	5.87 (5.37, 6.40)
1e-2	6.0e-4 (4.7e-4, 7.8e-4)	9.49 (9.16, 9.88)	3.2e-3 (2.2e-3, 4.4e-3)	2.94 (2.59, 3.35)
3e-3	1.1e-4 (1.0e-4, 1.2e-4)	5.90 (5.62, 6.20)	4.2e-4 (3.0e-4, 5.8e-4)	2.95 (2.68, 3.26)
1e-3	5.1e-5 (4.7e-5, 5.5e-5)	3.29 (3.13, 3.45)	3.6e-4 (2.5e-4, 4.8e-4)	1.54 (1.37, 1.74)
3e-4	2.3e-5 (2.1e-5, 2.5e-5)	1.42 (1.35, 1.49)	(not applicable)	0.48 (0.43, 0.54)
1e-4	(not applicable)	0.56 (0.53, 0.59)	(not applicable)	(not applicable)

Table 10: Average Jensen–Shannon divergence (JSD) and bytes/sec for various thresholds τ and a reference ($\tau = 1e-6$) using $p_{dna} \circ f_{dna2aa}$. 95% confidence intervals are given in parentheses. We limit the candidate-set size (n_{max}) to mitigate the combinatorial blow-up with increasing sequence length.

τ	$p_{dna} \circ f_{dna2aa}$ ($n_{max} = 5000$)		$p_{dna} \circ f_{dna2aa}$ ($n_{max} = 10000$)	
	average JSD / byte	bytes / sec	average JSD / byte	bytes / sec
1e-1	2.8e-2 (2.4e-2, 3.2e-2)	9.55 (8.44, 10.90)	2.8e-2 (2.5e-2, 3.3e-2)	9.54 (8.45, 10.82)
3e-2	3.2e-3 (2.8e-3, 3.6e-3)	2.90 (2.57, 3.26)	3.3e-3 (2.9e-3, 3.7e-3)	2.03 (1.74, 2.39)
1e-2	6.6e-4 (4.4e-4, 9.0e-4)	2.20 (1.99, 2.47)	7.4e-4 (5.0e-4, 1.0e-3)	1.42 (1.25, 1.63)
3e-3	1.6e-4 (7.8e-5, 2.7e-4)	1.89 (1.72, 2.11)	2.7e-4 (1.1e-4, 4.9e-4)	1.16 (1.03, 1.31)
1e-3	7.1e-5 (1.7e-5, 1.6e-4)	1.79 (1.62, 1.97)	6.6e-5 (1.7e-5, 1.5e-4)	1.08 (0.97, 1.22)
3e-4	4.9e-5 (9.1e-6, 1.1e-4)	1.73 (1.58, 1.93)	3.5e-5 (6.7e-6, 7.9e-5)	1.04 (0.93, 1.17)
1e-4	5.8e-5 (1.1e-5, 1.2e-4)	1.72 (1.56, 1.91)	2.1e-5 (9.9e-7, 7.9e-5)	1.02 (0.92, 1.16)
3e-5	3.0e-5 (7.9e-7, 7.9e-5)	1.71 (1.55, 1.89)	2.1e-5 (6.6e-7, 6.2e-5)	1.02 (0.92, 1.14)
1e-5	2.2e-5 (1.0e-6, 5.4e-5)	1.71 (1.56, 1.89)	3.9e-6 (5.1e-7, 8.9e-6)	1.02 (0.91, 1.15)
3e-6	1.0e-5 (2.3e-7, 2.9e-5)	1.70 (1.55, 1.89)	1.2e-5 (6.1e-7, 3.2e-5)	1.01 (0.91, 1.12)
1e-6	(not applicable)	1.71 (1.55, 1.90)	(not applicable)	1.02 (0.92, 1.14)
τ	$p_{dna} \circ f_{dna2aa}$ ($n_{max} = 15000$)		$p_{dna} \circ f_{dna2aa}$ ($n_{max} = 20000$)	
	average JSD / byte	bytes / sec	average JSD / byte	bytes / sec
1e-1	2.9e-2 (2.5e-2, 3.3e-2)	9.52 (8.46, 10.82)	2.9e-2 (2.5e-2, 3.3e-2)	9.35 (8.21, 10.65)
3e-2	3.2e-3 (2.8e-3, 3.5e-3)	1.63 (1.37, 1.94)	3.2e-3 (2.8e-3, 3.7e-3)	1.41 (1.18, 1.71)
1e-2	6.8e-4 (4.5e-4, 9.8e-4)	1.10 (0.96, 1.27)	8.3e-4 (5.0e-4, 1.3e-3)	0.91 (0.78, 1.07)
3e-3	2.2e-4 (8.2e-5, 4.2e-4)	0.88 (0.77, 1.00)	2.0e-4 (7.6e-5, 3.9e-4)	0.71 (0.62, 0.83)
1e-3	5.0e-5 (8.5e-6, 1.3e-4)	0.80 (0.71, 0.91)	6.6e-5 (1.7e-5, 1.5e-4)	0.64 (0.56, 0.73)
3e-4	2.8e-5 (3.6e-6, 7.2e-5)	0.77 (0.68, 0.88)	3.0e-5 (3.9e-6, 7.9e-5)	0.61 (0.55, 0.71)
1e-4	2.4e-5 (1.1e-6, 7.0e-5)	0.75 (0.66, 0.84)	6.0e-5 (1.8e-6, 1.6e-4)	0.60 (0.54, 0.69)
3e-5	6.0e-5 (1.0e-6, 1.6e-4)	0.74 (0.66, 0.84)	1.8e-4 (5.0e-5, 3.7e-4)	0.60 (0.53, 0.68)
1e-5	3.0e-7 (7.1e-9, 8.3e-7)	0.74 (0.66, 0.84)	7.8e-7 (5.3e-8, 2.1e-6)	0.59 (0.53, 0.68)
3e-6	9.3e-7 (1.1e-8, 2.7e-6)	0.73 (0.65, 0.83)	7.3e-7 (8.9e-9, 2.1e-6)	0.59 (0.53, 0.67)
1e-6	(not applicable)	0.74 (0.65, 0.84)	(not applicable)	0.60 (0.53, 0.69)
τ	$p_{dna} \circ f_{dna2aa}$ ($n_{max} = 25000$)		$p_{dna} \circ f_{dna2aa}$ ($n_{max} = 30000$)	
	average JSD / byte	bytes / sec	average JSD / byte	bytes / sec
1e-1	2.9e-2 (2.5e-2, 3.3e-2)	9.50 (8.31, 10.78)	2.8e-2 (2.5e-2, 3.3e-2)	9.52 (8.43, 10.99)
3e-2	3.3e-3 (2.9e-3, 3.7e-3)	1.28 (1.06, 1.60)	3.3e-3 (2.9e-3, 3.8e-3)	1.18 (0.96, 1.45)
1e-2	7.9e-4 (4.9e-4, 1.3e-3)	0.81 (0.70, 0.95)	8.2e-4 (4.9e-4, 1.2e-3)	0.72 (0.61, 0.86)
3e-3	2.3e-4 (8.1e-5, 4.7e-4)	0.62 (0.54, 0.72)	2.5e-4 (7.9e-5, 4.8e-4)	0.55 (0.47, 0.64)
1e-3	5.9e-5 (1.1e-5, 1.4e-4)	0.56 (0.49, 0.65)	6.0e-5 (1.1e-5, 1.4e-4)	0.49 (0.42, 0.57)
3e-4	2.6e-5 (3.5e-6, 6.8e-5)	0.53 (0.46, 0.61)	3.4e-5 (4.9e-6, 8.5e-5)	0.46 (0.41, 0.53)
1e-4	2.4e-5 (8.2e-7, 6.9e-5)	0.52 (0.46, 0.59)	2.4e-5 (1.0e-6, 8.0e-5)	0.45 (0.39, 0.51)
3e-5	7.2e-5 (1.9e-5, 1.5e-4)	0.51 (0.45, 0.59)	2.4e-5 (5.6e-7, 7.1e-5)	0.45 (0.39, 0.52)
1e-5	1.9e-6 (5.6e-8, 4.6e-6)	0.51 (0.45, 0.59)	1.7e-7 (5.7e-9, 3.8e-7)	0.44 (0.39, 0.51)
3e-6	1.3e-6 (1.2e-8, 3.3e-6)	0.51 (0.45, 0.58)	1.6e-6 (1.7e-8, 3.7e-6)	0.44 (0.38, 0.51)
1e-6	(not applicable)	0.51 (0.45, 0.59)	(not applicable)	0.44 (0.39, 0.51)

G.3 DECOMPOSITION SIZE

Tab. 11 and Fig. 18 show how the quotient and remainder sizes grow as τ decreases, explaining the throughput reduction observed in the JSD experiments.

For the all-IP-universal token-to-byte and DNA transducers, the remainder is empty ($|\mathbb{R}| = 0$) at every position, so only the quotient size is reported. In the token-to-byte setting, the mean quotient size grows from 62 at $\tau = 1e-1$ to over 35,000 at $\tau = 1e-5$, directly accounting for the throughput reduction at tight thresholds. The DNA transducer saturates early due to $n_{max} = 5000$: mean $|\mathbb{Q}|$ reaches 465 by $\tau = 3e-5$ and remains flat beyond that.

For f_{ptb} , which has non-IP-universal states, both $|\mathbb{Q}|$ and $|\mathbb{R}|$ are reported. $|\mathbb{Q}|$ grows steadily with a tighter τ , while $|\mathbb{R}|$ initially decreases as more candidates enter the quotient but then grows as the expansion loop over non-IP-universal states discovers additional remainder elements. The presence of a non-trivial remainder is the key structural difference from the all-IP-universal transducers: each

remainder element requires a full string probability $p_{\mathcal{X}}(\mathbf{x})$ rather than just a prefix probability, making it more expensive per element.

Table 11: Mean and maximum quotient size $|\mathcal{Q}|$ across sequence positions for three transducers at varying pruning thresholds τ . Results are computed on paragraph 1 of WikiText (833 bytes for $p_{\text{gpt2}} \circ f_{\alpha}$, 850 bytes for $p_{\text{gpt2}} \circ f_{\alpha} \circ f_{\text{ptb}}$) and on the longest protein in the test set (P83127, 12 amino acids for $p_{\text{dna}} \circ f_{\text{dna2aa}}$). The f_{α} and f_{dna2aa} transducers have all-universal states ($|\mathcal{R}| = 0$ everywhere). The f_{ptb} transducer has non-universal states, so we additionally report the remainder size $|\mathcal{R}|$.

(a) $p_{\text{gpt2}} \circ f_{\alpha}$			(b) $p_{\text{dna}} \circ f_{\text{dna2aa}}$		
τ	Mean $ \mathcal{Q} $	Max $ \mathcal{Q} $	τ	Mean $ \mathcal{Q} $	Max $ \mathcal{Q} $
1e-1	62	2,238	1e-1	104	344
3e-2	200	5,736	3e-2	288	1,274
1e-2	439	11,998	1e-2	346	1,329
3e-3	873	18,761	3e-3	439	2,011
1e-3	1,536	25,341	1e-3	454	2,027
3e-4	3,161	65,536	3e-4	462	2,044
1e-4	7,800	131,072	1e-4	463	2,044
3e-5	17,232	524,288	3e-5	465	2,046
1e-5	35,768	2,097,152	1e-5	465	2,046
			3e-6	465	2,046

(c) $p_{\text{gpt2}} \circ f_{\alpha} \circ f_{\text{ptb}}$				
τ	Mean $ \mathcal{Q} $	Max $ \mathcal{Q} $	Mean $ \mathcal{R} $	Max $ \mathcal{R} $
1e-1	1.3	31	1.0	113
3e-2	1.9	57	0.38	113
1e-2	3.6	142	0.48	25
3e-3	7.3	353	1.2	53
1e-3	16	686	3.5	129
3e-4	47	1,807	11.4	408
1e-4	128	5,101	33.9	1,195

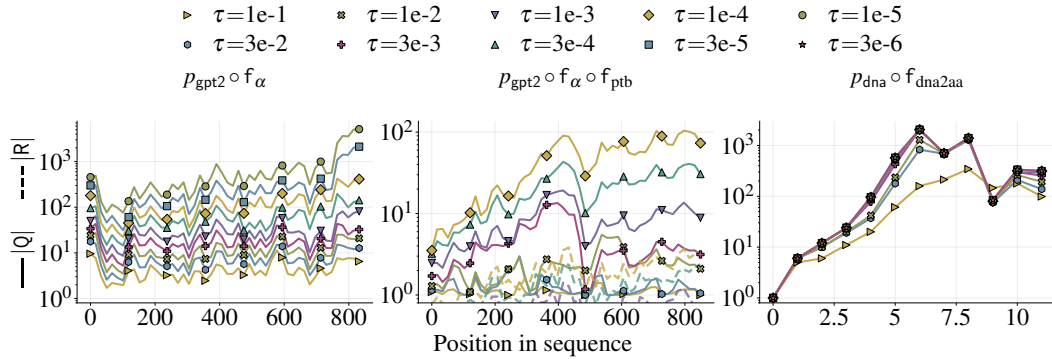


Figure 18: Growth of the quotient size $|\mathcal{Q}|$ (solid lines) and remainder size $|\mathcal{R}|$ (dashed lines) with sequence position for three transducer compositions at varying pruning thresholds τ . Left: $p_{\text{gpt2}} \circ f_{\alpha}$ on paragraph 1 of WikiText (833 bytes). Center: $p_{\text{gpt2}} \circ f_{\alpha} \circ f_{\text{ptb}}$ on paragraph 1 (850 bytes after transduction); dashed lines show $|\mathcal{R}|$, which is non-zero because f_{ptb} contains non-IP-universal states. Right: $p_{\text{dna}} \circ f_{\text{dna2aa}}$ on the longest protein in the test set (P83127, 12 amino acids). For f_{α} and f_{dna2aa} , all FST states are IP-universal, so $|\mathcal{R}| = 0$ everywhere. The f_{dna2aa} panel uses a candidate-set cap of $n_{\text{max}} = 5,000$, which limits the quotient size at lower thresholds and breaks monotonic growth at later positions.

G.4 CROSS-ENTROPY

Cross-entropy measures how well the transduced model assigns probability to held-out text; unlike JSD, it only requires evaluating $\overline{p_{\mathcal{Y}}}(y | \mathbf{y})$ for the observed next symbol rather than computing the full next-symbol distribution $\overline{p_{\mathcal{Y}}}(\cdot | \mathbf{y})$. Tab. 12 reports cross-entropy (in nats and bits per byte) together with throughput for $(p_{\mathcal{X}} \circ f_{\alpha})$. Because only a single probability is needed per position, throughput is higher than in the JSD tables above. Cross-entropy converges quickly as τ decreases: for all four models, the tightest thresholds yield nearly identical values, confirming that moderate pruning suffices for accurate sequence scoring.

Table 12: Cross-entropy and throughput for various thresholds τ using $p_{\mathcal{X}} \circ f_{\alpha}$. 95% confidence intervals are given in parentheses. $p_{\text{gpt2}} \circ f_{\alpha}$ at $\tau = 1\text{e-}5$ is computed over 6 paragraphs; all other configurations use 10.

τ	bytes / sec		Bits / byte		Cross-entropy	
	Mean	95% CI	Mean	95% CI	Mean	95% CI
$p_{\text{gpt2}} \circ f_{\alpha}$						
1e-1	82.61	(73.33, 92.34)	1.2434	(1.1884, 1.2936)	0.8619	(0.8237, 0.8966)
3e-2	49.10	(44.48, 54.24)	1.1466	(1.0978, 1.1949)	0.7948	(0.7609, 0.8282)
1e-2	28.46	(26.73, 30.33)	1.0652	(1.0199, 1.1068)	0.7383	(0.7070, 0.7672)
3e-3	14.20	(13.47, 14.98)	1.0385	(0.9956, 1.0806)	0.7199	(0.6901, 0.7490)
1e-3	6.46	(6.08, 6.84)	1.0293	(0.9909, 1.0664)	0.7134	(0.6868, 0.7392)
3e-4	2.18	(2.04, 2.33)	1.0220	(0.9831, 1.0604)	0.7084	(0.6815, 0.7350)
1e-4	0.75	(0.70, 0.80)	1.0220	(0.9823, 1.0610)	0.7084	(0.6809, 0.7355)
3e-5	0.35	(0.33, 0.39)	1.0200	(0.9781, 1.0633)	0.7070	(0.6779, 0.7370)
1e-5	0.34	(0.30, 0.38)	1.0025	(0.9461, 1.0550)	0.6949	(0.6558, 0.7313)
$p_{\text{llama1B}} \circ f_{\alpha}$						
1e-1	129.22	(112.82, 146.19)	0.9922	(0.9467, 1.0405)	0.6877	(0.6562, 0.7212)
3e-2	90.74	(82.63, 99.33)	0.9128	(0.8682, 0.9542)	0.6327	(0.6018, 0.6614)
1e-2	47.81	(44.04, 51.52)	0.8626	(0.8252, 0.9027)	0.5979	(0.5720, 0.6257)
3e-3	26.15	(24.71, 27.73)	0.8402	(0.8037, 0.8790)	0.5823	(0.5571, 0.6093)
1e-3	14.89	(14.18, 15.69)	0.8364	(0.8001, 0.8725)	0.5797	(0.5546, 0.6048)
3e-4	6.80	(6.46, 7.18)	0.8358	(0.7999, 0.8724)	0.5793	(0.5545, 0.6047)
1e-4	2.62	(2.49, 2.77)	0.8362	(0.8018, 0.8699)	0.5796	(0.5558, 0.6030)
3e-5	1.42	(1.35, 1.49)	0.8361	(0.8002, 0.8717)	0.5796	(0.5547, 0.6042)
1e-5	0.73	(0.69, 0.77)	0.8360	(0.8002, 0.8717)	0.5795	(0.5546, 0.6042)
$p_{\text{llama8B}} \circ f_{\alpha}$						
1e-1	88.65	(79.18, 99.61)	0.8176	(0.7757, 0.8661)	0.5667	(0.5377, 0.6003)
3e-2	76.39	(71.27, 81.35)	0.7392	(0.7007, 0.7759)	0.5124	(0.4857, 0.5378)
1e-2	52.05	(49.41, 54.93)	0.7153	(0.6778, 0.7507)	0.4958	(0.4698, 0.5203)
3e-3	28.81	(27.18, 30.44)	0.6959	(0.6627, 0.7282)	0.4824	(0.4594, 0.5047)
1e-3	16.86	(16.01, 17.82)	0.6913	(0.6584, 0.7251)	0.4791	(0.4564, 0.5026)
3e-4	9.73	(9.24, 10.25)	0.6870	(0.6513, 0.7179)	0.4762	(0.4515, 0.4976)
1e-4	4.35	(4.15, 4.58)	0.6870	(0.6557, 0.7221)	0.4762	(0.4545, 0.5005)
3e-5	2.60	(2.47, 2.73)	0.6869	(0.6533, 0.7208)	0.4761	(0.4528, 0.4996)
1e-5	1.57	(1.49, 1.66)	0.6869	(0.6552, 0.7180)	0.4761	(0.4541, 0.4977)
$p_{\text{phi4}} \circ f_{\alpha}$						
1e-1	42.39	(37.95, 47.19)	0.8714	(0.8217, 0.9208)	0.6040	(0.5695, 0.6382)
3e-2	34.48	(31.73, 37.33)	0.7748	(0.7317, 0.8180)	0.5371	(0.5072, 0.5670)
1e-2	24.89	(23.05, 26.59)	0.7547	(0.7165, 0.7959)	0.5231	(0.4966, 0.5517)
3e-3	16.55	(15.34, 17.92)	0.7301	(0.6959, 0.7690)	0.5061	(0.4824, 0.5330)
1e-3	9.91	(9.41, 10.52)	0.7241	(0.6882, 0.7595)	0.5019	(0.4770, 0.5264)
3e-4	5.81	(5.51, 6.14)	0.7170	(0.6803, 0.7509)	0.4970	(0.4716, 0.5205)
1e-4	2.55	(2.41, 2.70)	0.7163	(0.6824, 0.7493)	0.4965	(0.4730, 0.5194)
3e-5	1.54	(1.46, 1.62)	0.7162	(0.6793, 0.7490)	0.4965	(0.4709, 0.5192)
1e-5	0.86	(0.81, 0.91)	0.7162	(0.6828, 0.7502)	0.4964	(0.4733, 0.5200)

G.5 BENCHMARKING THE COMPUTATIONAL SHORTCUT

We benchmark the computational shortcut inherent in the prefix decomposition described in §4, which allows us to decompose the precover into remainder and quotient representatives. We generate suboptimal decompositions by randomly selecting n IP-universal states in the transducer (see §4) and treating them as non-IP-universal in our algorithms (see §5). This gradually decreases the size of the quotient and increases the remainder correspondingly. Tab. 13 shows the average JSD between the original and modified distributions over the first 256 bytes of the first 5 paragraphs of the `wikitext-2-raw-v1` dataset (Merity et al., 2017). For each value of n , we repeat the sampling of new non-universal states three times, and report the mean JSD.

The distributions diverge rapidly, and after converting roughly 15–20% of IP-universal states, the algorithm repeatedly encounters dead ends. This number varies between runs; as shown in Fig. 19, each repeat exhibits a distinct step function: JSD remains low until a particular high-connectivity state is converted, then jumps by 2–3 orders of magnitude and plateaus. In the PTB transducer, one IP-universal state (state 193) serves as a routing hub with 274 arcs spanning 245 output symbols. When this state is converted, frontiers containing it move from the quotient Q to the remainder R , causing the expansion loop to require fallback scoring (Fig. 10). Different runs encounter this hub at different values depending on the permutation order, producing the staircase pattern. This shows that IP-universal states have a hierarchical importance structure: distribution quality is governed by a small number of high-connectivity hub states, while the majority can be converted with negligible impact ($\text{JSD} \leq 1e-4$).

Table 13: Average Jensen–Shannon divergence (JSD) for the PTB transducer ($\tau = 1e-3$) after randomly converting n of the IP-universal states to non-IP-universal. 95% confidence intervals are given in parentheses. JSD is computed against the unmodified transducer ($n = 0$).

Converted States (n)	$p_{\text{llama1B}} \circ f_{\alpha} \circ f_{\text{ptb}}$	$p_{\text{llama8B}} \circ f_{\alpha} \circ f_{\text{ptb}}$	$p_{\text{phi4}} \circ f_{\alpha} \circ f_{\text{ptb}}$
0	(not applicable)	(not applicable)	(not applicable)
2	$3.9e-5$ (3.5e-5, 4.3e-5)	$1.3e-4$ (7.4e-5, 2.1e-4)	$6.6e-5$ (3.1e-5, 1.1e-4)
5	$9.5e-4$ (7.5e-4, 1.2e-3)	$9.0e-4$ (7.5e-4, 1.1e-3)	$7.8e-4$ (6.4e-4, 9.4e-4)
8	$9.8e-4$ (8.0e-4, 1.2e-3)	$9.2e-4$ (7.7e-4, 1.1e-3)	$8.1e-4$ (6.6e-4, 9.6e-4)
11	$3.0e-2$ (2.6e-2, 3.3e-2)	$2.8e-2$ (2.5e-2, 3.1e-2)	$2.6e-2$ (2.3e-2, 2.9e-2)
14	$2.9e-2$ (2.6e-2, 3.3e-2)	$2.8e-2$ (2.5e-2, 3.1e-2)	$2.6e-2$ (2.3e-2, 2.9e-2)
16	$2.9e-2$ (2.6e-2, 3.2e-2)	$2.8e-2$ (2.5e-2, 3.2e-2)	$2.6e-2$ (2.3e-2, 2.9e-2)
19	$2.9e-2$ (2.6e-2, 3.3e-2)	$2.8e-2$ (2.5e-2, 3.2e-2)	$2.6e-2$ (2.3e-2, 2.9e-2)

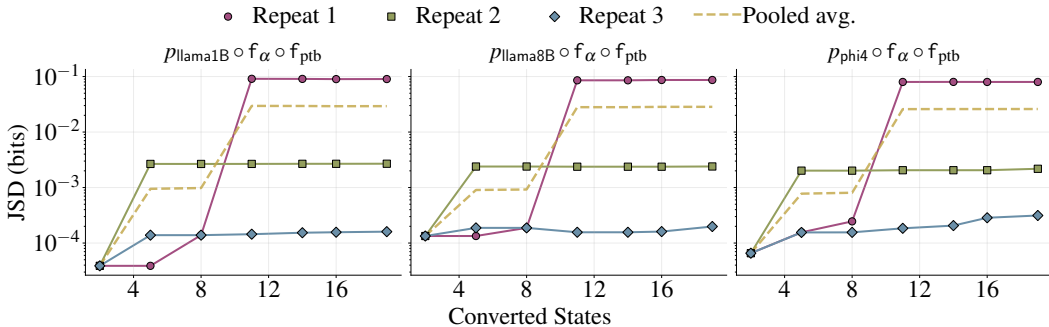


Figure 19: Per-repeat Jensen–Shannon divergence (JSD) vs. number of states converted from IP-universal to non-IP-universal for the PTB transducer ($\tau = 1e-3$). Each repeat uses a different random conversion order. The abrupt jumps are caused by individual high-connectivity states, whose conversion causes a jump in JSD.

H STATE-BASED DECOMPOSITION

The algorithms presented in the main text enumerate source *strings*: the quotient $\mathcal{Q}(y)$ and remainder $\mathcal{R}(y)$ are represented as explicit sets of strings. When these sets are infinite, the string-enumeration approach does not terminate without pruning.

An alternative is to operate on the *state space* of the precover DFA rather than its string space. Since the precover DFA P_y (§5.1) has finitely many states, a state-based traversal always terminates, even when $\mathcal{Q}(y)$ or $\mathcal{R}(y)$ are infinite. The key idea is to represent the quotient and remainder as DFAs Q and R —automata that *accept* the (possibly infinite) sets $\mathcal{Q}(y)$ and $\mathcal{R}(y)$ respectively—rather than enumerating their elements. The full precover is then recovered as $\mathcal{P}(y) = \llbracket Q \rrbracket \sqcup \llbracket R \rrbracket$.

The algorithm in Fig. 20 performs a BFS over the states of P_y . At each state s , it checks whether s is *universal*—i.e., whether the sub-automaton rooted at s accepts \mathcal{X}^* (see `is_cylinder`). If so, s is marked as a quotient member and accepting state, and its successors are not explored, since all extensions from a universal state are covered. If s is accepting but not universal, it is marked as a remainder member and accepting state, and exploration continues through its outgoing arcs.

The result is a pair of DFAs that share the same state space and truncated arc set but differ in their accepting states. The quotient automaton Q has the universal states as accepting states, and arcs leaving universal states are dropped (since the BFS does not expand past them); thus $\llbracket Q \rrbracket = \mathcal{Q}(y)$, accepting exactly the quotient elements. The remainder automaton R uses the same truncated arc set but marks only the non-universal accepting states; thus, $\llbracket R \rrbracket = \mathcal{R}(y)$.

```

247 def dfa_decomposition(f, y):
248     P_y ← trim(determinize(proj_x(f ∘ y^*)))
249     q ← QUEUE(l_y)
250     V ← ∅; arcs ← ∅
251     Q ← ∅; R ← ∅
252     while q:
253         s ← q.pop()
254         if s ∈ V: continue
255         V.add(s)
256         if s ∈ F_y:
257             if is_cylinder(s):
258                 Q.add(s)
259                 continue # do not expand
260             else:
261                 R.add(s)
262         for x ∈ X:
263             s' ← step_y(s, x)
264             if s' = ∅: continue
265             q.push(s')
266             arcs.add(s  $\xrightarrow{x}$  s')
267     return DFA(V, arcs, Q), DFA(V, arcs, R)
268 def is_cylinder(s):
269     V ← {s}; q ← QUEUE({s})
270     while q:
271         s ← q.pop()
272         if s ∉ F_y:
273             return False
274         for x ∈ X:
275             s' ← step_y(s, x)
276             if s' = ∅: return False
277             if s' ∉ V:
278                 V.add(s'); q.push(s')
279     return True

```

Figure 20: State-based decomposition of the precover into DFAs. *Left*: BFS over the precover DFA P_y . Universal states become accepting in Q ; non-universal accepting states become accepting in R . Arcs leaving universal states are not collected. *Right*: `is_cylinder` is the same universality BFS as in Fig. 3, but takes a DFA state directly rather than computing it from a source string via `run_y`.

Comparison with string-based algorithms. The state-based algorithm always terminates in finite time—even when $\mathcal{Q}(y)$ or $\mathcal{R}(y)$ are infinite—because P_y has finitely many states. The resulting DFAs Q and R provide compact, finite representations of these potentially infinite sets.

However, implementing the autoregressive interface (§C.1) still requires enumerating the strings accepted by these machines: computing $\vec{p}_y(y)$ via Eq. (8a) sums $p_x(x)$ over elements of $\mathcal{Q}(y)$ and $\mathcal{R}(y)$, and when these sets are infinite, the sum must be truncated regardless. Thus, while the DFA representation guarantees a finite decomposition, it does not, on its own, yield finite-time scoring.

I RELATED WORK

Modern language models define probability distributions over sequences of tokens (see §2). For efficiency and vocabulary (a.k.a. their alphabet) management, they usually rely on subword schemes such as BPE (Sennrich et al., 2016; Gage, 1994) or Unigram (Kudo, 2018). Although these approaches have been remarkably successful, their units often don’t coincide with linguistic boundaries, and any given string typically admits an exponential number of tokenization variants with non-zero probability mass under the language model. Recent work has tackled this issue by enforcing canonical tokenization to remove probability mass from noncanonical encodings (Vieira et al., 2025b), while Geh et al. (2024) have shown that aggregating the probability mass of noncanonical tokenization choices carries a useful signal that can boost downstream accuracy.

Subword segmentation also gives rise to the prompt-boundary problem (Vieira et al., 2025a), where imperceptible changes to the final characters of a prompt (e.g., appending a single whitespace) can push the encoded token sequence onto a completely different path in token space, causing the model to abandon otherwise highly probable continuations. To overcome these issues, Vieira et al. (2025a) introduce an algorithm for transforming token-based language models into language models over characters. Although their contribution centers around characters, the underlying idea can be generalized (as shown in this work).

Many applications need a method to accurately convert the probability mass learned on subword tokens to other types of units, such as bytes, words, or morphemes in NLP, or amino acids in computational biology, as pointed out in §1. An additional example is found in psycholinguistics, where researchers often require fine-grained estimates of surprisal, e.g., to predict a reader’s likelihood of skipping a word based on how predictable its first three characters are (Rayner et al., 1982; Blanchard et al., 1989). To this end, recent studies have tackled the challenges posed by subword tokenization (Nair & Resnik, 2023; Beinborn & Pinter, 2023; Pimentel & Meister, 2024; Oh & Schuler, 2024; Giulianelli et al., 2024). For example, Oh & Schuler (2024) and Pimentel & Meister (2024) argue that leading whitespace tokenization introduces a confounder in surprisal estimates and instead advocate for incorporating the probability of trailing whitespaces into such calculations.

Furthermore, Pimentel & Meister (2024) give a bespoke procedure for converting token-based language models to word-based language models. However, their method does not model the contextually sensitive nature of English word segmentation, e.g., it treats both periods in Ex. (1) identically, where English orthography does not. Additionally, the justification of the procedure requires that there exists a set of distinguished end-of-word markers that appear at the end of a token, if at all. We now consider how such a transducer can be constructed. Let f_α be a transducer that converts a token alphabet to a character alphabet, and D be the set of delimiters. The transducer f_D is given in Fig. 21. Given a language model $p_{\mathcal{X}}$ over \mathcal{X} , we can then compose them into a transducer $p_{\mathcal{X}} \circ f_\alpha \circ f_D$ to get a transduced language model over separator-delimited words. However, such an approach would be rather naïve. Unfortunately, delimiter-based separation would not be able to distinguish when the dot should be its own symbol or not, as in ex. (3).

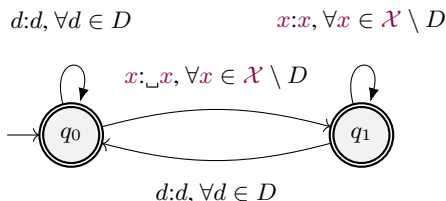


Figure 21: A simple FST that segments character streams into words without contextual information, inserting $_$ at the start of each word.

The delimiter-based approach also fails for most BPE-based language models because of the clustering of delimiter candidates. For instance, GPT-4o’s alphabet contains the token $_{10880}$, which consists

solely of end-of-word symbols. Under PTB guidelines, for example, 10880 should be broken into three consecutive orthographic words 10880 . In contrast, we argue that the proper tokenization scheme for psycholinguistic modeling should be specified based on the goals of the study and not based on the properties of any one specific tokenizer.

Tokenization challenges are not unique to modeling natural language. In computational biology, DNA, RNA, and protein sequences are long, unsegmented strings over small alphabets that pose challenges in tokenization. Researchers thus alternate between different tokenization schemas, such as k-mers, learned subwords, and motif-aware segmenters (Ji et al., 2021; Nguyen et al., 2023; Dotan et al., 2024; Wang et al., 2024; Qiao et al., 2024). Because language models are often trained under different tokenization schemas, their autoregressive predictions—step-by-step probabilities and conditional distributions—are not directly comparable across tokenization schemes.

Transducer-based approaches to tokenization are well-established—WordPiece (Wu et al., 2016) can be implemented as a transducer (Song et al., 2021), and deterministic finite automata have been constructed for BPE (Berglund & van der Merwe, 2023; Berglund et al., 2024). Moreover, transducers also have a long history in language modeling (Mohri, 1997) and have been adopted for constrained decoding, where an FST enforces lexical or structural constraints (Allauzen et al., 2014; Ghazvininejad et al., 2016; Stahlberg et al., 2019; Willard & Louf, 2023; Koo et al., 2024; Cognetta et al., 2025).

Closely related are neural finite-state transducers (Lin et al., 2019) and earlier neural FST hybrids (Rastogi et al., 2016), which assign (neural) weights to transitions and compute prefix/sequence probabilities as path-sums over all paths consistent with a given output. Our construction admits a similar view: we marginalize over all source strings (paths) that map to a given output. However, rather than learning transition weights, we focus on transducing an off-the-shelf pretrained LM, enabling efficient inference via quotient-remainder decomposition.

In this study, we generalize character-level conversion and extend Vieira et al. (2025a) into a framework that enables transforming a language model into another language model, beyond the limited setting of strict-prefix monotonic mappings. We support conversions between sets of units and unit-preserving transformations, provided that the mapping between them can be described by a finite-state transducer.

J LIMITATIONS

Empirical scope. Although our framework theoretically enables transduction of any language model to any unit of interest, given a valid transducer, we test only a limited set of architectures (GPT-2, LLaMA 3, and Phi-4) and target specific units (bytes, Penn Treebank tokens, and amino acids). Future research could broaden the analysis to a wider range of models, datasets, and units.

Expressiveness. Our analysis has focused on functional finite-state transducers and regular languages. Future work could consider dynamically built transducers and distributions over more expressive languages, as well as stochastic maps encoded by non-functional transducers—where the notion of universality would need to be adjusted.

Approximation quality. Our pruning-based inference algorithm performs well when the source language model concentrates most of its probability mass on a small number of prefixes that map to the current target prefix under the transducer—i.e., when the effective size of the quotient and remainder after pruning is small. When the mass is dispersed across many source prefixes (such as in the DNA to amino-acid case), pruning must discard a larger fraction of the total probability, and the approximation degrades. An importance-sampling approach (§ C.3) could provide a less systematically biased alternative.

Speed. The speed of our algorithms and implementations may not suit every use case. Obtaining the full distribution (for example, for decoding or model comparisons) currently requires speeds of around 10–20 bytes/sec. While this is not prohibitive for many tasks, it leaves ample room for improvement.

Marginalization. A core property of transduced language models is the *marginalization*: the transduction sums source-string probabilities to compute target-string probabilities, aggregating mass across all source strings that map to the same target. Since natural language allows the same meaning to be expressed in multiple ways, a transduction could normalize these to obtain a more representative output distribution over the space of interest. Consider, for instance, a math problem: “If 12 students are younger than Tom and 12 students are older, how many are there in total?” The answer could be ‘25’, or ‘twenty-five’, or perhaps ‘12+1+12’. If any of these have significant probability mass, we would like to sum them. In chain-of-thought reasoning, we can similarly imagine summing and normalizing probabilities across samples from the system, an approach known as *self-consistency* (Wang et al., 2023). We hope to see transduced language models applied in such settings in future work.